Simulations of 2014 Hydrodynamics and Water Quality in the Massachusetts Bay System using the Bays Eutrophication Model

Massachusetts Water Resources Authority
Environmental Quality Department
Report 2016-03

Citation:

Zhao L, Chen C, Beardsley RC, Codiga DL, Leo WS. 2016. **Simulations of Hydrodynamics and Water Quality in the Massachusetts Bay System during 2014 using the Bays Eutrophication Model.** Boston: Massachusetts Water Resources Authority. Report 2016-03. 103p.

Acronyms

Related to models used

BEM	Bays Eutrophication Model (water quality model UG-RCA and hydrodynamics model MB-FVCOM together)
FVCOM	Finite-Volume Community Ocean Model
GOM1-FVCOM	FVCOM applied to the Gulf of Maine and Georges Bank
MB-FVCOM	FVCOM applied to Massachusetts Bay
RCA	Row Column Advanced (RCA), a water quality model from Hydroqual
UG-RCA	Unstructured-grid version of RCA
WRF	Weather Research and Forecast meteorological model

Related to modeled quantities

DIN	Dissolved Inorganic Nitrogen (Sum of N in NH_4^+, NO_3^-, and NO_2^-)
DO	Dissolved Oxygen
DOC, DON, DOP	Dissolved Organic Carbon, Nitrogen, and Phosphorous
NH_4^+, NO_3^-, NO_2^-	Ammonium, Nitrate, Nitrite
PO_4^{3-}, SiO_3^{2-}	Phosphate, Silicate
POC, PON, POP	Particulate Organic Carbon, Nitrogen, and Phosphorous
SOD	Sediment Oxygen Demand

Simulations of 2014 Hydrodynamics and Water Quality

in the Massachusetts Bay System using the Bays Eutrophication Model

Submitted to

Massachusetts Water Resources Authority
Environmental Quality Department
100 First Avenue
Charlestown Navy Yard
Boston, MA 02129
(617) 242-6000

Prepared by

Liuzhi Zhao and Changsheng Chen

School for Marine Science and Technology

University of Massachusetts-Dartmouth

New Bedford, MA 02744

Robert C. Beardsley

Woods Hole Oceanographic Institution

Woods Hole, MA 02543

Daniel L. Codiga and Wendy S. Leo

Massachusetts Water Resources Authority

Boston, MA 02129

June 2016

EXECUTIVE SUMMARY

The hydrodynamics (including temperature, salinity, and currents) and water quality (including nutrients, chlorophyll, and dissolved oxygen) of Massachusetts Bay, Cape Cod Bay, and Boston Harbor during 2014 were simulated by University of Massachusetts Dartmouth. Methods were the same as in 2013 simulations (MWRA Technical Report, http://www.mwra.state.ma.us/harbor/enquad/pdf/2015-03.pdf). Hydrodynamic results were in good agreement with available observations for the geographic and vertical structure, and temporal variability, of temperature and salinity distributions (including density stratification) and currents (non-tidal and tidal).

The water quality simulation captured general patterns in observed seasonal variations, geographic distributions, and vertical structure for many variables. This included the spring reduction in near-surface dissolved inorganic nitrogen, due to phytoplankton uptake, and its fall replenishment when stratification broke down. It also included seasonal dissolved oxygen variations, with peak values in spring at shallow depths due to solubility and phytoplankton growth and late summer minima deep in the water column when stratification inhibits reaeration. In addition to those more bay-wide patterns, near the seafloor local to the outfall (within 10-20 km) dissolved inorganic nitrogen was elevated. Model-observation agreement was modest for dissolved and particulate organic nitrogen and weakest for particulate organic carbon, particularly its vertical structure, and for chlorophyll. In general, as in prior years, most modeled water quality variables exhibited a smaller range of values, and smaller surface-bottom differences during stratified conditions, as compared to observations. The simulations support the conclusion of the field monitoring program, that bay-wide ecological function is not appreciably influenced by the outfall.

Focused investigations of model characteristics were made regarding two notable features of the 2014 observations. The first notable feature was that the observed spring phytoplankton bloom was modest in strength and delayed by about a month compared to a typical year, likely due to unusually late cold winter temperatures. Although not all aspects of the simulated spring bloom agreed well with observations, prominent features were consistent with them including later than typical decreases in surface nutrients, increases in particulate organic carbon, and increases in deep chlorophyll. The second notable feature was that the observed development of stratification included an unusual storm mixing event, and the observed breakdown of stratification was earlier than typical in the upper water column but later than typical at depth. Most of these short-timescale variations and features in the vertical structure of stratification were captured well by the model.

Table of Contents

Table of Figures

1. Introduction

1.1 *Project overview*

The Massachusetts Water Resources Authority (MWRA) has established a long-term monitoring program to evaluate the impact of MWRA sewage treatment plant effluent on the water quality and ecosystem function of Massachusetts Bay, Cape Cod Bay, and Boston Harbor. The monitoring program primarily consists of a series of ongoing field observation campaigns and includes complementary water quality modeling as required by the permit for effluent discharge into Massachusetts Bay. The water quality simulations are carried out using the Bays Eutrophication Model (BEM), which consists of the UG-RCA (Unstructured Grid - Row Column Advanced) water quality model and the MB-FVCOM (Massachusetts Bay - Finite Volume Community Ocean Model) hydrodynamic model. This report presents simulation results for the 2014 calendar year.

1.2 *Background on oceanographic processes influencing water quality*

Massachusetts Bay and Cape Cod Bay (Figure 1-1) comprise a temperate coastal embayment system. Readers unfamiliar with its geography and the current understanding of its physical and biological oceanographic processes are referred to the introductory summaries found in sections 1.2 and 1.3 of MWRA Technical Report 2011-13 (Zhao et al., 2012), in the annual MWRA water column monitoring report (e.g., for calendar year 2014, Libby et al., 2015), and in references cited by them. (All MWRA Technical Reports, including those just cited, are available online at http://www.mwra.state.ma.us/harbor/enquad/trlist.html.) A brief summary follows here.

System hydrodynamics are characterized by a persistent general circulation pattern driving the flow of offshore Gulf of Maine waters into Massachusetts Bay via the Western Maine Coastal Current off Cape Ann, then southward before returning offshore just to the north of Cape Cod, with a portion of the flow first passing through Cape Cod Bay to the south. Rough estimates of the water residence time are about a month based on the surface currents, somewhat longer at mid-depth or deeper where currents are weaker, and also longer in Cape Cod Bay than in Massachusetts Bay. While this slow general circulation is important in determining long-term average transport pathways, superposed on it are stronger and more variable wind-driven currents, and oscillatory tidal motions. Temperatures follow the characteristic temperate seasonal pattern of minima in late winter and peaks in late summer. Salinities are freshest inshore and in the upper several meters, and

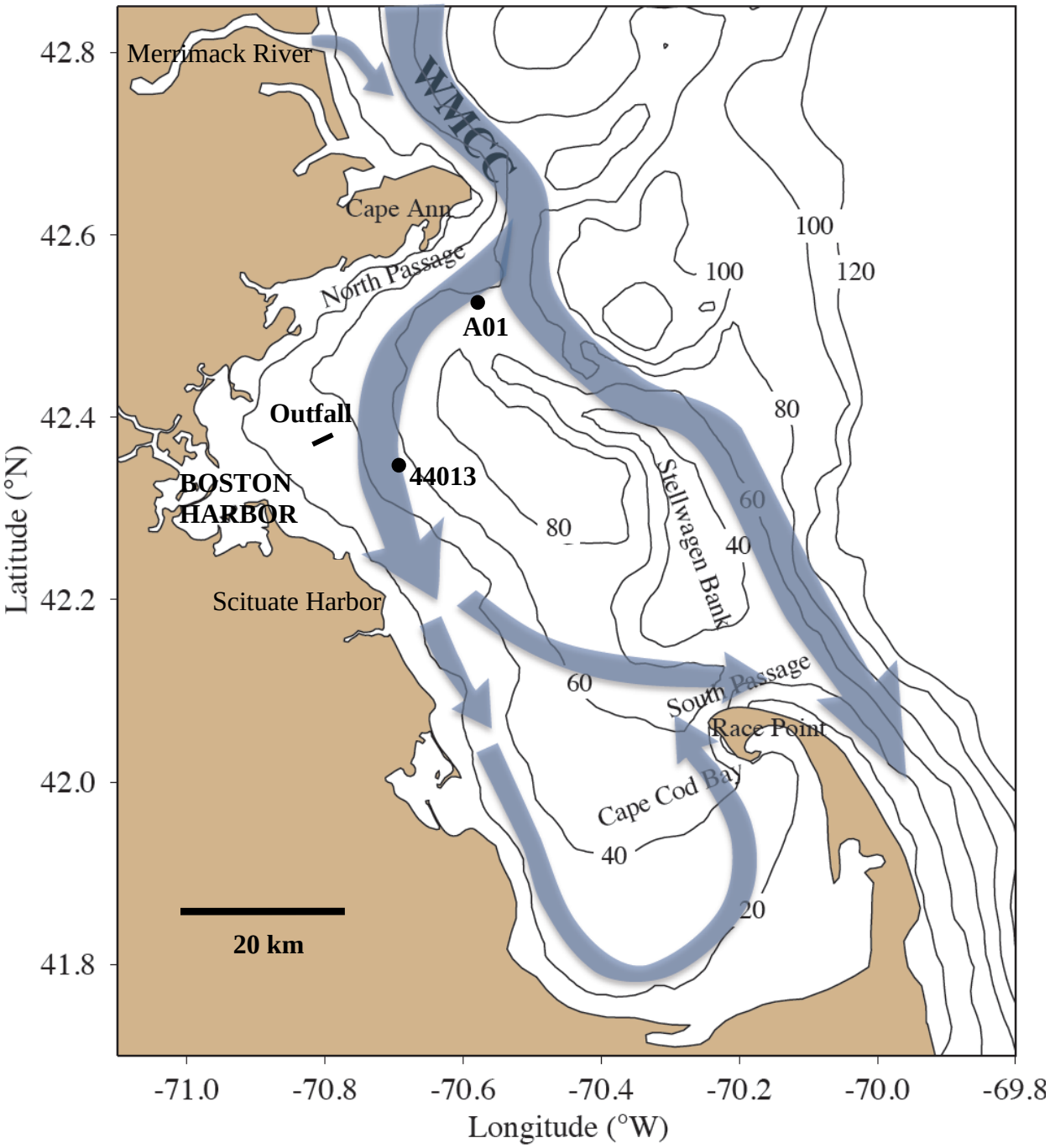

Figure 1-1. Geography, bathymetry, schematic long-term mean circulation.

WMCC = Western Maine Coastal Current.
A01 = Oceanographic mooring (NERACOOS).
44013 = Weather buoy (NDBC).
Contours = water depth in meters.
Figure adapted from Xue et al. (2014).

vary mainly in response to riverine inputs—including those delivered by the Western Maine Coastal Current and the Merrimack River outflow to the north, and via Boston Harbor—in addition to being influenced by regional changes offshore. There is a seasonal cycle in vertical structure that includes transitions between well-mixed conditions, present from fall through early spring due to higher winds and atmospheric cooling, and strong density stratification during the late spring and summer due mainly to preferential heating of surface water by the atmosphere.

The biology of the system is plankton-based and exhibits clear seasonal cycles that are tied closely to those hydrodynamic features, but with more pronounced spatial and interannual variability. Phytoplankton abundance typically peaks most strongly during bloom-favorable conditions in the late winter and early spring, as temperatures rise, light increases, and nutrients remain plentiful near the surface due to the active vertical mixing. Following the transition from spring to summer, near-surface nutrient concentrations become depleted, as density stratification impedes the vertical mixing that replenishes them. Zooplankton abundance and biomass generally peak in late summer, following the spring increase in phytoplankton prey levels. Primary productivity is commonly sustained at modest levels through summer and typically there is a second increase in phytoplankton during fall, when vertical mixing increases again and delivers nutrients to the surface while temperature and light conditions are still favorable before winter. Dissolved oxygen concentrations are influenced by a combination of biological and physical processes; the net result is a seasonal peak in late spring, due to phytoplankton production increasing winter levels already high due to strong reaeration, then steady decreases to a late summer minimum due to respiration and reduced reaeration. Oxygen is depleted more strongly at depth, where stratification limits reaeration.

1.3 *Summary of observed 2014 conditions*

To provide context for descriptions of model simulations of 2014 throughout this report, a brief summary is given here of the most relevant observed conditions based on MWRA monitoring results (Libby et al., 2015). Nutrient levels were lower than typical during the earliest MWRA vessel-based survey, in February. Together with evidence from satellite images and moorings this suggested the possibility that phytoplankton productivity, which leads to reduced nutrients, was higher than typical through the winter months. There are some indications that winter nutrient concentrations have been lower than typical in other recent years, but in the context of the 23 years

of monitoring it is unusual. The year 2014 had rainfall similar to a typical year, but was noteworthy for early spring temperatures that were lower than average, particularly in March and April. The spring increase in phytoplankton abundance was modest and, consistent with the colder temperatures, later than typical. Annual-mean abundance of phytoplankton and particulate organic carbon levels were at or near the lowest measured by 23 years of MWRA vessel-based surveys, although satellite and mooring observations suggest modest blooms occurred in both spring and fall that may not have been captured well by the 2014 surveys. During summer, winds that drive upwelling were the strongest in 23 years, and could have been responsible for observed increases to summer phytoplankton levels measured in the harbor and inshore areas. Zooplankton abundance reached its peak in late summer as is typical, and annual-mean levels were near or at the highest measured in past years. From late spring through the summer, deep dissolved oxygen levels were lower than typical but within the range of past years' variability. The onset of strong winds caused destratification and oxygen replenishment to occur by late October, earlier than typical.

2. Methods

2.1 *Overview*

The present-day BEM is the result of extensive development begun in the early 1990s. Complete background information is in MWRA technical reports, where the model development and updating process has been documented. MWRA Technical Report 2015-02 (Zhao et al., 2015a) provides a comprehensive listing (their Table 1.1) of MWRA technical reports about the modeling (up to and including simulations of 2011), including for each report a summary of its topic, highlighted aspects of its content, the full citation, and (when viewed electronically) a hyperlink to the downloadable PDF file in the online repository. Section 1.4 of Zhao et al. (2012) reviews some of the key improvements incorporated to modeling methods, with emphasis on recent years. Simulations of years 2008 and later use MB-FVCOM for hydrodynamics and UG-RCA for water quality. The methods used in the 2014 simulations, with the minor exception that the FVCOM hydrodynamics code was updated from version 2.6 to version 3.1, are the same as for simulations of 2013 (Zhao et al., 2015b). A brief summary is as follows.

The model grids consist of three domains. The largest domain is the regional Gulf of Maine FVCOM hydrodynamic model (GOM1-FVCOM; lower panel, Figure 2-1). Nested within the GOM1-FVCOM domain is the higher-resolution grid of the Massachusetts Bay FVCOM (MB-FVCOM) hydrodynamic model (upper panel, Figure 2-1). The MB-FVCOM domain extends offshore to an open boundary along an arc southeastward from north of Portsmouth, New Hampshire that passes about 25 km offshore from Cape Cod. Circulation in MB-FVCOM along this boundary, including tidal variability, is driven ("forced") by circulation of the GOM1-FVCOM simulation. The third and smallest domain is that for the UG-RCA water quality model, which is the same as the MB-FVCOM grid except that it extends less far offshore, having an open boundary along an arc from near Cape Ann to the eastern shore of Cape Cod (upper panel, Figure 2-1). In MB-FVCOM and UG-RCA, horizontal resolution ranges from about 0.29 km near the coast to 0.7-2.5 km at the eastern boundary of UG-RCA and 5-10 km near the MB-FVCOM nested boundary. In the vertical, the model has 30 grid levels. In areas shallower than 60 m deep, the levels are uniformly distributed; in deeper areas, the shallowest and deepest levels are concentrated in constant-thickness boundary layers, between which the remaining levels are uniformly distributed. The hydrodynamic models are forced at the surface by the data-assimilative Weather Research and

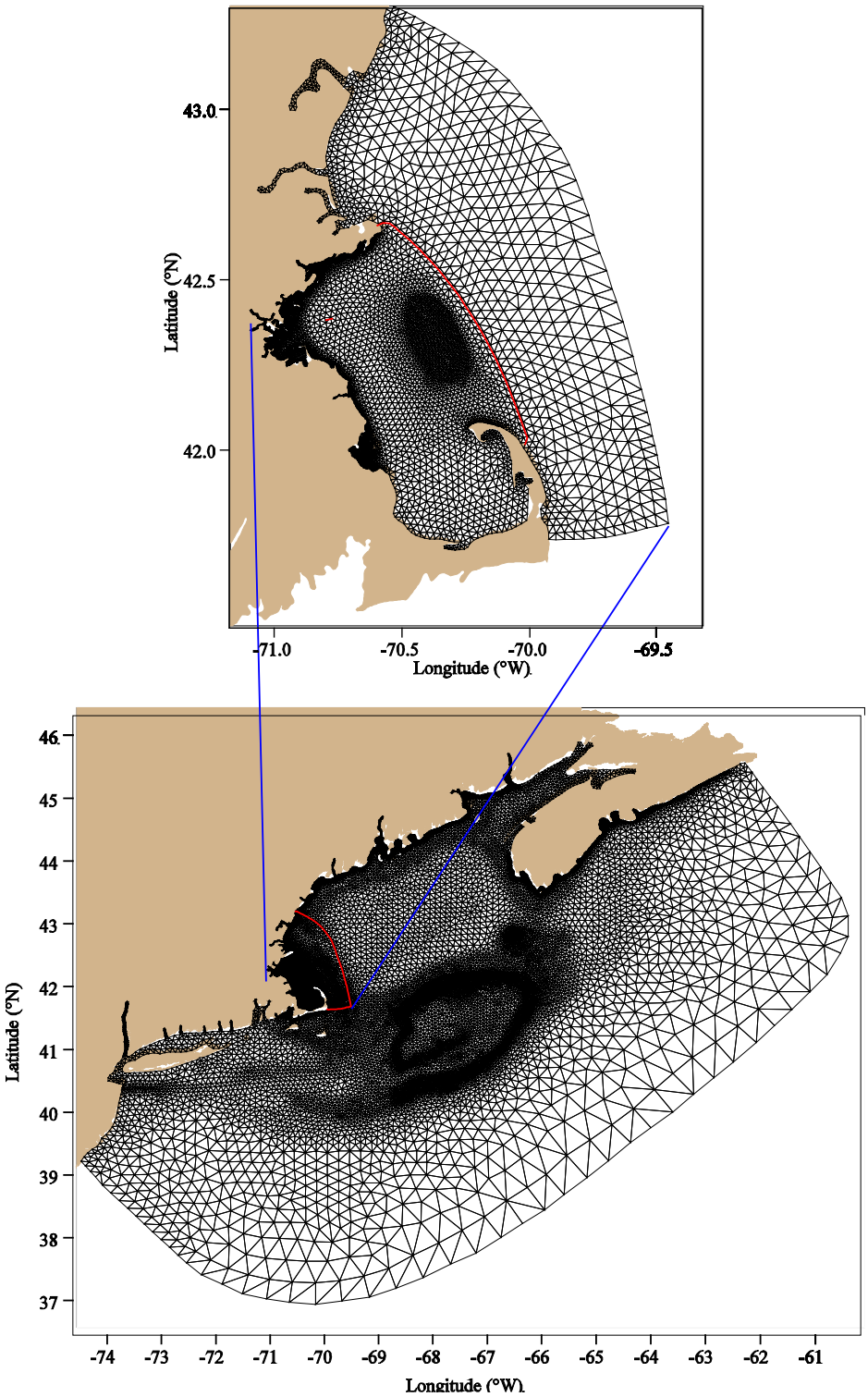

Figure 2-1. Model grids.

Lower panel: Gulf of Maine grid, GOM1-FVCOM; the red line shows the offshore boundary of the nested Massachusetts Bay grid, MB-FVCOM. Upper panel: nested MB-FVCOM domain; red line shows offshore boundary of the smaller domain of the water quality model, UG-RCA.

Forecast (WRF) meteorological model, along the coast by freshwater inputs from rivers, and at the seafloor by the MWRA outfall. In addition to satellite sea surface temperature, the models assimilate all available observed temperature and salinity profiles and moored timeseries collected throughout their geographic coverage areas.

The water quality model UG-RCA is driven using the circulation and eddy diffusivity of the MB-FVCOM hydrodynamic model output. UG-RCA is an unstructured grid version of RCA-v3.0 (Hydroqual, 2004), which simulates 26 water column parameters and 23 sediment variables, a subset of which are shown in a schematic diagram of modeled processes (Figure 2-2). Three phytoplankton functional groups are included: a winter-spring group favoring low temperatures, low light, and high nutrients (representative of diatoms); a summer group that favors higher temperature and light conditions, and tolerates lower nutrients (representative of a mixture of species including dinoflagellates); and a fall group most responsive to moderate temperatures and lower nutrients (representative of a second diatom group). Growth of phytoplankton is based on solar radiation and nutrient availability. Grazing by zooplankton, which are not directly modeled, is treated as a transformation of mass in the phytoplankton groups to particulate and dissolved organic matter at rates that increase linearly with temperature. Nutrients (including nitrate NO_3^-, nitrite NO_2^-, ammonium NH_4^+, phosphate PO_4^{3-}, and dissolved silica SiO_3^{2-}) are formed through mineralization of organic substances in the water column and at the sediment-water interface. Cycling of labile and refractory forms of dissolved and particulate organic carbon, nitrogen, and phosphorous is included. DO is computed by the reaeration flux at the sea surface, sediment oxygen demand at the bottom, and biological and biogeochemical dynamics in the water column including phytoplankton photosynthetic production, consumption by respiration, biogeochemical oxygen demand through the mineralization of particulate and dissolved organic matter, and nitrification. Open boundary condition fields are specified using MWRA monitoring program observations and the method of objective analysis (e.g., Tian et al., 2009). Nutrient and carbon loadings of the MWRA outfall are specified using data from the Deer Island Treatment Plant.

2.2 *Freshwater sources, assimilated observations, and water column irradiance*

Freshwater sources to MB-FVCOM consist of 13 river outlets, one of which combines two rivers, and the MWRA outfall discharge (Figure 2-3). River discharge was obtained from the US Geological Survey (http://waterdata.usgs.gov/ma/nwis). Following Menzie et al. (1991) the Charles

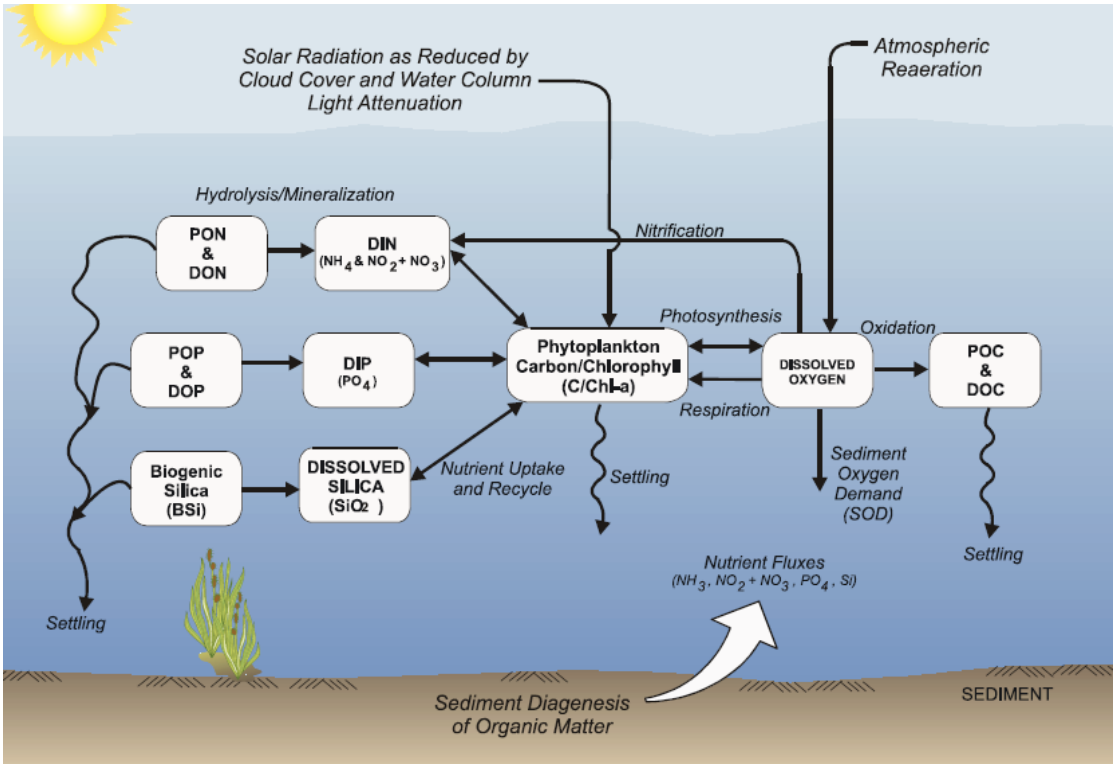

Figure 2-2. Water quality model dynamics, schematic (reproduced from Hydroqual, 2004).

River discharge was scaled up by a factor of 1.13 to account for the watershed area downstream of the gauge; Mystic River discharge, for which there were no observations available, was assumed to be 0.195 times the corrected Charles River discharge. Daily freshwater flow from the outfall was provided by MWRA.

Data assimilated by MB-FVCOM and GOM1-FVCOM included sea surface temperature (SST) and temperature/salinity profiles from vessel-based surveys. The SST used is a daily satellite-derived product from the National Center for Environmental Prediction with with 0.1×0.1 degree resolution (http://polar.ncep.noaa.gov/sst/ophi/). It was assimilated by the nudging method as described in Chen et al (2013), on a daily basis. First the model was run without data assimilation for one day, and used to compute the model daily mean temperature. Next, nudging with a daily temporal window as applied using error defined as the difference between the model daily mean and the satellite SST. In this way the modeled daily means were improved, while variability on shorter timescales than a day was not affected.

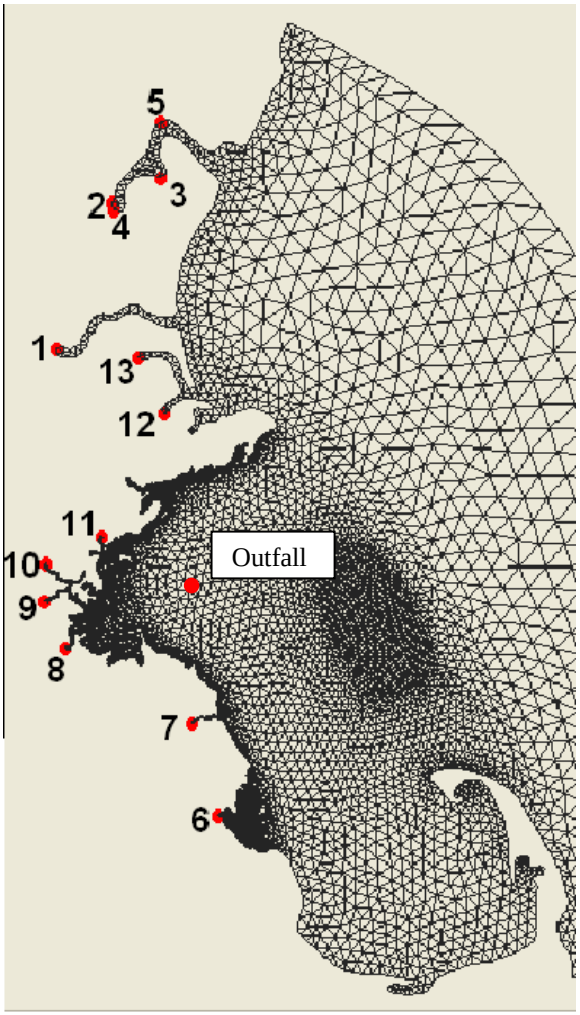

1. Merrimack & Spicket Rivers
2. Exeter River
3. Winnicut River
4. Lamprey River
5. Isinglass River
6. Jones River
7. North River
8. Neponset River
9. Charles River
10. Mystic River
11. Saugus River
12. Ipswich River
13. Parker River

Figure 2-3. Freshwater source locations.

The non-Outfall red dots (sizes are not proportional to river flow) indicate the grid nodes where river water enters the hydrodynamic model.

The assimilated temperature/salinity profile observations (locations shown in Figure 2-4) were obtained from multiple sources including MWRA, the Northeast Fisheries Science Center (http://www.nefsc.noaa.gov/epd/ocean/MainPage/ioos.htm), and the National Ocean Data Center (https://www.nodc.noaa.gov/GTSPP/, Sun and co-authors, 2010). General characteristics of these profile datasets are described in the appendix of Li et al. (2015), including their typical temporal frequency and their depth resolution and water column coverage, which vary from site to site. They are first interpolated to standard depths (0, 5, 10, 15, 20, 25, 30, 35, 40, 50, 60, and 75 m, and at 25m intervals to the seafloor where deeper than 75 m) and then assimilated. The assimilation method is optimal interpolation (described on page 189 of Chen et al. 2013). The horizontal correlation radius for assimilation is 20 km, and each observation is assimilated only by the model grid vertical layer that contains the standard depth of the observation. The temporal window for assimilation is 3 days, so timescales less than 3 days are not captured; however, this is sufficient for the purposes of the water quality model, which is not focused on such higher frequency variability.

Light has a fundamental influence on BEM water quality dynamics because it is a primary factor determining phytoplankton growth. Treatment of light in the water column by BEM has been described in past model reports (Hydroqual 1993; Beardsley et al. 1995; Hydroqual 1995; Hydroqual 2002a,b; Jiang and Zhou 2004) and the UGA-v3 User Manual (Hydroqual, 2004). Because there have been modifications through the years, the method is summarized in some detail here, as follows. Shortwave radiation from the WRF meteorological model is used to compute the planar irradiance I_o of photosynthetically active radiation (PAR) incident on the sea surface. This includes spatiotemporal variations, as described in Section 3.1 below, where a comparison to observations from Deer Island is provided. The surface-incident light is attenuated in the water, such that planar irradiance of PAR I decreases with depth as

$$I(x,y,z,t) = \bar{I}_o(x,y,t)\mathrm{e}^{-[\mathrm{K_{Base}(x,y)+K_{Chl}(x,y,z,t)}]\,z}$$

In this expression, x and y are eastward and northward coordinates; z is depth (positive downward, zero at sea surface); t is time; $\bar{I}_o$ is the planar PAR irradiance incident on the sea surface averaged over the prior three days; K_{Base} is the baseline or non-algal extinction coefficient; and K_{Chl} is the extinction coefficient due to phytoplankton self-shading. The functional form of K_{Base} is

$$K_{Base}(x,y) = \begin{cases} 0.3\ m^{-1} & for\ (x,y)\ in\ Boston\ Harbor \\ 0.16 + 0.42e^{-0.065\,H(x,y)}\ m^{-1} & for\ (x,y)\ in\ bays\ north\ of\ Scituate\ Harbor \\ 0.16 + 0.06e^{-0.045\,H(x,y)}\ m^{-1} & for\ (x,y)\ in\ bays\ south\ of\ Scituate\ Harbor \end{cases}$$

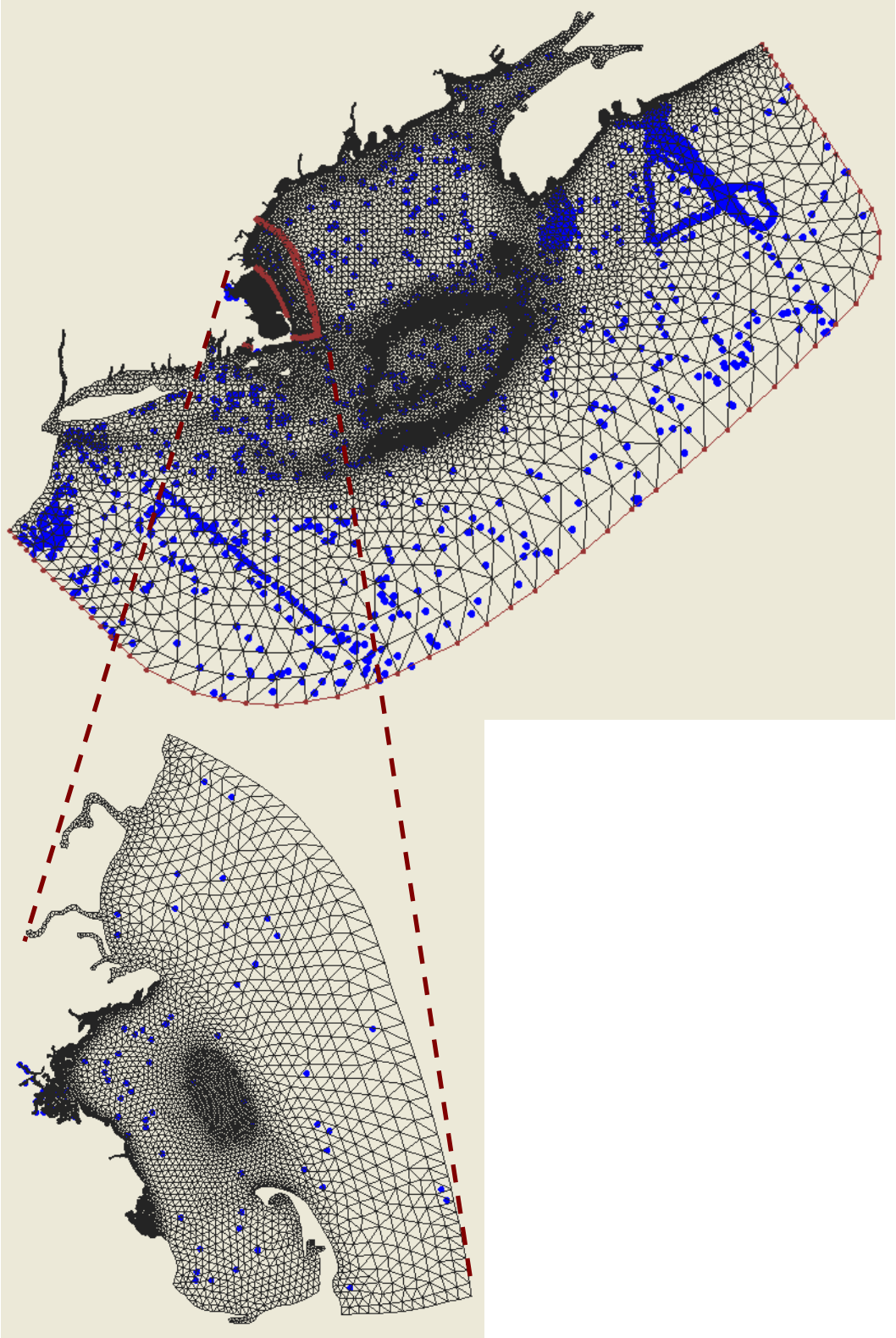

Figure 2-4. Locations of assimilated temperature/salinity profile observations.

where H(x,y) is the bathymetric depth in meters, and the location of Scituate Harbor is shown in Figure 1-1. The expression for K_{Chl} is

$$K_{Chl}(x, y, z, t) = k_c \times [Chl(x, y, z, t)]$$

where k_c = 0.017 m^2 $(mg\ chl)^{-1}$ is the constant phytoplankton self-shading coefficient and [*Chl(x,y,z,t)*] is the chlorophyll concentration as a function of space and time in the model.

Comparisons of model and observed light fields to each other are presented in Section 5.1 below using extinction coefficients. The observed extinction coefficient has been calculated by least-squares fits of exponentials to vertical profiles of scalar PAR irradiance measured by a spherical 4-pi upwelling/downwelling sensor. The model extinction coefficient used in the comparisons is the vertical mean of $K_{Base}(x,y) + K_{Chl}(x,y,z,t)$, a quantity that is based on the downwelling planar PAR irradiance, equivalent to what would be measured by a flat-disc cosine sensor. These observed and modeled extinction coefficients are compared directly to each other under the generally applicable assumptions that upwelling irradiance contributes minimally to the 4-pi measurements, that differences in the attenuation of planar and scalar PAR irradiance are of minor importance, and that depth dependence of the extinction coefficient is modest such that the depth-mean value is representative of conditions at all depths.

3. Forcing conditions

3.1 *Wind, heat flux, light, and rivers*

The main characteristics of 2014 wind forcing are revealed by comparisons to the long-term mean and standard deviation of previous years from 1995 to 2013 (Figure 3-1). The seasonal pattern of vector-averaged velocities (top frame) was generally similar to the long-term mean, but with higher magnitudes during the summer months. The wind speeds (second frame) also followed the seasonal pattern of the long-term mean but with weaker magnitudes than average in summer. The higher than typical summer vector-average velocities are thus indicative that summer winds in 2014, while of weak magnitude, were unusually persistent in direction. The wind stress magnitude (third frame) was above average in July, and the north-south wind stress (bottom frame), a diagnostic for summer upwelling, was at least one standard deviation higher than the long-term mean during most of the summer.

The main attributes of the 2014 air-sea heat flux are seen on comparing it similarly to the long-term mean and standard deviation (Figure 3-2). The seasonal pattern in 2014 (top frame) had negative heat flux (loss of heat or cooling) during winter and positive heat flux (heating) during summer, as does the long-term mean. The cumulative flux (middle frame) results emphasize that 2014 had a notably higher than average heat flux during January-February and November-December; in addition, the 2014 heat flux was as high as or higher than the long-term mean throughout most of the remainder of the year. The anomaly of 2014 relative to the long-term mean (bottom frame) was therefore substantially positive throughout the year and led to a substantially higher cumulative anomaly than the long-term mean.

The surface irradiance forcing applied to the BEM water quality model, from the data-assimilative WRF model, for 2014 has been compared to observations from Deer Island (Figure 3-3). The observations were collected by a flat-disc (cosine) sensor directly measuring downwelling planar irradiance of PAR in μEinsteins m^{-2} s^{-1} each 15 minutes, on a building rooftop at the MWRA Deer Island facility, and used to compute daily means. To facilitate the comparison, the daily-mean WRF total downwelling shortwave irradiance (in W m^{-2}) was multiplied by 0.437 (see Fig. 2-2 of Chen et al, 2010) to arrive at the corresponding daily-mean downwelling PAR in W m^{-2}, then divided by 0.2174 (see p8 of Chen et al, 2010) to yield the estimated daily-mean downwelling PAR in μEinsteins m^{-2} s^{-1}. Although for some of the shorter-timescale variations there

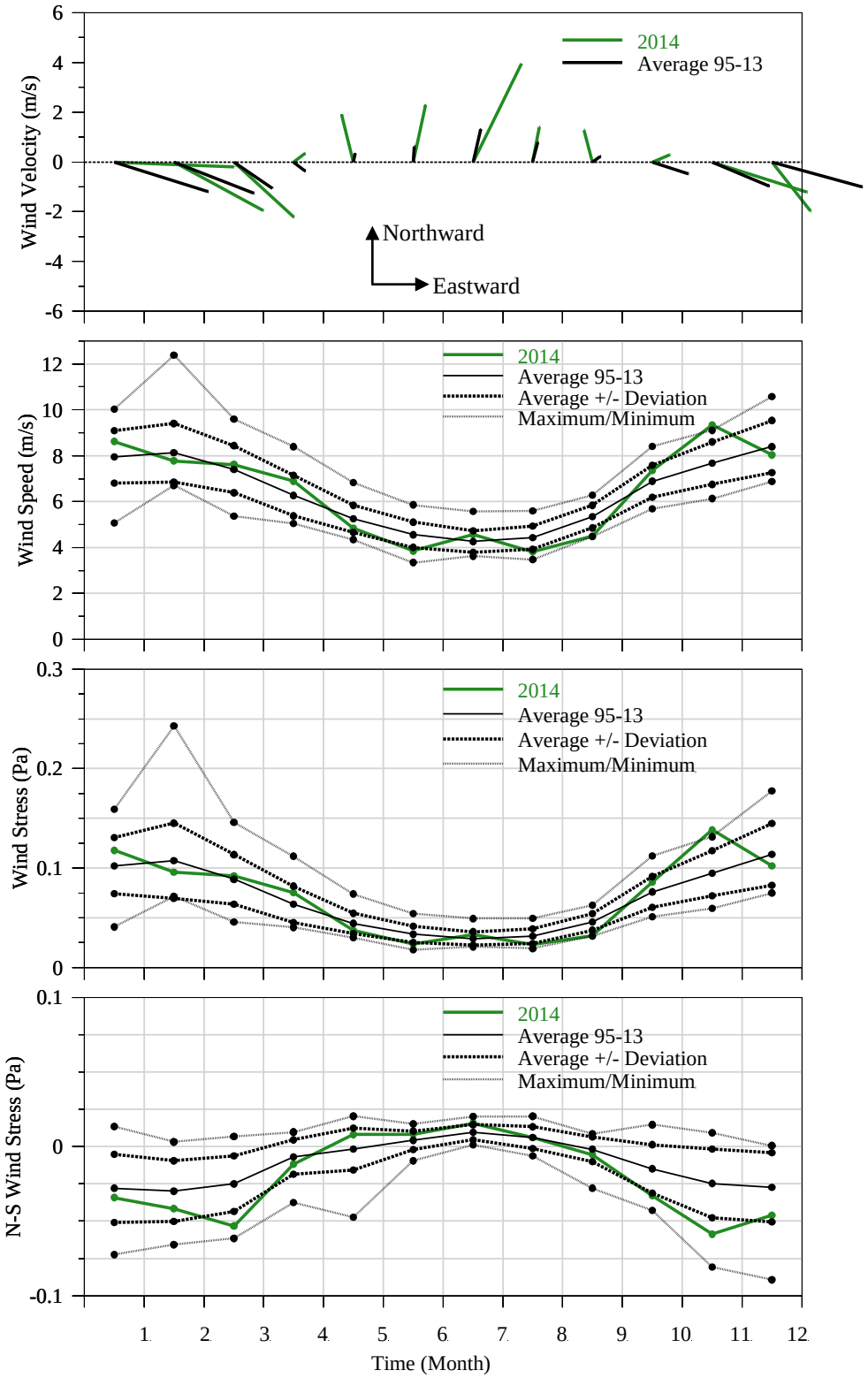

Figure 3-1. Surface wind forcing, monthly averages.

Top frame: Vector-averaged wind velocities. Second frame: Wind speed. Third frame: Wind stress magnitude. Bottom frame: North-south component of wind stress, an indicator for wind-driven upwelling.

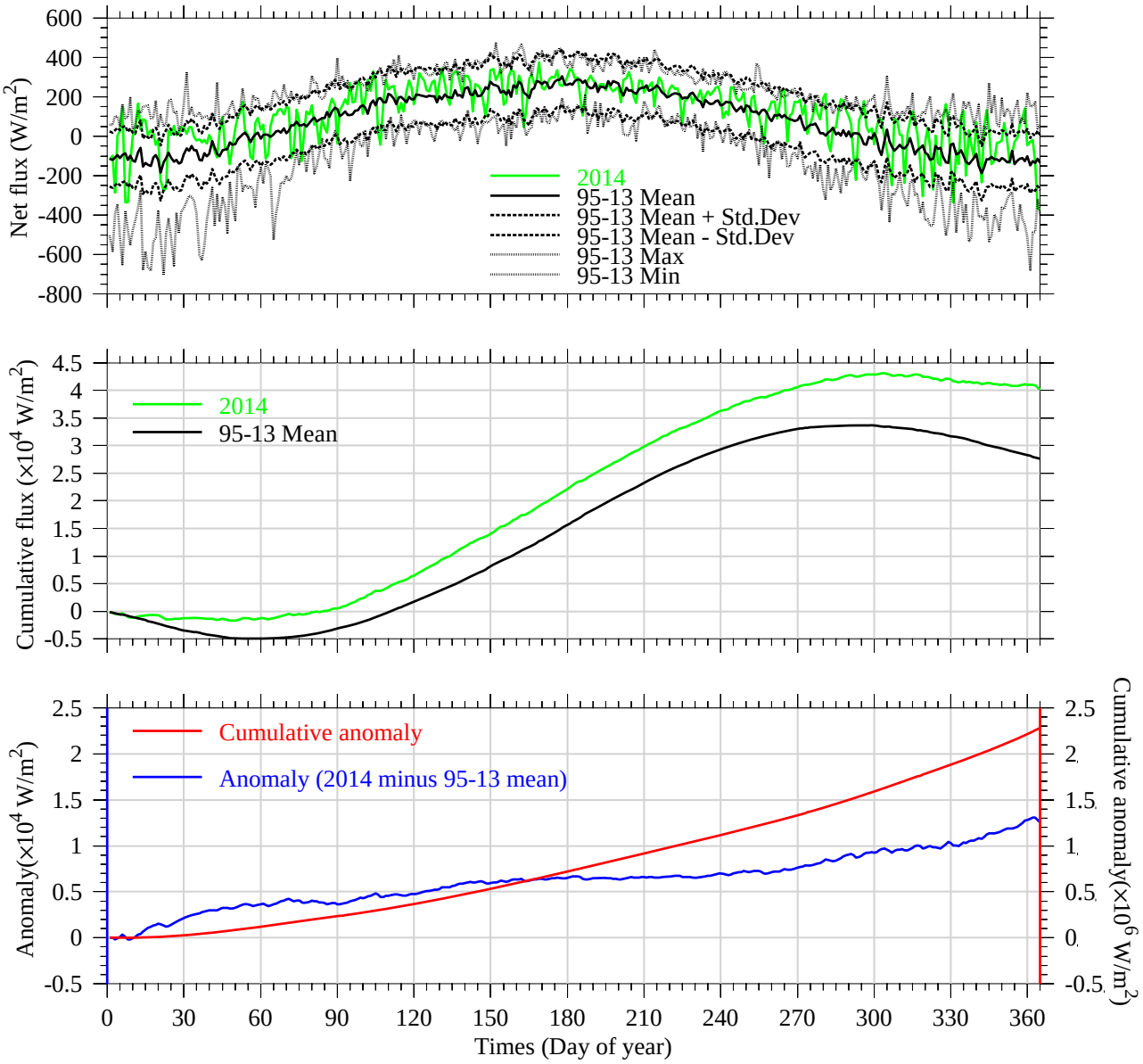

Figure 3-2. Surface heat flux.

Top frame: Net heat flux into ocean. Middle frame: Cumulative net heat flux relative to January 1. Bottom frame: Anomaly of 2014 net heat flux (blue, left vertical axis) relative to 1995-2013 average; cumulative anomaly relative to January 1 (red, right vertical axis).

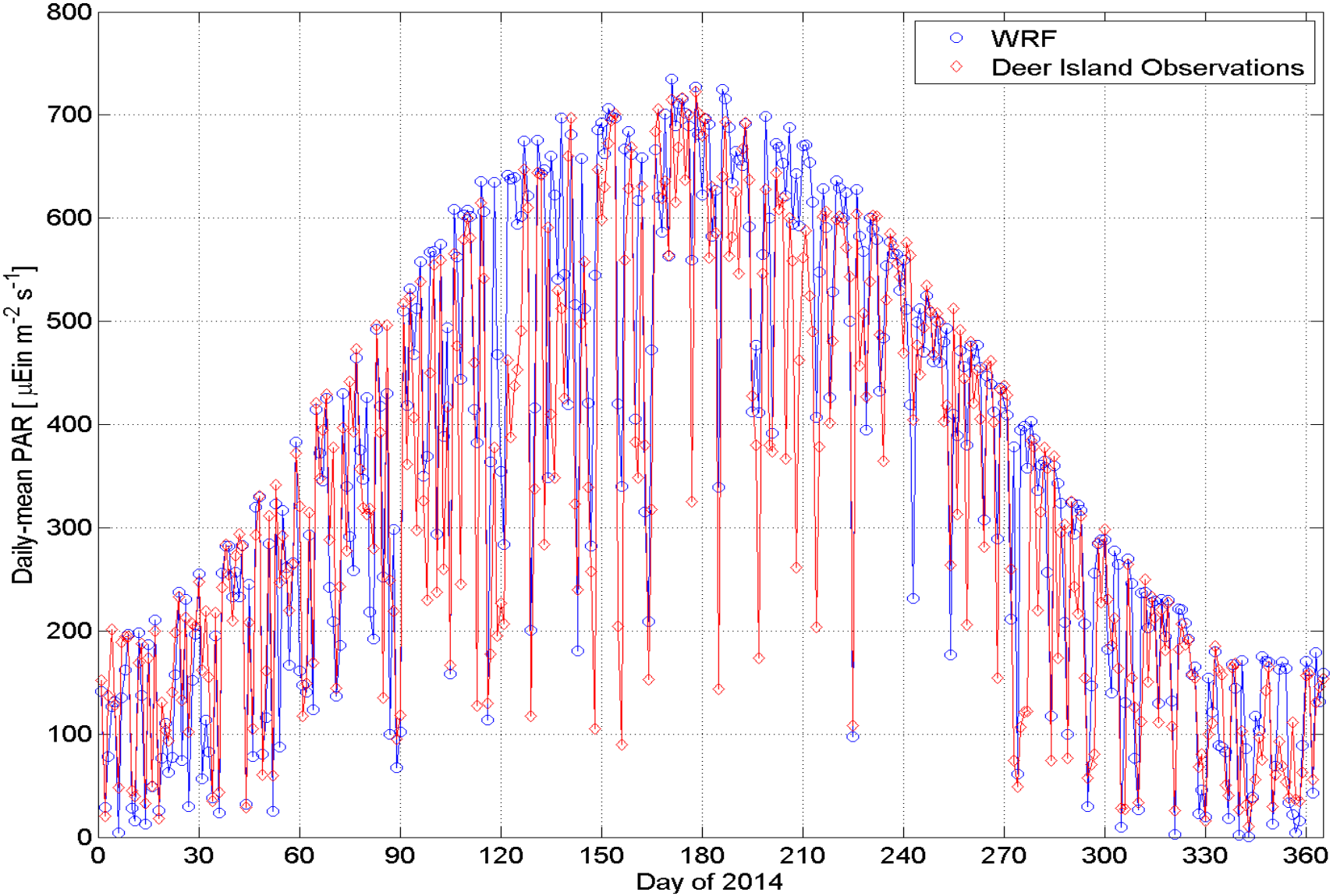

Figure 3-3. Deer Island surface irradiance: WRF model compared to observations.

WRF = Weather Research and Forecast

are notable discrepancies between the WRF and observed values, for others there is good agreement. The differences could be due in part to the fact that the observations are at a single point while the WRF values are for the nearest model grid element, therefore necessarily an average of conditions over an area at least several km across. The comparison demonstrates that the WRF irradiance matches well the seasonal pattern and much of the shorter-timescale variations in the observations, with minimal systematic bias. Irradiance forcing for the water quality model is thus considered sufficiently detailed and accurate to simulate surface conditions for primary producers.

The largest riverine influence on Massachusetts Bay is the Merrimack River, which on entering coastal waters north of the bay joins the Western Maine Coastal Current and flows into the bay off Cape Ann (Figure 1-1). Features of the 2014 Merrimack River volume transport are made clear by comparisons to the long-term mean and standard deviation (Figure 3-4). The 2014 flow (upper frame) followed the long-term mean conditions quite closely, with cumulative values slightly lower than the long-term average for most of the year (middle frame), such that the cumulative anomaly (bottom frame) was negative and modest in amplitude.

3.2 *Loading of organic carbon, nitrogen, and phosphorous*

There are both oceanic and non-oceanic sources of organic materials and nutrients to the bays. The oceanic component stems from exchange with adjacent offshore waters of the Gulf of Maine. These offshore waters are not characterized by particularly high concentrations, but the volume of the exchange is very large. A systemwide budget for total nitrogen in the bays, based on results from BEM simulations of 1992 conditions, concluded that approximately 93% originated offshore in the Gulf of Maine (Hunt et al., 1999; Hydroqual, 2000). Consequently, oceanic input is by far the single largest source of organic materials and nutrients to the bays. While conditions change from year to year and it is recognized there have been long-term changes to loads since 1992, the estimated 93% oceanic fraction remains broadly representative of today's conditions, and is likely crudely applicable to organics and nutrients other than total nitrogen.

The smaller non-oceanic sources include rivers, terrestrial runoff other than rivers (referred to as non-point sources), atmospheric deposition, and sewage outfalls (referred to as point sources). Point sources include both the MWRA outfall and non-MWRA outfalls. To help put the MWRA outfall contribution in context, estimates of the non-oceanic sources have been made and compared (Figure 3-5). In 2014 the non-MWRA outfalls contributed most to organic carbon loading, followed by the MWRA outfall, atmospheric deposition, non-point sources and rivers. The MWRA

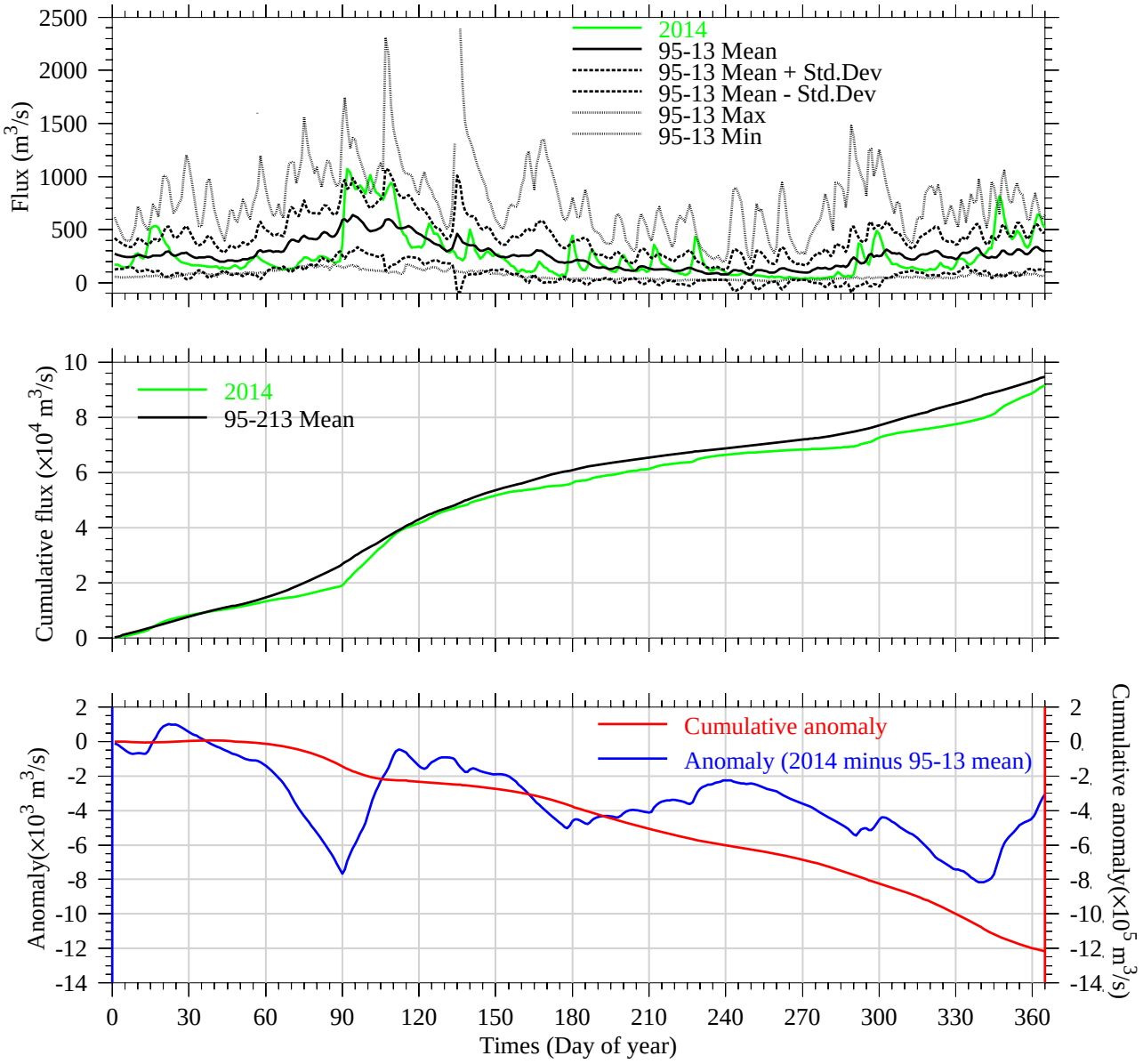

Figure 3-4. Merrimack River daily/cumulative flux, and anomaly relative to long-term mean.

Top frame: Merrimack River volume flux. Middle frame: Cumulative flux relative to January 1. Bottom frame: Anomaly of flux in 2014 relative to 1995-2013 average (blue, left vertical axis); cumnulative anomaly relative to January 1 (red, right vertical axis).

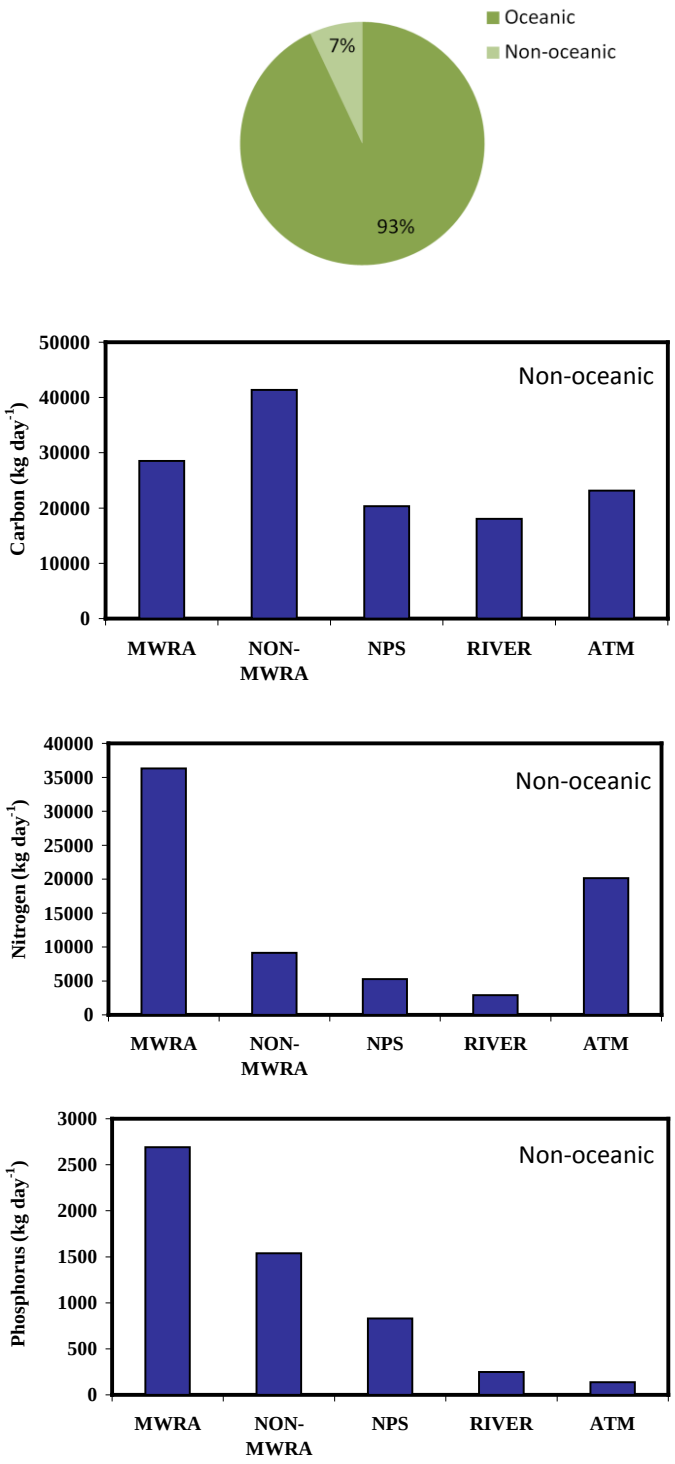

Figure 3-5. Mean daily 2014 non-oceanic loads (carbon, nitrogen, phosphorous).

MWRA = MWRA Outfall; NON-MWRA = Non-MWRA point sources; NPS = Non-point sources; RIVER = River loadings. ATM = Atmospheric deposition.

Top pie chart: Representative estimate of oceanic/non-oceanic sources of total nitrogen (see text).

outfall was the largest input to nitrogen loading, followed by atmospheric deposition, non-MWRA outfalls, non-point sources, and rivers. For phosphorus loading, the MWRA outfall again contributed the largest portion, followed by non-MWRA outfalls, non-point sources, rivers, and atmospheric deposition. Note that for non-MWRA outfalls, use has been made of the only available dataset (Menzie-Cura and Associates, 1991), for which there are recognized limitations to applicability given that treatment levels at some non-MWRA outfalls have changed since that study.

For the MWRA outfall the annual mean volume flow in 2014 (Figure 3-6) was slightly lower than the average over the past 10 years, and higher than in 2012 and 2013 which were both relatively dry years. The 2014 outfall carbon load was also slightly below the average over the past 10 years. The 2014 nitrogen load was slightly higher, by an amount not inconsistent with the typical range of inter-annual variations, than the previous peak value which occurred in 2009. The 2014 phosphorous load was comparable to that of the past 5 years.

3.3 *Open boundary of the UG-RCA water quality model*

The open boundary condition values for UG-RCA at the offshore edge of its grid domain (red line in upper frame of Figure 2-1) are determined using field survey observations from the MWRA monitoring program in Massachusetts and Cape Cod Bays and the objective analysis method (Tian et al., 2009). These observations are collected during 9 surveys annually, at 14 stations in the two bays. Figure 3-7 shows the representative subset of these 14 stations that is used, for clarity of presentation, below in the water quality section of this report; all 14 stations are shown, for example, in Figure 3-1 on page 10 of Werme et al (2015). Open boundary condition results for April 15, June 15, August 15, and October 15 illustrate the seasonal cycle (Figure 3-8 and Figure 3-9; colorscale ranges are the same as in earlier reports for ease of comparison). As explained in Zhao et al. (2012), for dissolved organic carbon and biogenic silica (not shown), which are no longer being sampled, a seasonal cycle constructed by averaging observations from 1992-2010 is used. The field observations on which the objective analysis method is based are collected relatively infrequently, and located at large distances from the open boundary, particularly for the South Passage near Cape Cod. It is therefore recognized that, while the method is appropriate and effective, the results include a high degree of uncertainty.

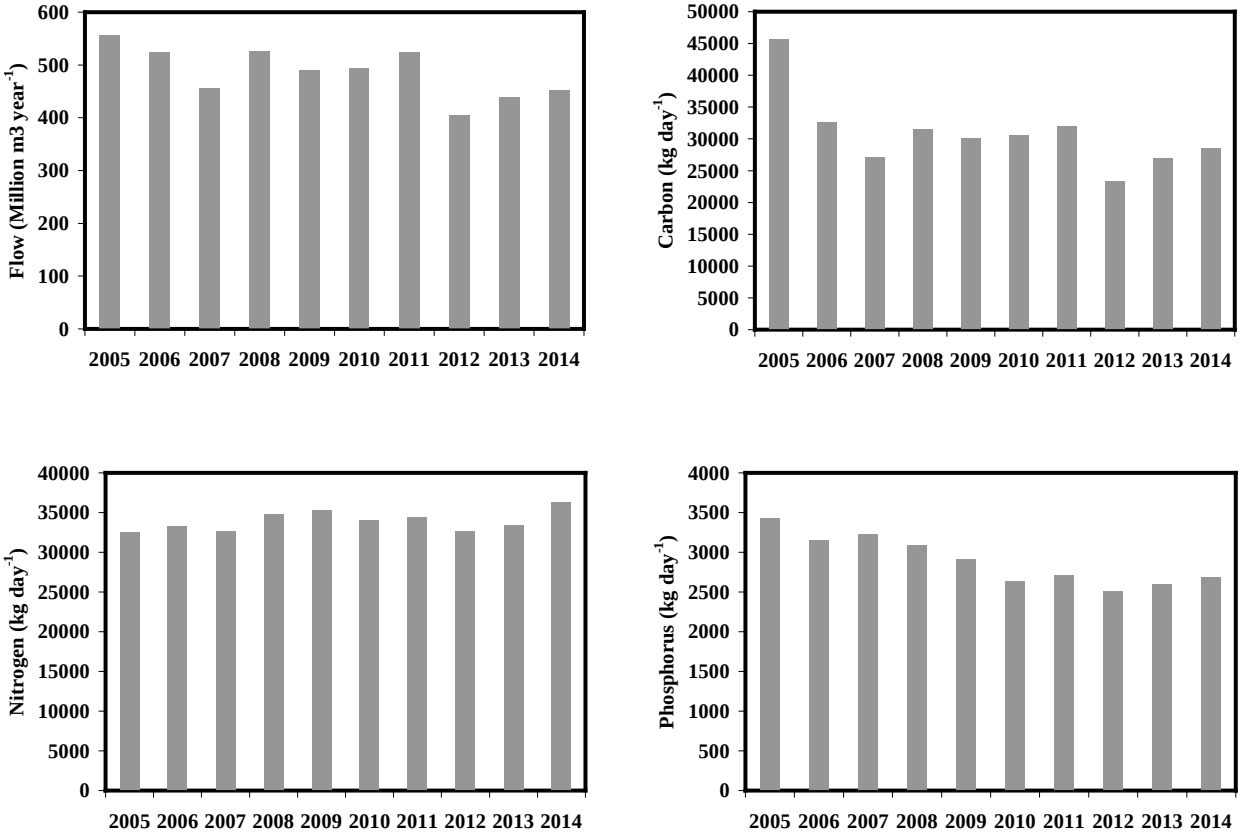

Figure 3-6. MWRA outfall mean annual flow and carbon/nitrogen/phosphorous loads, 2005-14.

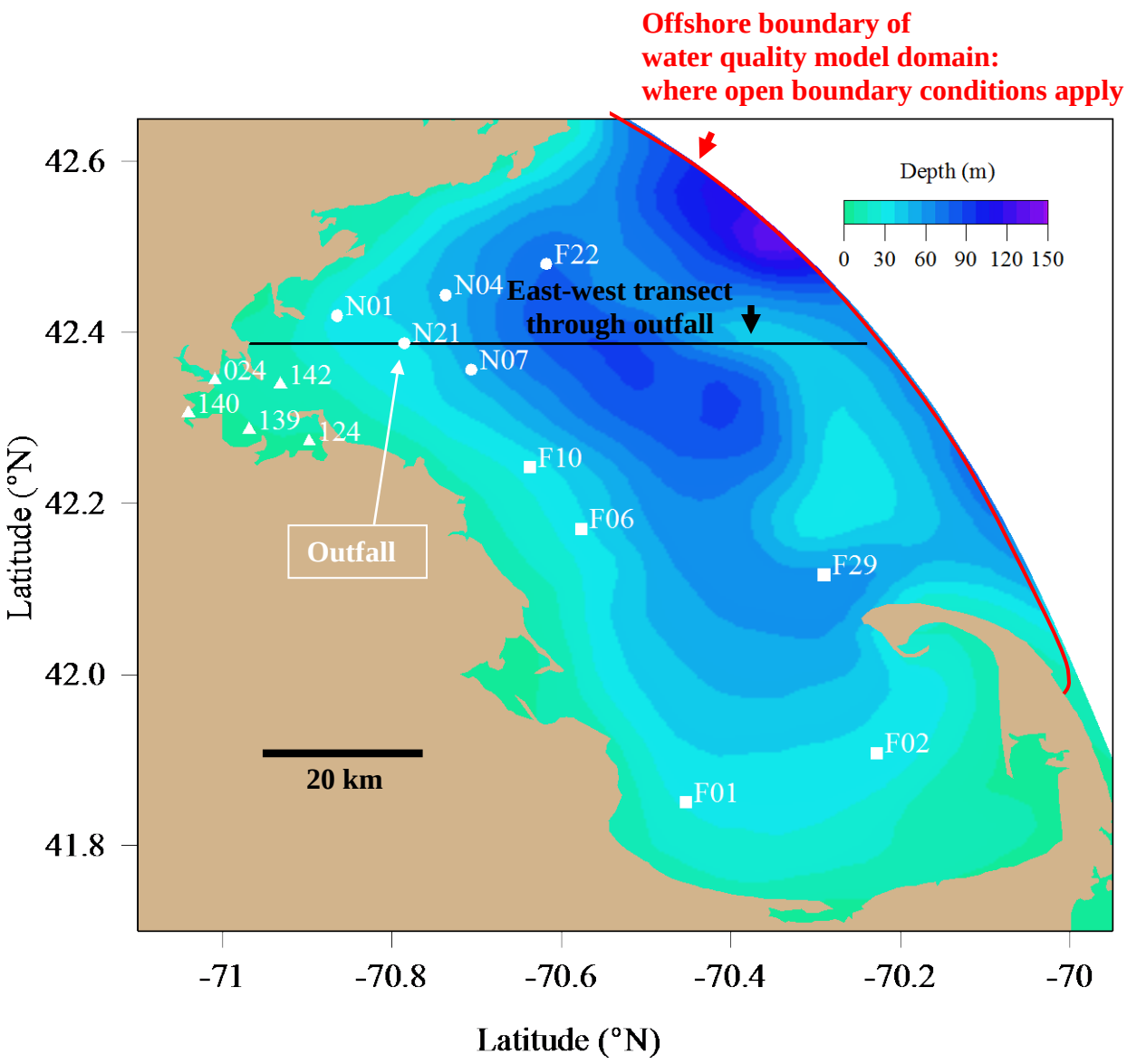

Figure 3-7. Station groups: northern (circles), southern (squares), and harbor (triangles).

For reference in later figures:
Red arc = Offshore boundary, water quality model domain, where open boundary conditions apply.
Black line = East-west transect through outfall.

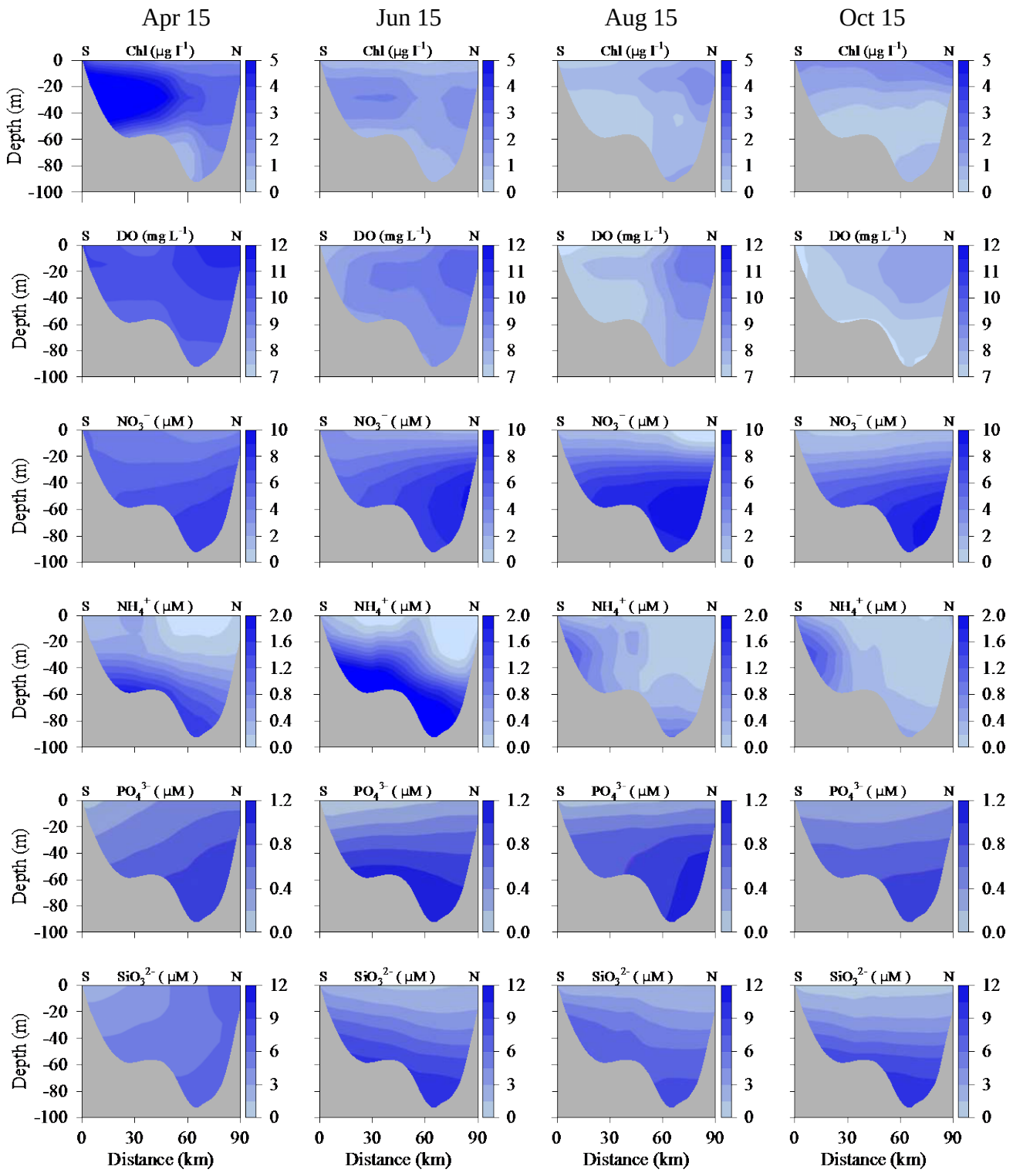

Figure 3-8. Open boundary forcing, water quality model: chlorophyll, oxygen, and nutrients.

Horizontal axis: distance along offshore arc (red in Figure 3-7) of open boundary, from its southernmost point; left endpoint ("S", distance 0 km) is the southernmost end of arc at Cape Cod and right endpoint ("N", distance 90 km) is the northernmost end of arc off Cape Ann.

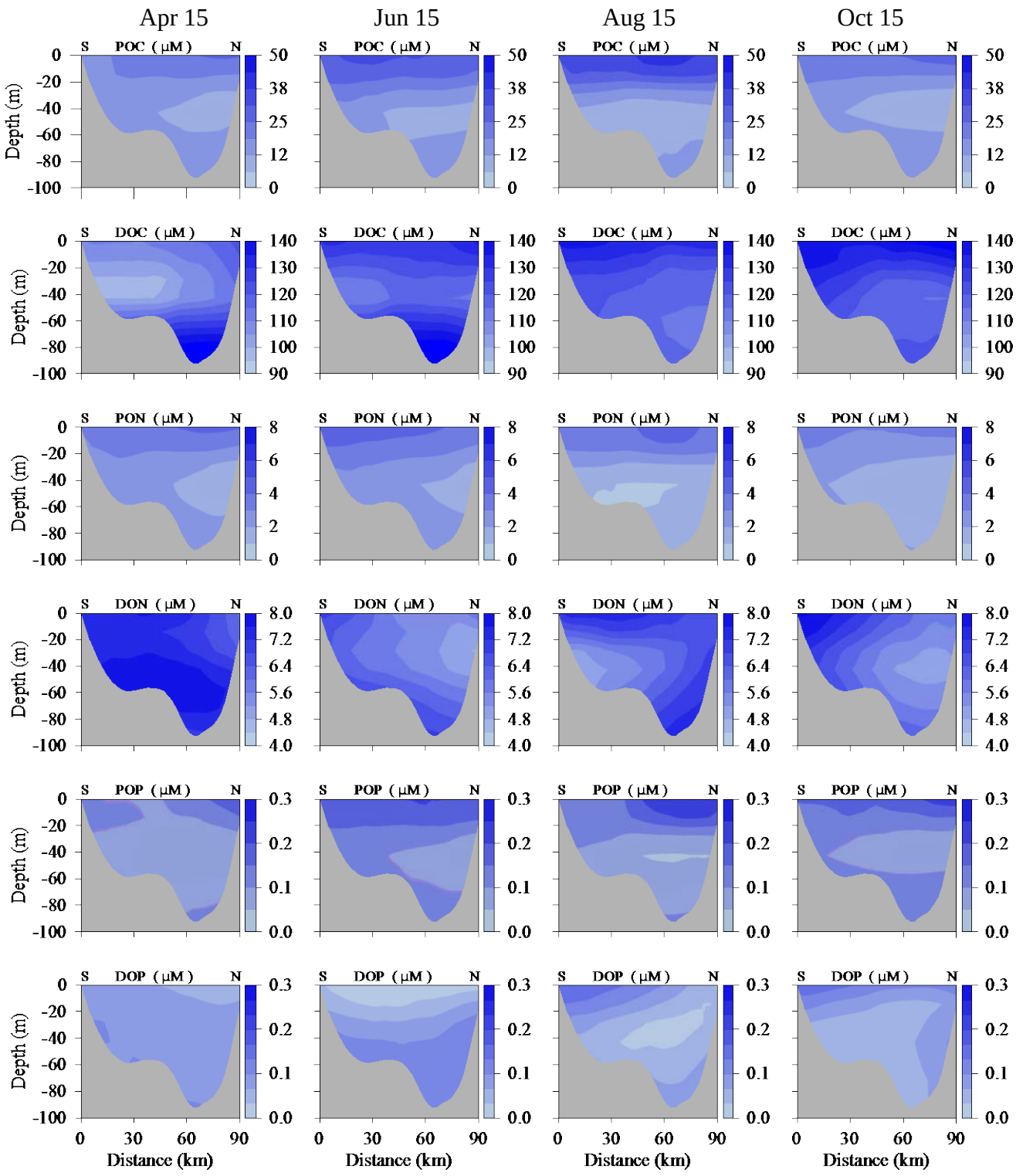

Figure 3-9. Open boundary forcing, water quality model: organics. Presented as in Figure 3-8.

POC = Particulate Organic Carbon, DOC = Dissolved Organic Carbon
PON = Particulate Organic Nitrogen, DON = Dissolved Organic Nitrogen
POP = Particulate Organic Phosphorus, DOP = Dissolved Organic Phosphorus

4. Hydrodynamics

The focus of BEM is water quality, which is strongly influenced by physical processes such as the evolution of temperature and salinity patterns and water circulation. The fidelity of the UG-RCA water quality simulations therefore depends on the capability of the MB-FVCOM hydrodynamic model to capture realistic Massachusetts Bay physical processes. This section describes the hydrodynamic model characteristics and performance.

4.1 *Model-observation comparisons*

Comparisons between the model results and observations from 2014 make clear the level of agreement between them for the time evolution of the geographic and vertical structure of temperature (Figure 4-1) and salinity (Figure 4-2). Salinity is given in units on the Practical Salinity Scale throughout this report. Stations in these figures include locations spanning Massachusetts Bay (N01, F22, N07, F06), in and near Cape Cod Bay (F01, F02, F29), and in Boston Harbor (F23; Figure 5-5 shows the location of F23, near the harbor mouth, 1 km east of station 142 which is shown in Figure 3-7). Vessel-based observations from 9 survey dates in 2014 are shown as individual symbols, from both shallow and deep depths, at each station in Figure 4-1 and Figure 4-2. In addition, in the panels for Station F22, time series observations are shown from Mooring A01, located about 5 km northeast from F22 and operated by University of Maine as part of the Northeast Regional Association of Coastal and Ocean Observing Systems. Stratification developed in April, peaked in August, and was eliminated by the end of October. The model generally captured the seasonal cycle, and most event-timecale characteristics, of observed temperature and salinity. This indicates the effectiveness of data assimilation of both satellite sea surface temperatures and *in situ* hydrographic measurements. The most notable differences between the model and observations were model temperatures not cold enough to match observations in February at some stations (F23, F06, F22), and some near-surface model temperatures not matching two anomalously cold survey results during the summer at stations F06 and F02. At most stations the observed deep salinities were higher than the model and the assimilation tended to increase them as intended.

For more complete spatial information, model-observation comparisons have been made of the monthly-mean geographic structure, during a series of months spanning the seasonal cycle, of near-

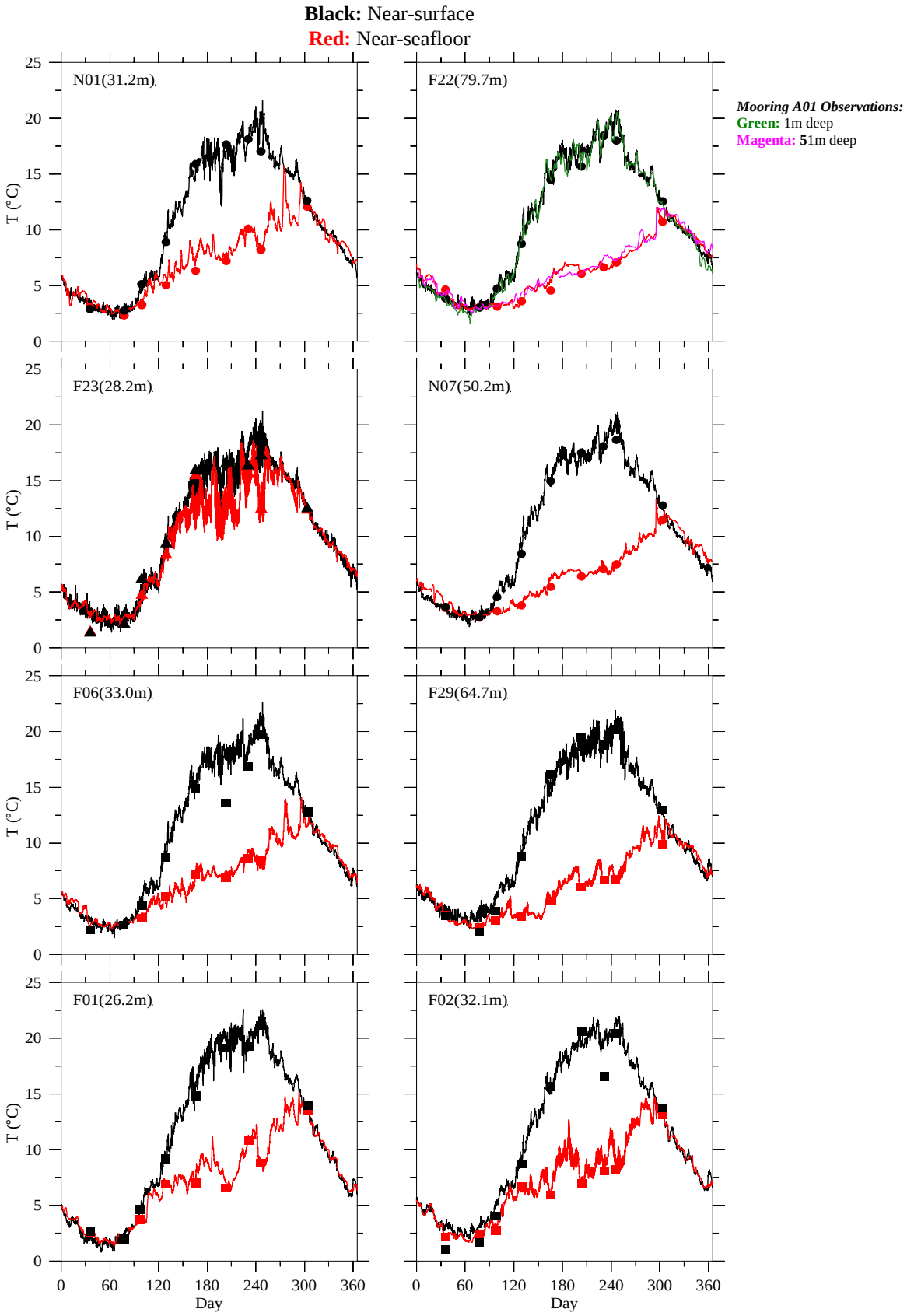

Figure 4-1. Temperature time series, model-observation comparison.

Model results: black/red lines. MWRA vessel-based survey observations: black/red symbols.

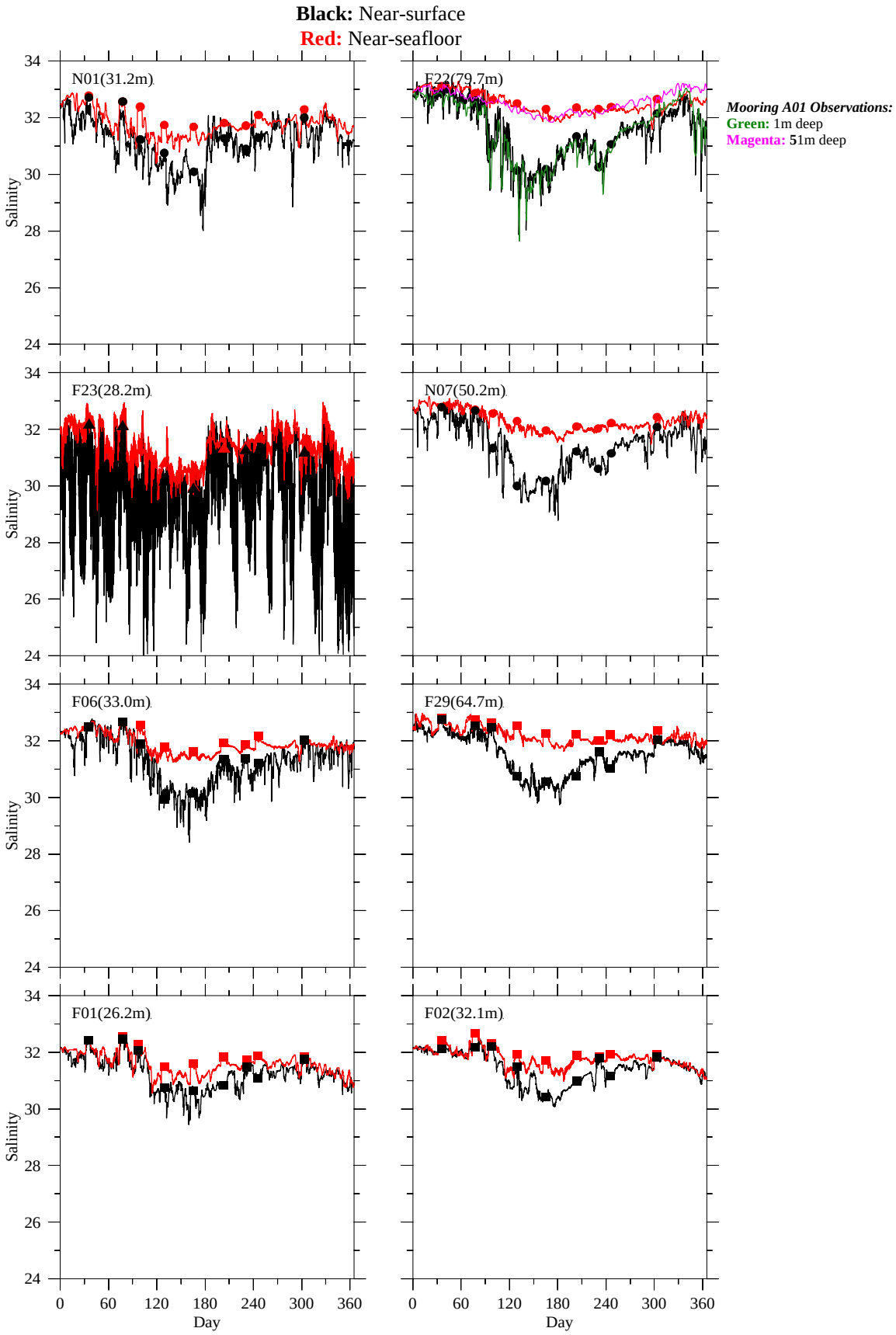

Figure 4-2. Salinity time series, model-observation comparison.

Shown as in Figure 4-1. Salinity units: Practical Salinity Scale.

surface and near-bottom temperature (Figure 4-3a,b) and salinity (Figure 4-4a,b). The observed fields in these figures are computed using measurements from all stations (black dots) sampled during each month-long period. For most months there was a one-day survey in Massachusetts Bay and Cape Cod Bay, and Boston Harbor stations were sampled weekly or biweekly (for more detail on harbor station locations see, e.g., Taylor, 2015). The model fields in these figures are computed using model outputs from the dates and locations corresponding to the associated set of observations.

The seasonal cycle and general spatial structure of the model fields is in reasonably good agreement with the observed fields. The most notable model-observation differences for shallow temperatures (Figure 4-3a) were that model results were typically more spatially uniform than the observations; relative to observations the model results were also colder in June and warmer in October. For deep temperatures (Figure 4-3b) the agreement was better, with the most notable model-observation differences being that the model had more pronounced horizontal gradients than observations in October. The model shallow salinities (Figure 4-4a) have a more gentle offshore gradient than the observations during August, and to a lesser degree also during February and April. The model deep salinities (Figure 4-4b) were not as spatially uniform as observations during August. The model captured the general spatial pattern of onshore freshening throughout the year.

Comparisons between modeled and observed 2014 non-tidal currents are shown in Figure 4-5a,b at the Mooring A01 site in northeastern Massachusetts Bay off Cape Ann, the only location where time series observations are available. (Tidal currents, while important in controlling vertical mixing and dispersal of materials, are not examined in this report. Tidal currents in these simulations are very similar to tidal currents in other similarly-configured FVCOM simulations spanning the Gulf of Maine, and have been shown (e.g. see Appendix of Chen et al., 2011) to be in very good agreement with observed tidal currents.) The model-observations comparisons of non-tidal currents include time variations and vertical structure, with wind forcing included for context. In order to isolate the non-tidal variability of interest, consisting mainly of weather-related and seasonal changes, the tidal variability has been removed using a low-pass filter (38-hr half-power period, PL66TN; e.g., Limeburner 1985) and the results subsampled to 6 hour resolution. Observations at 2 m deep were not available from Jan – May.

As expected, the main features of the winds (from the WRF model) are weather-band changes on timescales of about 3-10 days. These features include: wind directions spanning the full range;

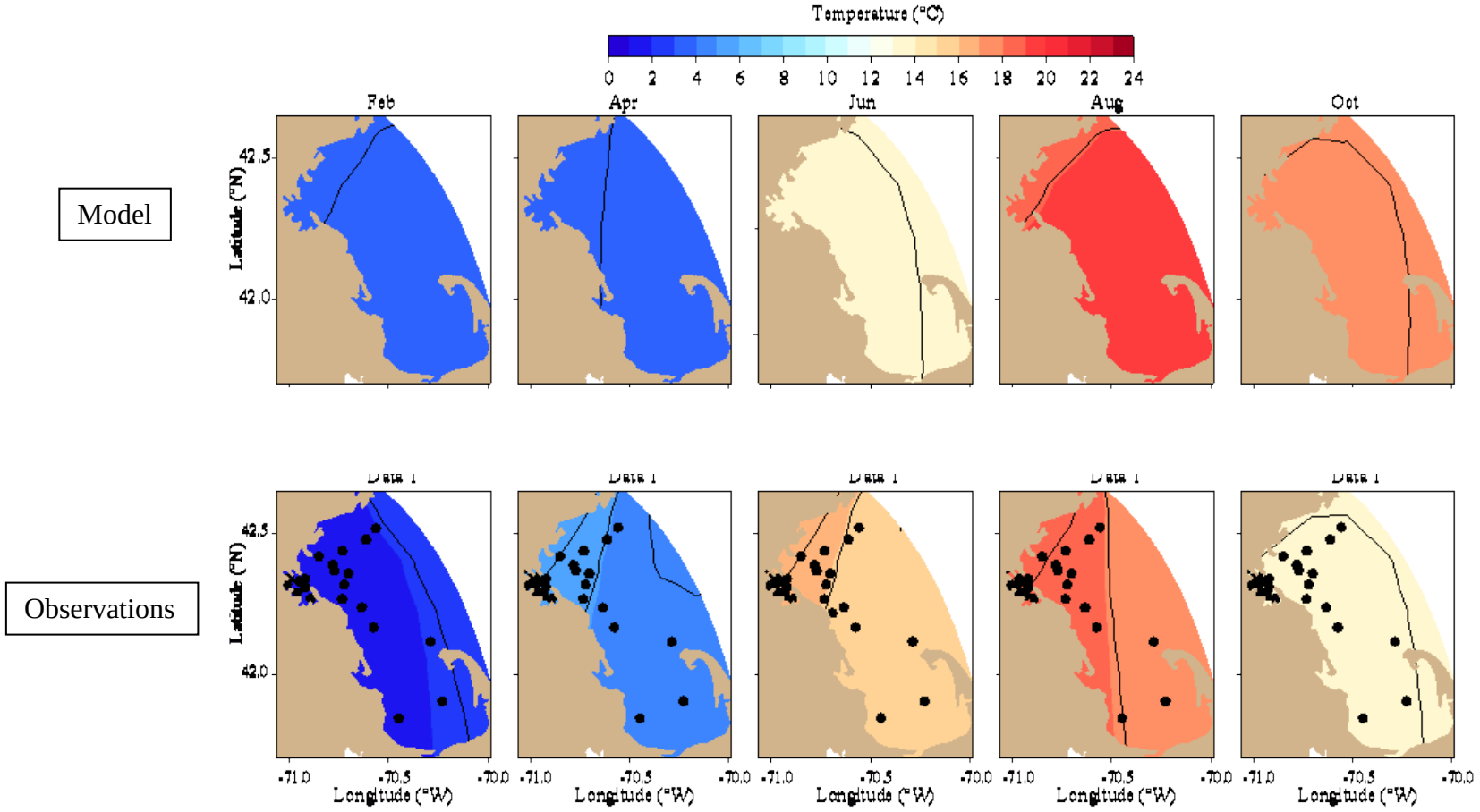

Figure 4-3a. Temperature spatial structure, at/near sea surface, model-observation comparison.

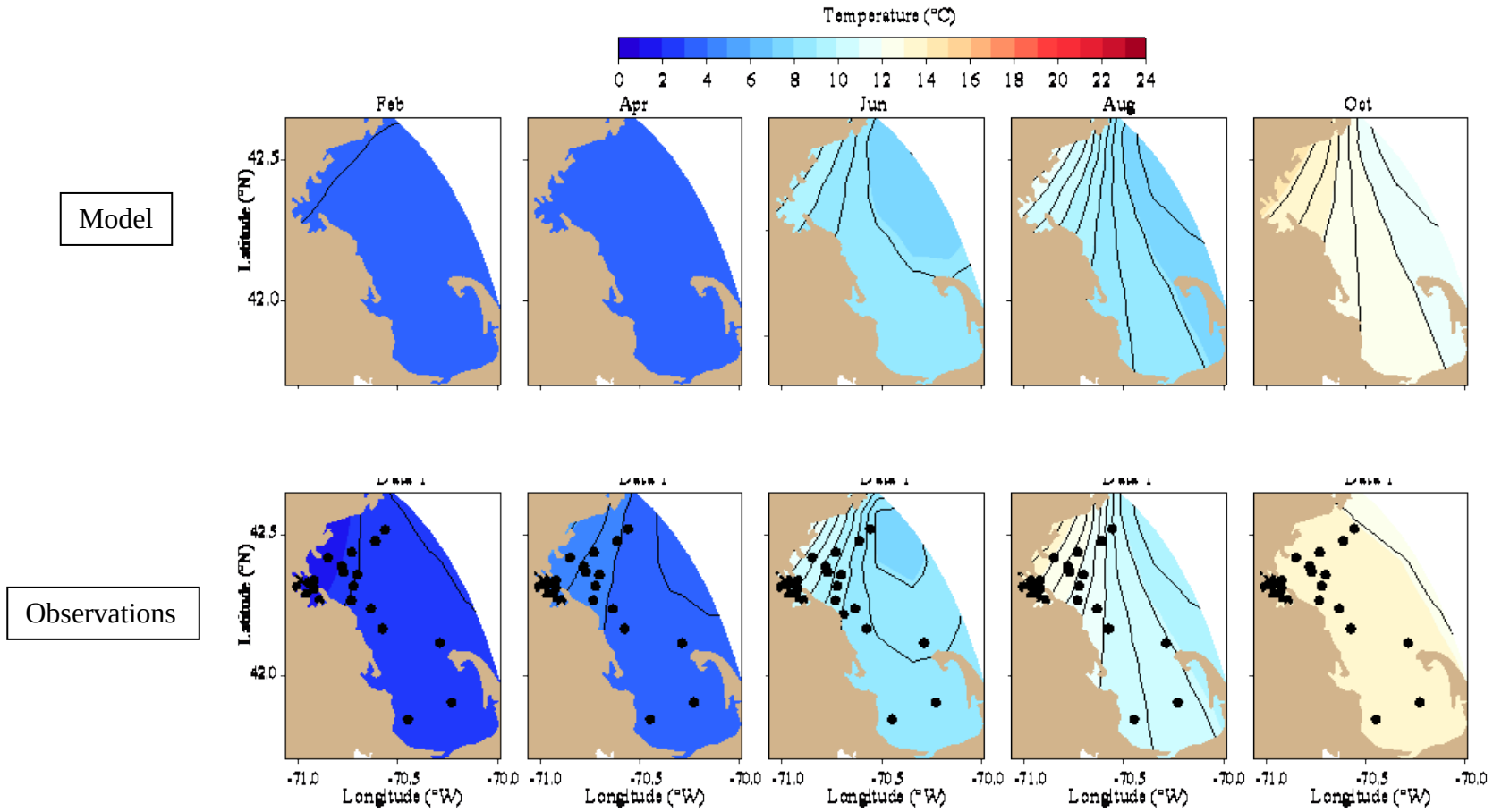

Figure 4-3b. Temperature spatial structure, at/near seafloor, model-observation comparison.

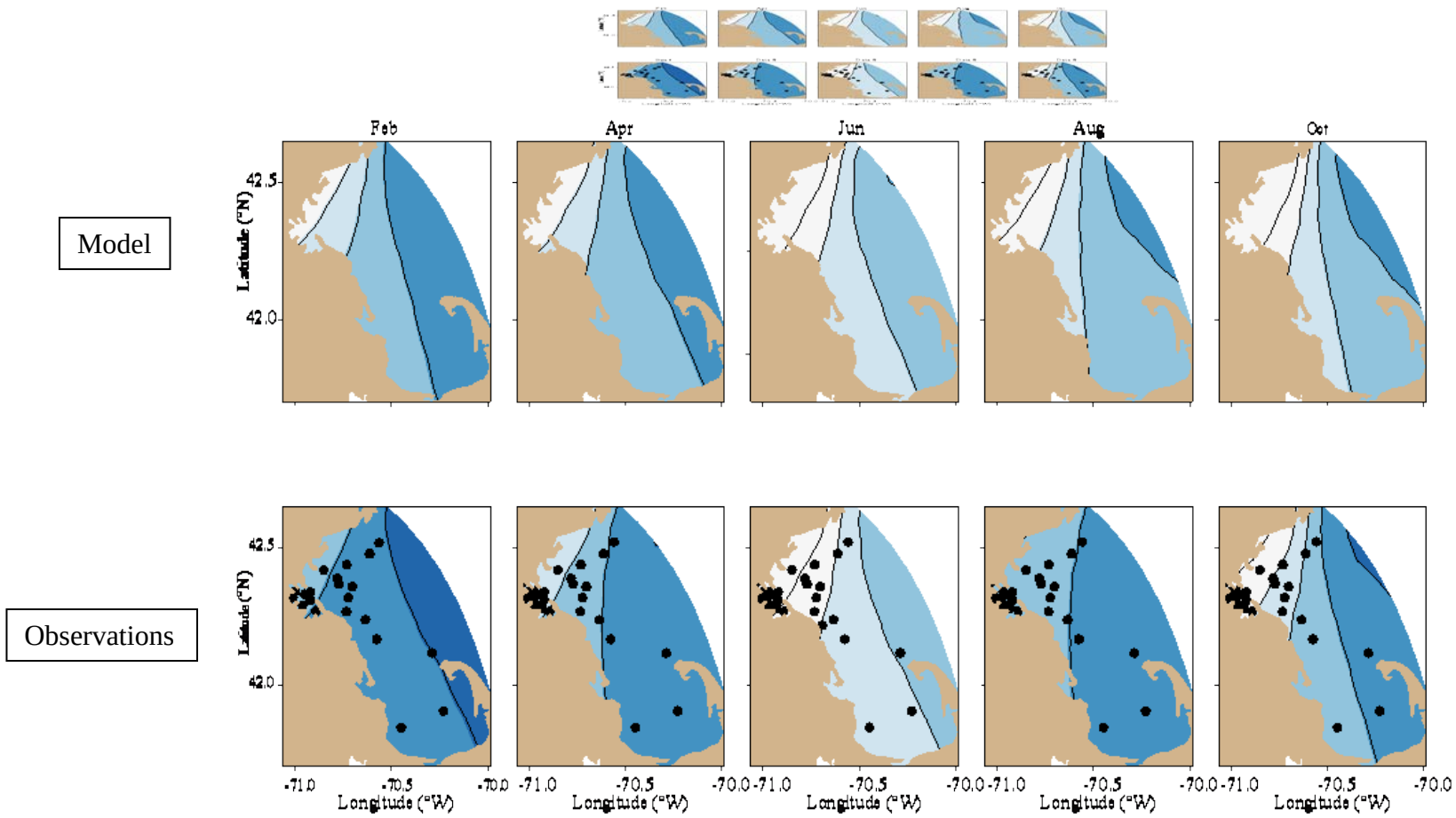

Figure 4-4a. Salinity spatial structure, at/near sea surface, model-observation comparison.

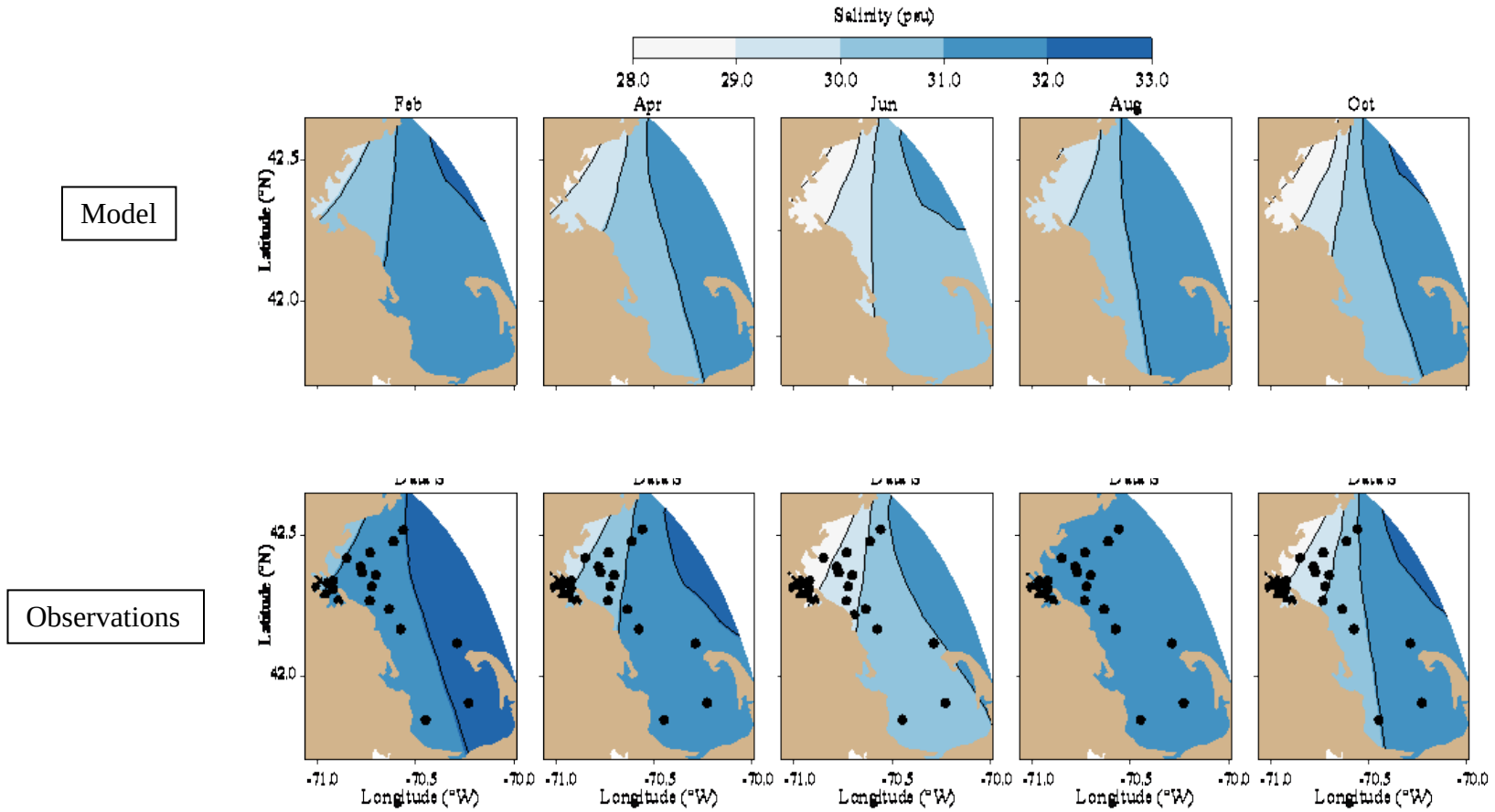

Figure 4-4b. Salinity spatial structure, at/near seafloor, model-observation comparison.

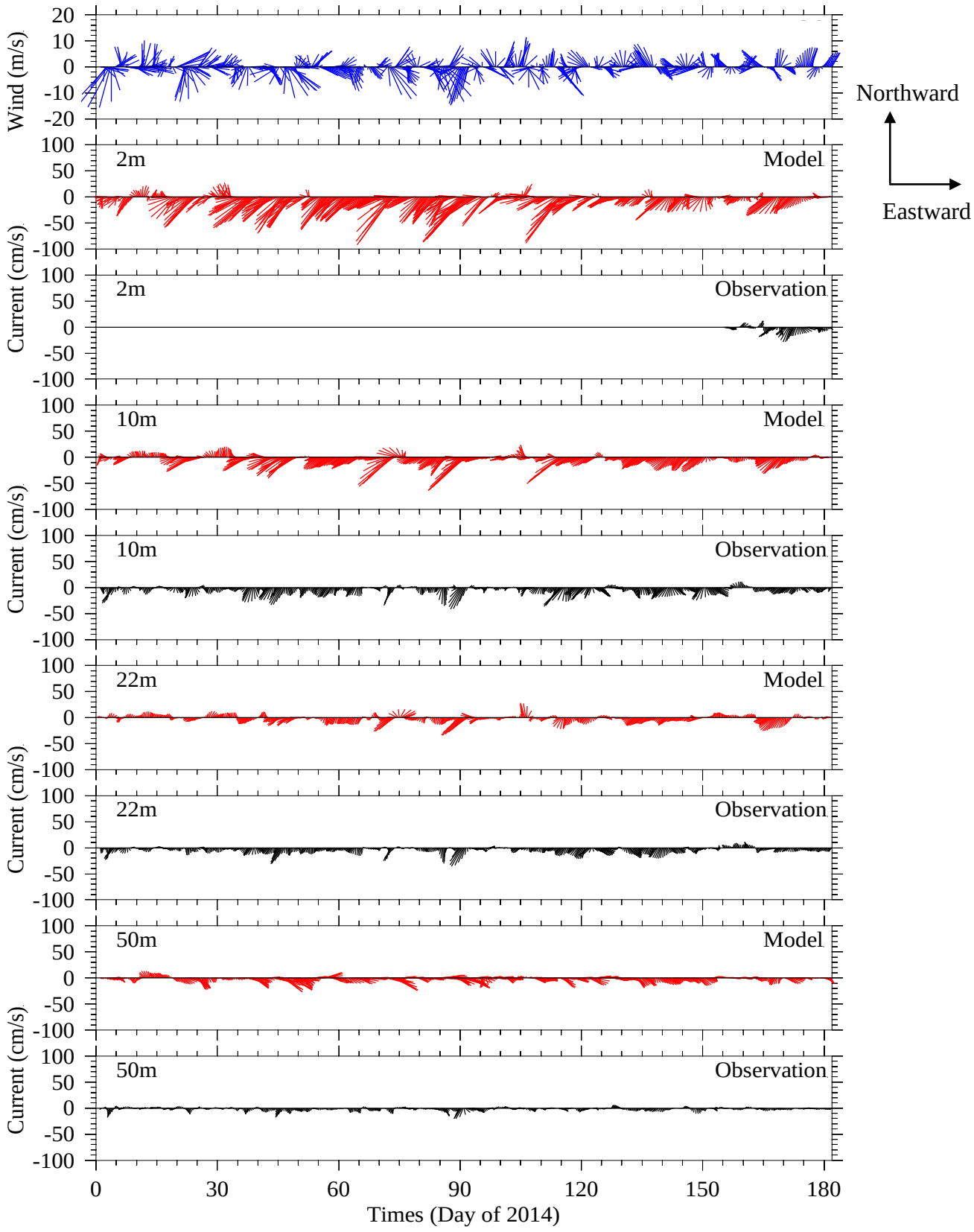

Figure 4-5a. Currents time series model-observation comparison, Jan – Jun.

Sticks point in the direction of flow, away from zero line; north/eastward flow up/rightward.

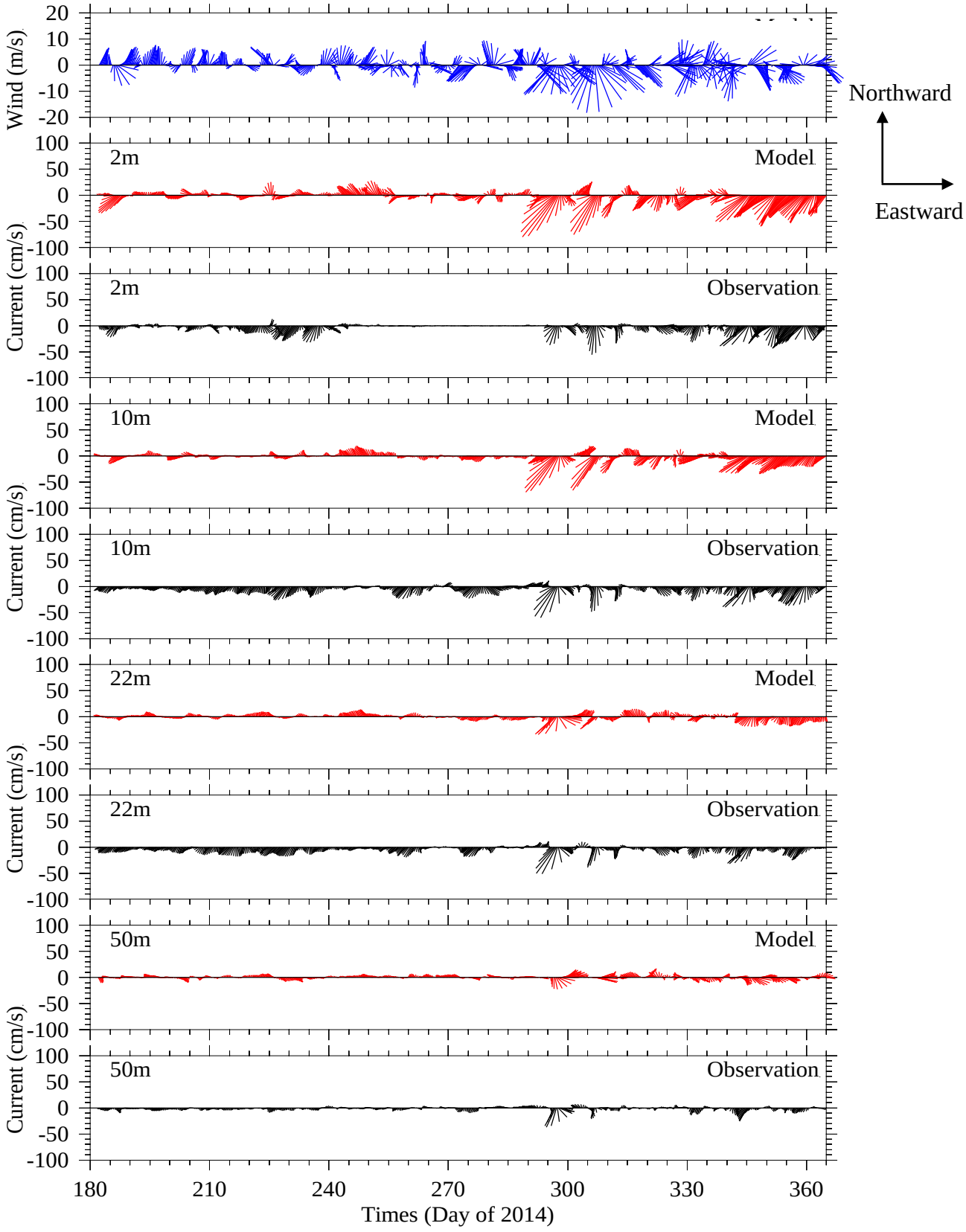

Figure 4-5b. Currents time series model-observation comparison, Jul - Dec.

generally weaker magnitudes in the summer; and a tendency for longer-term (monthly or longer) average winds to be weaker than weather-band changes and directed towards the east year round, southward in winter, and northward in summer.

Measured currents are generally toward the south and west at this location (see Figure 1-1; observations were not available from 2m deep prior to early June) and the model adequately captures this aspect of the observations. The most prominent model-observation differences are that at shallower depths the model currents are stronger and directed more eastward than observations, while at the deeper depths, particularly in the first half of the year, the model currents are more westward than observed. Most of the individual storm events seen in the observed currents occur in the model currents, and for some events the timing and direction of the flow is similar in the model and observations. These detailed comparisons of the time variations and vertical structure of currents in the model to direct observations at a particular site form a challenging test of the hydrodynamic simulation performance. Agreement is sufficient to conclude that the hydrodynamic model represents observed processes adequately to support the water quality modeling.

4.2 *Model monthly-mean temperature, salinity, and circulation*

Based on the above comparisons having demonstrated a level of agreement between the 2014 simulation and available observations, this subsection presents a more complete view of the monthly-averaged simulation temperature, salinity, and circulation throughout the year.

Model temperatures followed the expected seasonal cycle (Figure 4-6a,b) with peak values in summer and early fall and minima in late winter. Horizontal gradients are notable, with inshore temperatures generally colder during winter and spring and warmer during summer and fall. From May to October the surface temperatures (Figure 4-6a) are markedly higher than bottom temperatures (Figure 4-6b). Model salinities (Figure 4-7a,b) have a weaker seasonal cycle than temperature, particularly at depth. Water near the coastlines is generally fresher year-round, both at the surface (Figure 4-7a) and the seafloor (Figure 4-7b). At the surface, from April to June the offshore extent of relatively fresh water increased, first in the southern Gulf of Maine and then in Massachusetts Bay, where it then decreased from July to September.

The temporal progression of the geographic pattern of 2014 monthly-mean currents at the surface (Figure 4-8a) and at 15 m deep (Figure 4-8b) is consistent with the schematic in Figure 1-1 and characterized by the following main features. At the surface (Figure 4-8a), flow in Massachusetts and Cape Cod Bays was generally directed southward and strongest from February

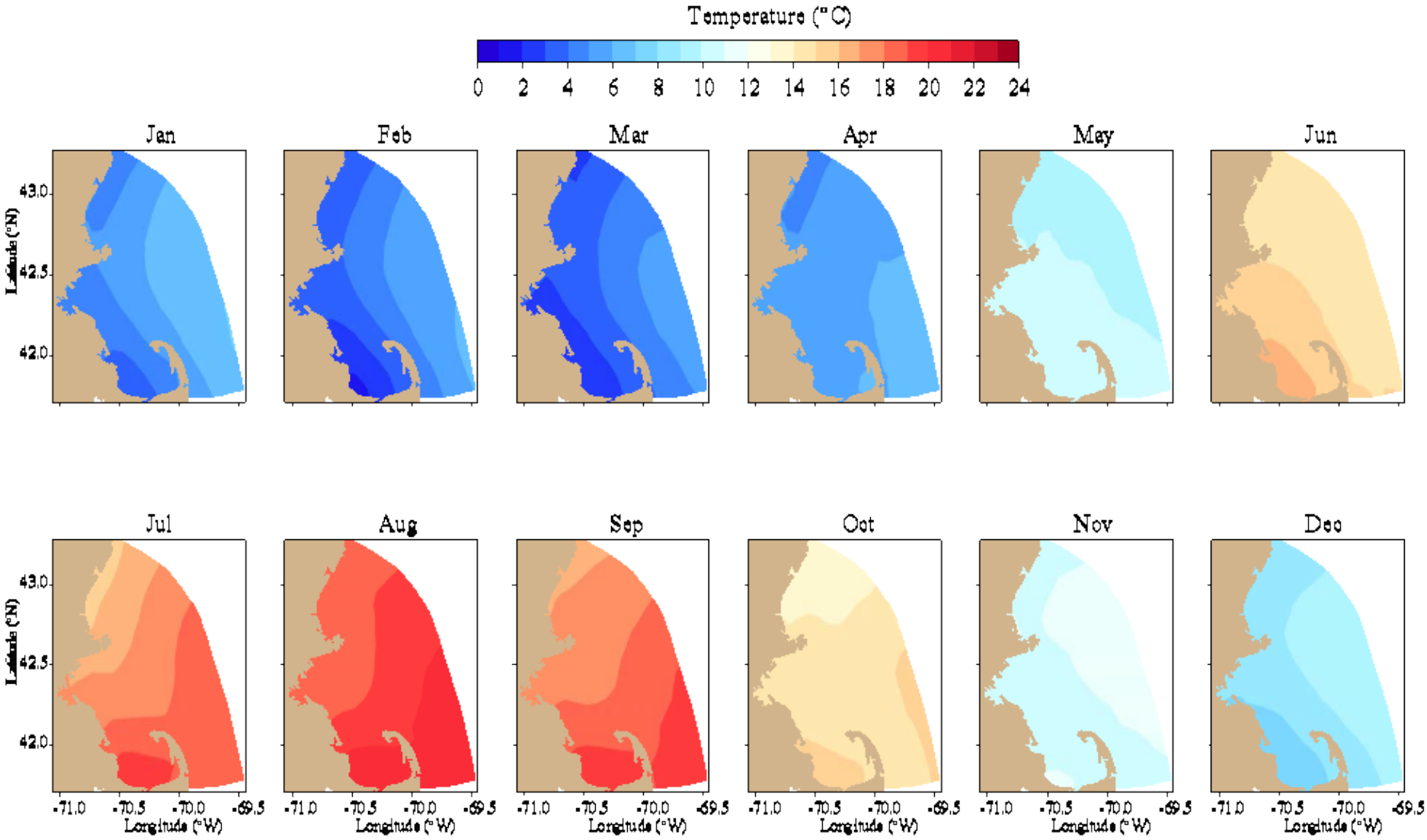

Figure 4-6a. Model temperature, monthly-mean spatial structure, at sea surface.

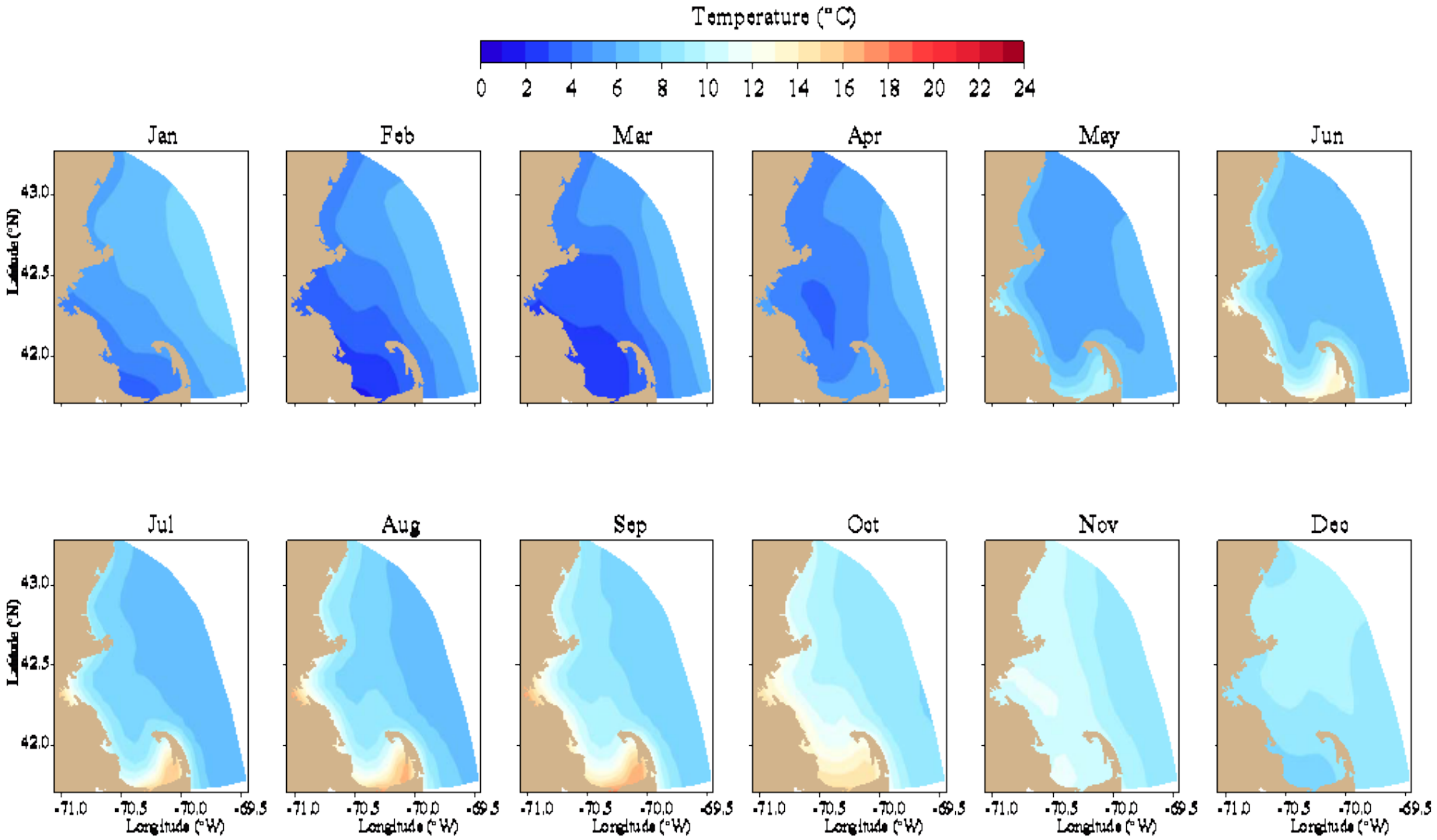

Figure 4-6b. Model temperature, monthly-mean spatial structure, at seafloor.

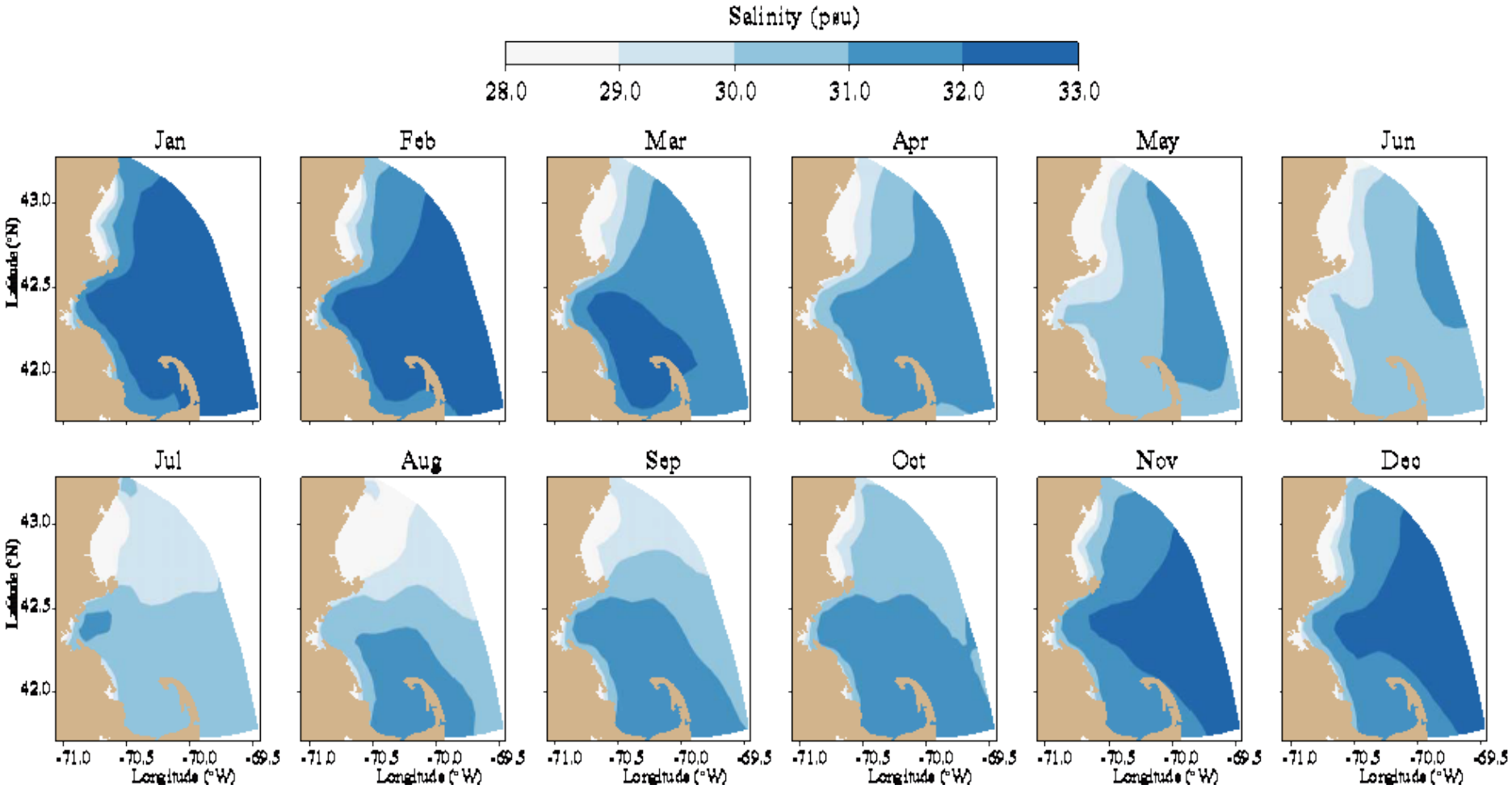

Figure 4-7a. Model salinity, monthly-mean spatial structure, at sea surface.

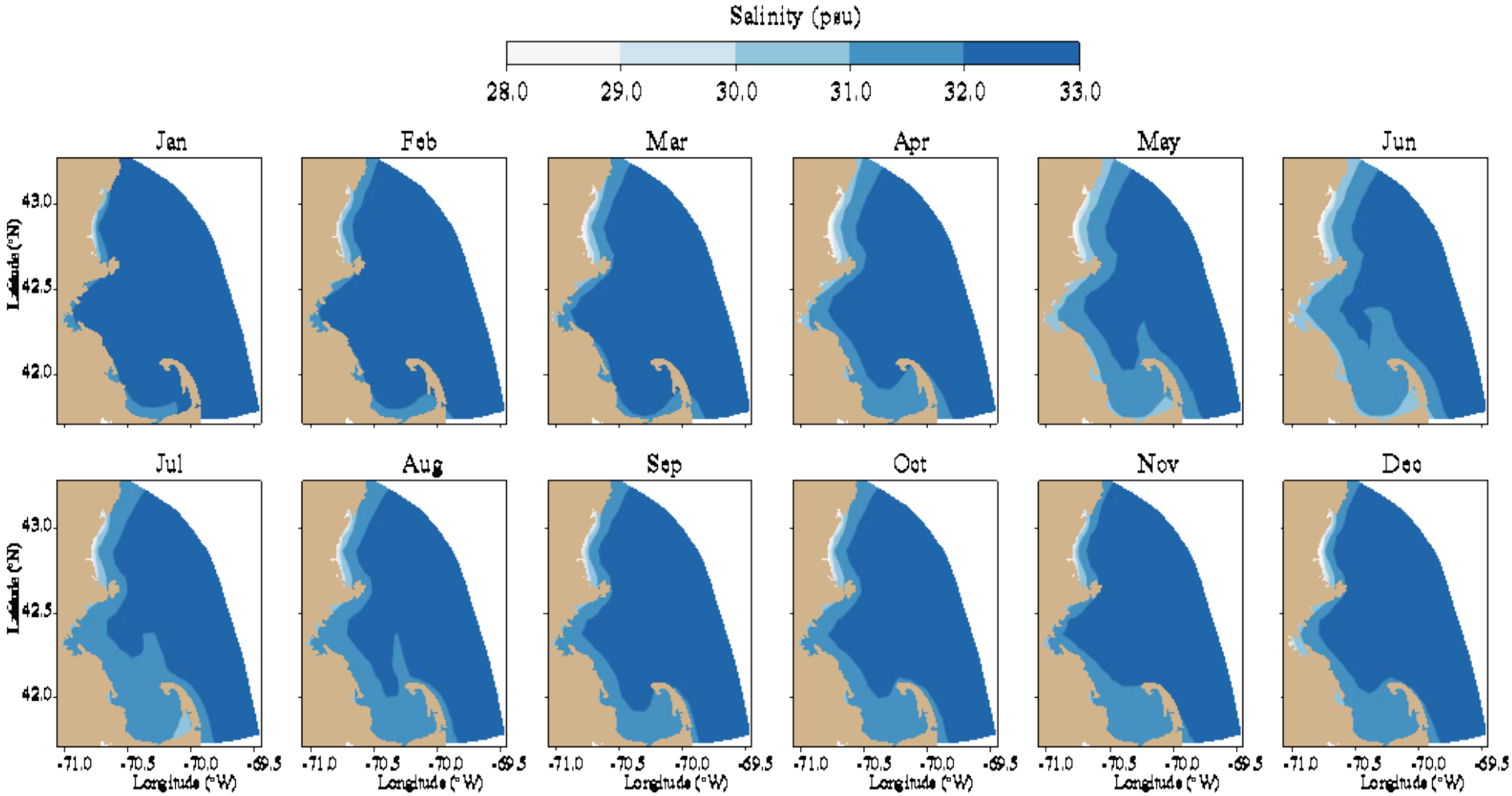

Figure 4-7b. Model salinity, monthly-mean spatial structure, at seafloor.

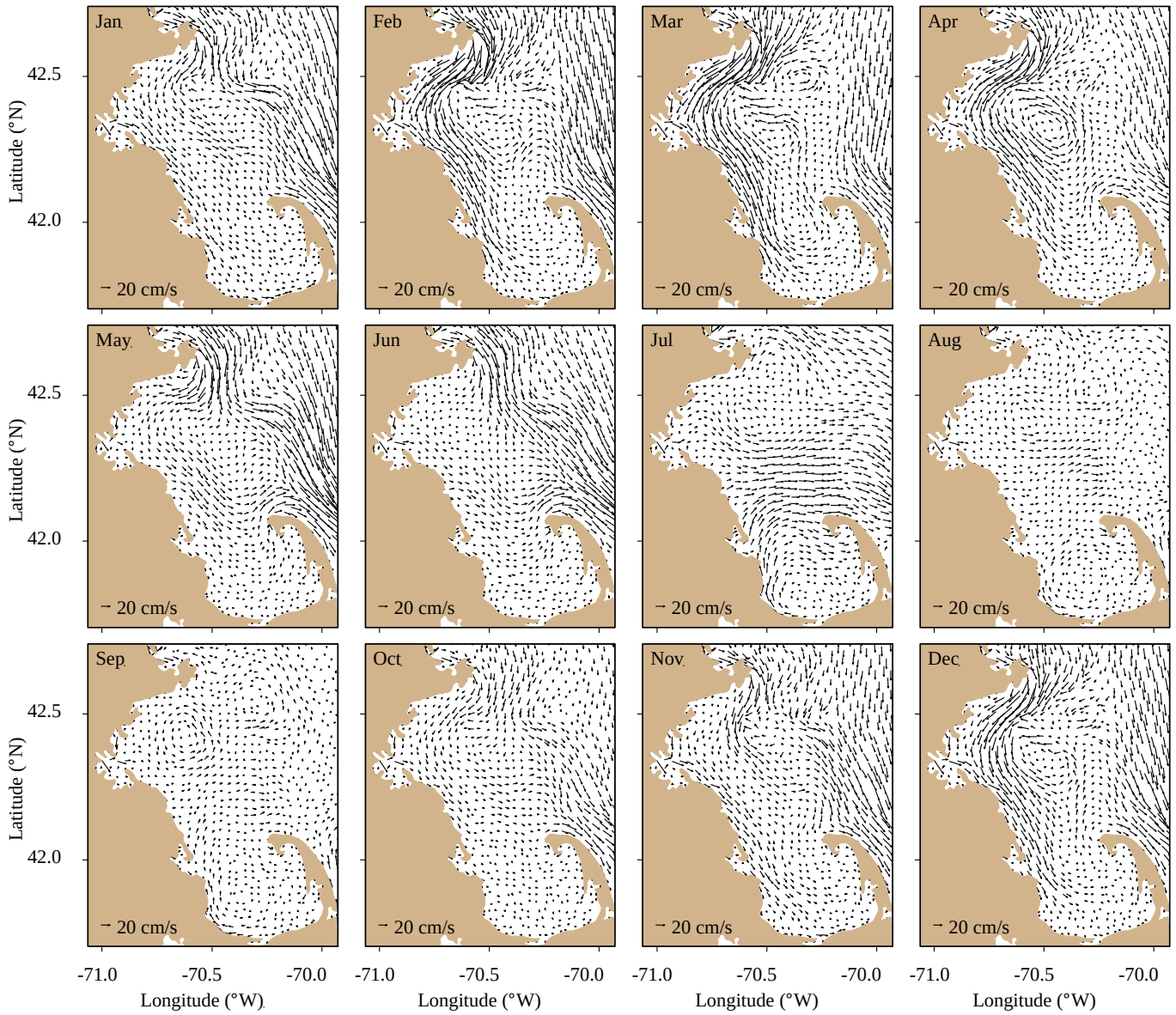

Figure 4-8a. Model currents, monthly-mean spatial structure, at sea surface.

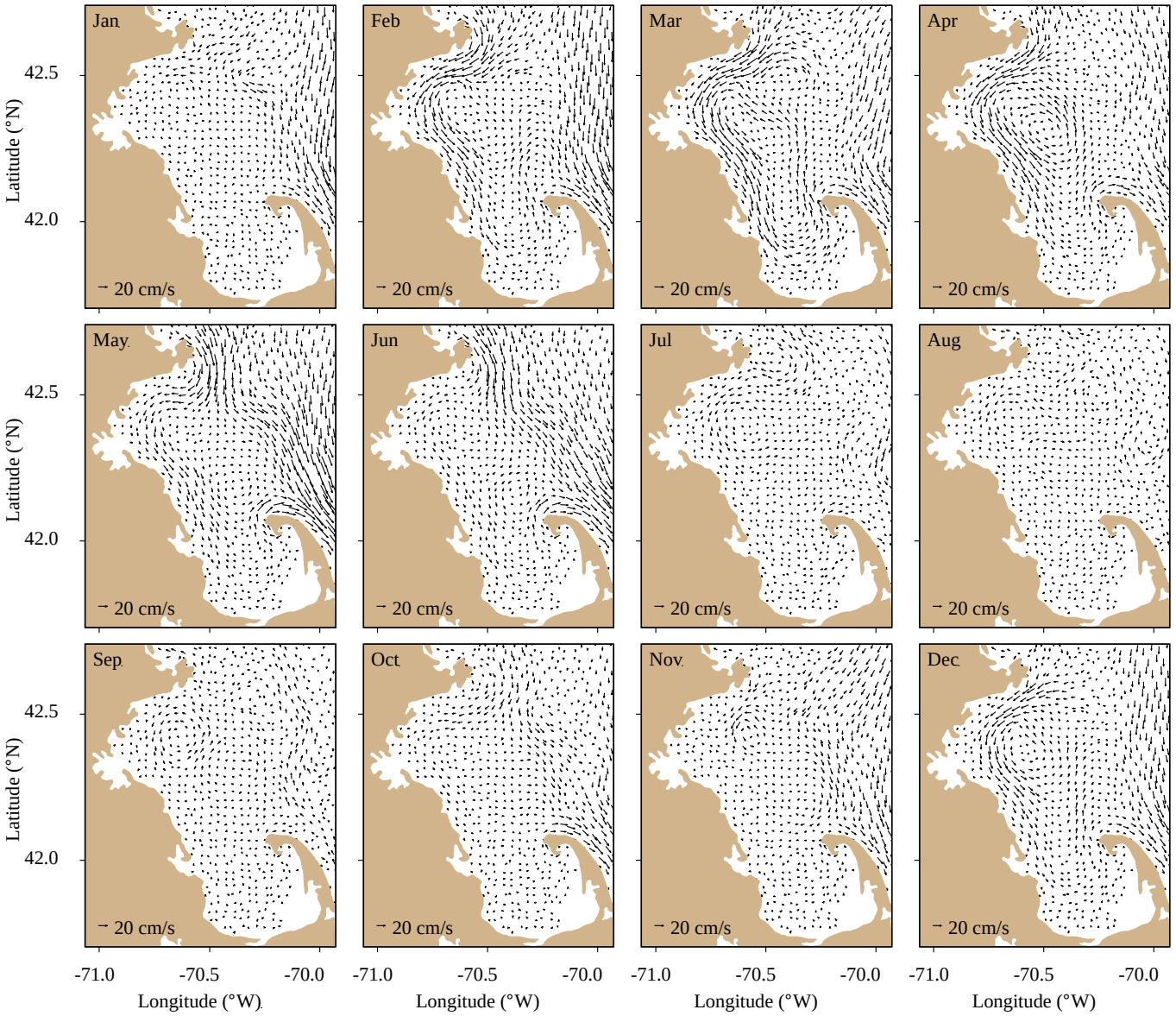

Figure 4-8b. Model currents, monthly-mean spatial structure, 15 m deep.

to April, during spring runoff, and in December. During these months currents were most intense within about 15 km of shore, reaching up to 30-40 cm/s; they originated in the Western Maine Coastal Current north of Cape Ann, extended along the Massachusetts Bay coastline, and entered the western side of Cape Cod Bay. During the rest of the year flows were generally weaker, 10-20 cm/s at most, and not well organized spatially with the exception that in July there was a broad region of eastward offshore motion of surface waters associated with the strong upwelling-favorable 2014 summer winds. In waters offshore of the bays a southward current extends from Cape Ann to east of Cape Cod during some months (notably January, May, and June). A feature common to many months is offshore flow in the Southern Passage, south of Stellwagen Bank and north of the tip of Cape Cod.

At 15 m deep (Figure 4-8b) the flow patterns are typically the same as at the surface, with the main difference being that currents are generally not stronger than 10 cm/s, and are thus substantially weaker than currents at the surface. Exceptions include some locations and months with the most intense surface flows (for example, offshore from Cape Cod in May), for which the 15-m deep currents have strengths that are only weakly reduced compared to the surface currents. This is indicative that these stronger flows extend a greater distance beneath the sea surface.

5. Water quality

Model-observation correlation and regression analyses of key water quality variables from the 2014 simulation are presented in Figure 5-1, including surface chlorophyll, surface inorganic nutrients (nitrate NO_3^-, ammonium NH_4^+, and silicate SiO_3^{2-}), and seafloor dissolved oxygen (DO) concentration (mg L^{-1}) and DO saturation (%). These comparisons use observations from all Massachusetts Bay and Cape Cod Bay sites sampled by MWRA during 2014, comprising a total of 14 stations (see, for example, Figure 3-1 on page 10 of Werme et al 2015). (For clarity of presentation as noted above, figures in the remainder of this section use a subset of 10 such stations, as shown in Figure 3-7.) In 2014 there was no meaningful correlation for near-surface chlorophyll, silicate, or ammonium. The model significantly underestimated chlorophyll when its concentration was higher than about 2 µg L^{-1}. For surface NO_3^- the correlation is better than in past years, although substantial scatter is evident as typifies simulations of earlier years. A better-defined relationship is seen for DO concentration, which has a correlation coefficient of 0.90. The DO saturation was not directly modeled, rather it was calculated based on temperature, salinity and DO concentration using the approximate relation given in equation 2.3 of Zhao et al. (2012); biases in the simulation for these parameters could be factors that contribute to the lower correlation coefficient for DO percent saturation than for DO concentration.

The remainder of this section describes the 2014 annual progressions of a representative set of water quality model variables from representative locations. Individual figures generally show results of model-observation comparisons for stations from one of the three groups in Figure 3-7 (northern, southern, and harbor), or monthly-mean model output along an east-west transect (shown in Figure 3-7) that originates at the coast, passes through the outfall site, and extends offshore across Stellwagen Basin and Stellwagen Bank.

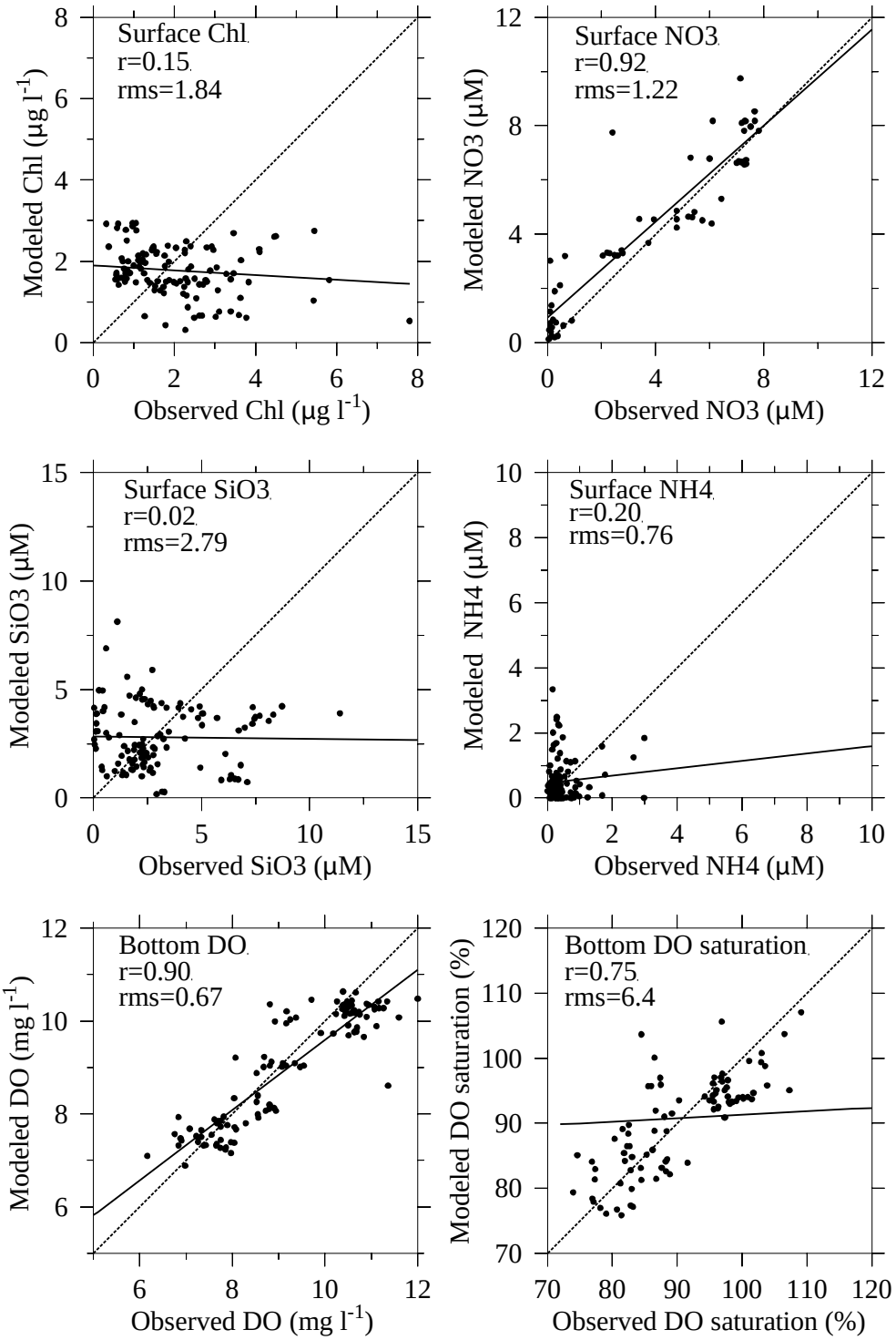

Figure 5-1. Model-observation correlations/regressions for key water quality parameters.

All stations outside Boston Harbor; regressions are solid lines, dashed lines indicate equality between observed and modeled results.

5.1 *Light*

Model and observations are compared using extinction coefficients for PAR attenuation in the water column, as described in Section 2.2. At stations in the northern group (Figure 5-2a) and southern group (Figure 5-2b) spanning Massachusetts Bay and Cape Cod Bay, the model extinction coefficient results include annual-average values that differ modestly from site to site, and have substantial temporal variations that generally include a peak in late spring in association with chlorophyll self-shading. At all stations the range of temporal variability in the model is much lower than that in the observations. The modeled values are generally within the range of observations and systematic bias is typically minor, with the most pronounced bias consisting of higher than observed values at the outfall/N21 site and lower than observed values at F01 in Cape Cod Bay.

The extinction coefficient results for the harbor group of stations (Figure 5-2c) are similar to those in the bays, with respect to site-to-site variations in the model being modest and generally consistent with the observations. In contrast, the temporal variability of the model in the harbor is much less than outside the harbor. At sites in the harbor (station 140, and to a lesser extent station 124) where the temporal variability of observations is more pronounced than in the bay, this leads to larger model-observation differences.

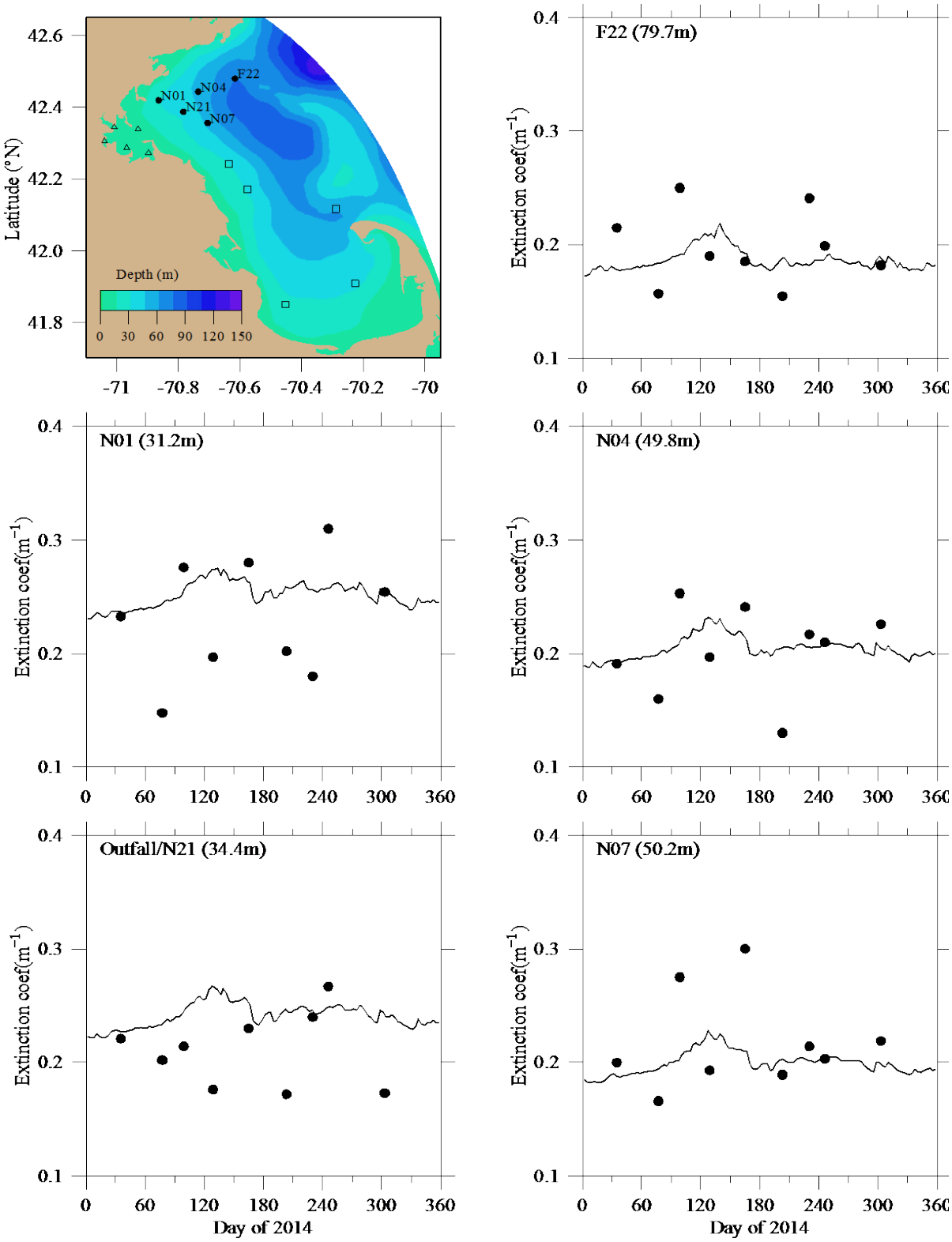

Figure 5-2a. Light extinction. Northern stations. Line: Model. Symbols: Observations.

In this and all similar plots to follow, at the upper left of each frame is a label showing "station name (bathymetric depth at station)".

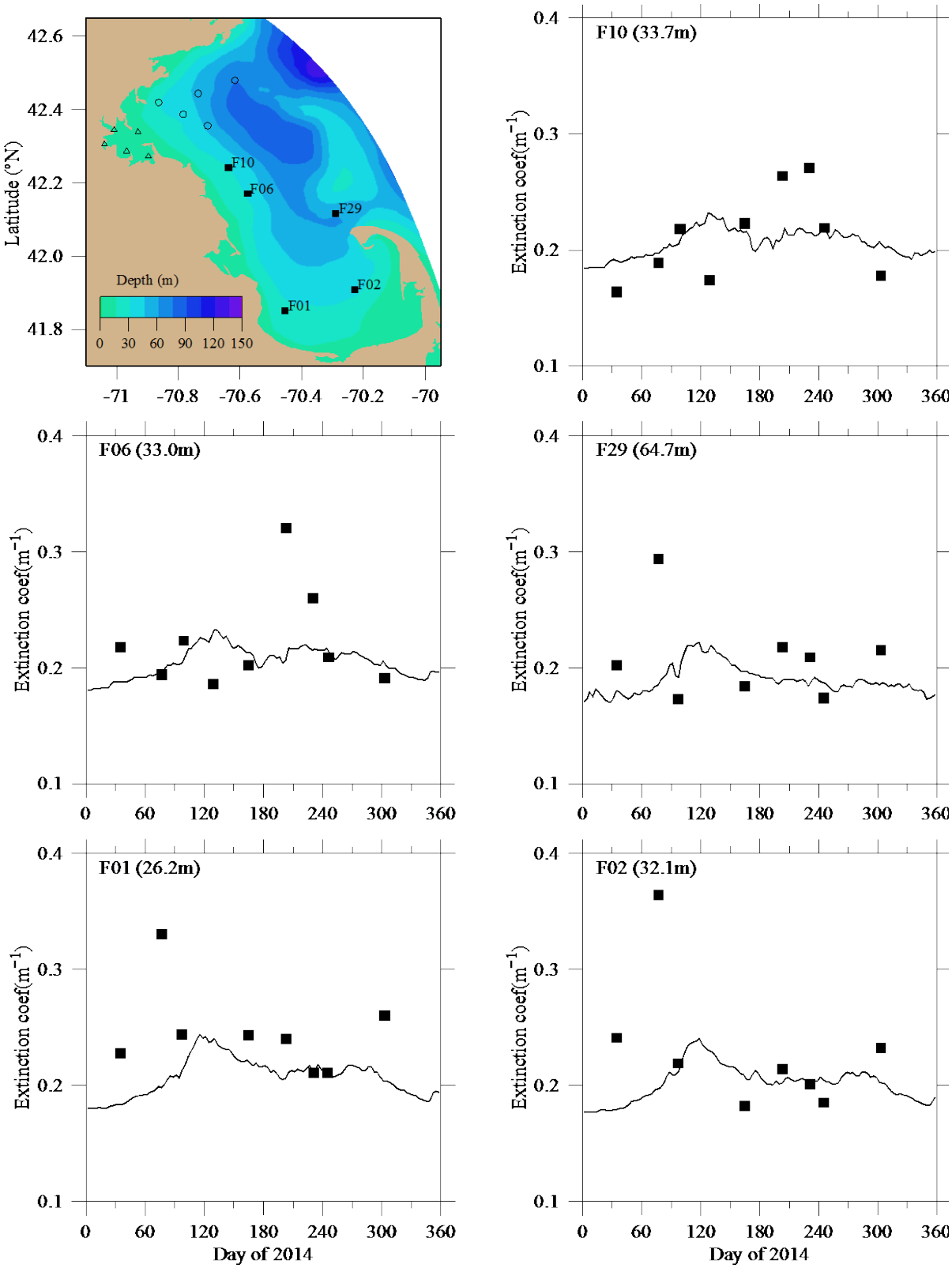

Figure 5-2b. Light extinction. Southern stations. Line: Model. Symbols: Observations.

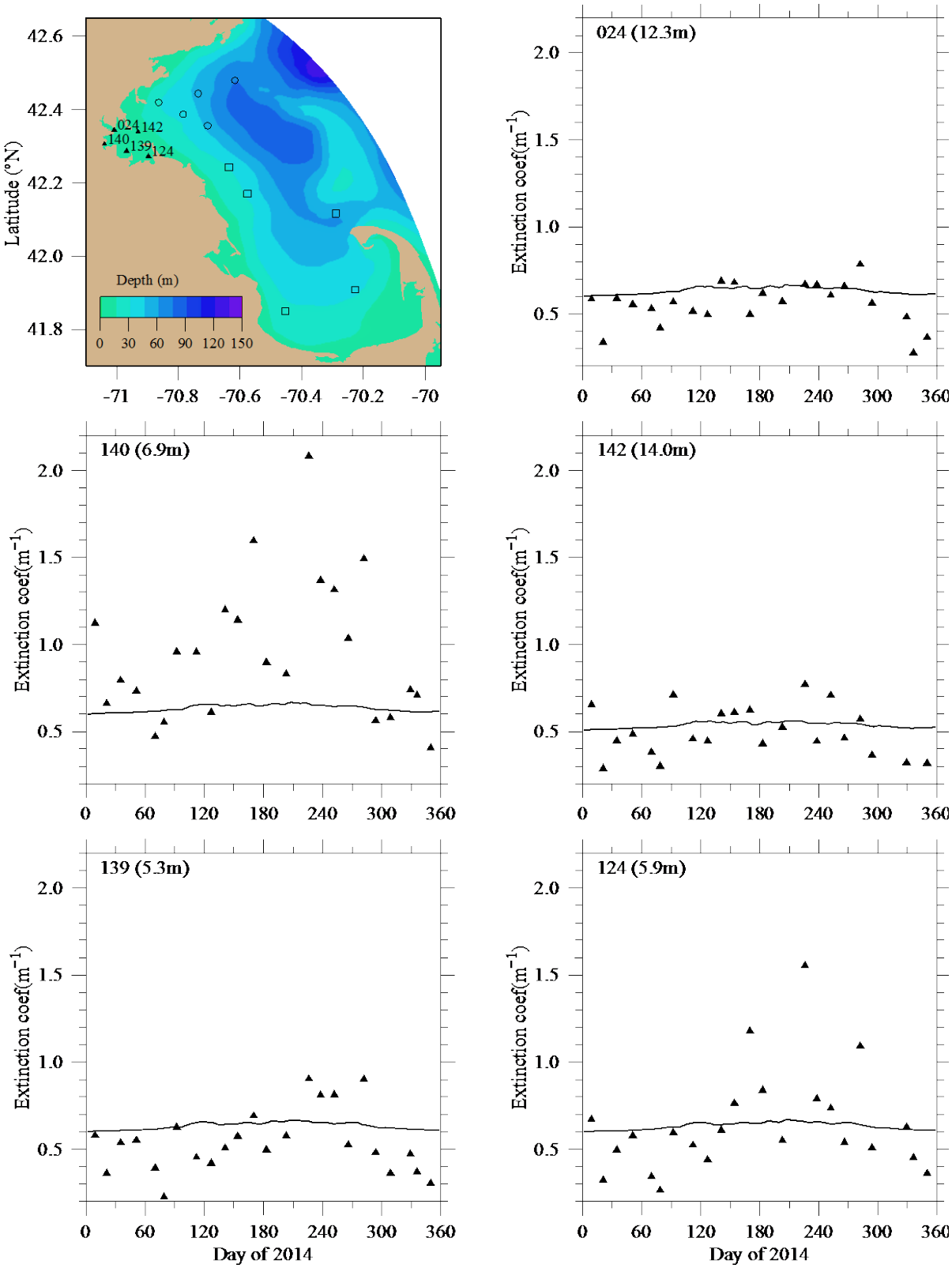

Figure 5-2c. Light extinction. Harbor stations. Line: Model. Symbols: Observations.

5.2 *Dissolved inorganic nitrogen*

Dissolved inorganic nitrogen (DIN) is the sum of the nitrogen in ammonium (NH_4), nitrate (NO_3), and nitrite (NO_2). Typical seasonal variations in modeled and observed DIN occurred during 2014 at the northern and southern station groups (Figure 5-3a,b). At the start of the year the shallow and deep DIN concentrations were comparable. By late April the shallow values were drawn down to nearly zero by phytoplankton consumption, and they remained low through summer. Deep concentrations remained relatively unchanged throughout the year, particularly for the northern group. By November the shallow values had increased to again be comparable to deep due to reinvigorated vertical mixing during fall. Similarly to 2013, in 2014 at the outfall/N21 site some observations (notably Feb, Mar, Nov) had higher concentrations near the surface, in contrast to other stations; the simulation did not capture this feature, which is likely associated with the details of circulation within the zone of initial dilution (e.g. Blumberg et al., 1996), and if so would not be expected to be represented particularly well in the model. At stations in and near Cape Cod Bay (F29, F01, F02; Figure 5-3b) the measured early-year concentrations (until at least late April) were very low both near the surface and near the seafloor, which the model did not capture.

At many stations, the near-seafloor concentrations in the model underestimated the observed values. At most of these stations the seafloor is substantially deeper than the euphotic zone, so DIN uptake by phytoplankton does not occur near the bottom. It is possible this model underestimation of deep DIN is due to local nutrient sources not captured well by the model, such as groundwater sources (Becker 1992, Jiang et al. 2007) which the model bases on historical estimates without inclusion of geographic variations. An exception to model underestimation of deep DIN occurs at the outfall/N21 station, where for most of the year the model concentrations substantially exceeded measured.

For harbor stations the magnitudes and seasonal cycles of DIN in the model were generally similar to observations (Figure 5-3c). At some sites (stations 024, 124) the model exhibited similar patterns as outside the harbor, with shallow and deep concentrations diverging during summer. This contrasted the observations, for which late spring nutrient depletion occurred both near the surface and near the seafloor.

The modeled signature of the outfall in DIN is made clear (Figure 5-3d) by monthly-mean concentrations on the east-west transect. The highest DIN levels occur near the seafloor, and within about 10 km of the outfall, year-round. Away from the outfall, during winter conditions (Jan-Feb

and Oct-Dec) vertical gradients are weak in association with more vigorous vertical mixing, while for the rest of the year concentrations in the upper water column are substantially lower than at depth due to near-surface phytoplankton uptake when stratification impedes vertical exchange. These patterns in 2014 were similar to simulations of prior years.

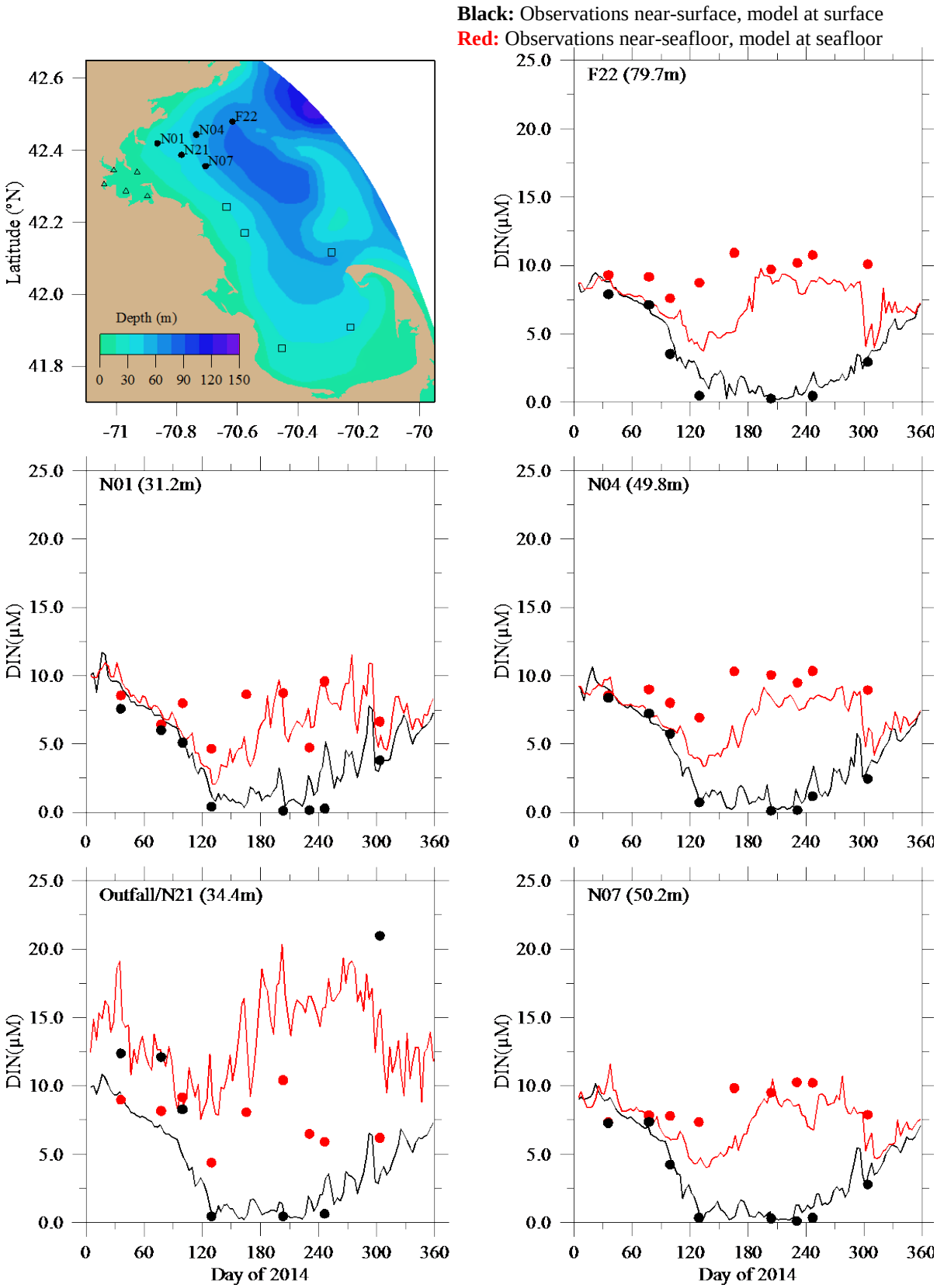

Figure 5-3a. Dissolved inorganic nitrogen. Northern stations. Model-observation comparisons.

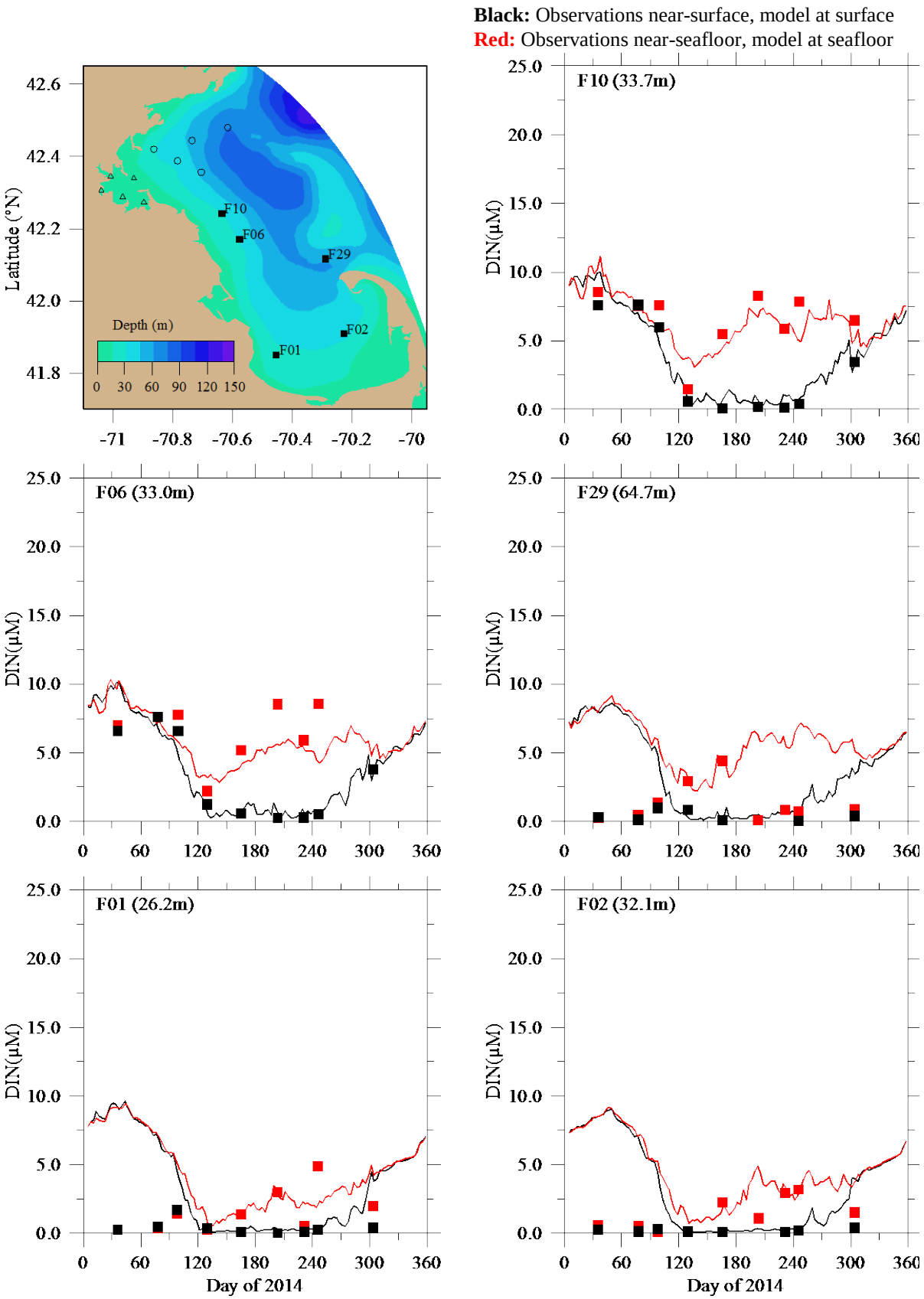

Figure 5-3b. Dissolved inorganic nitrogen. Southern stations. Model-observation comparisons.

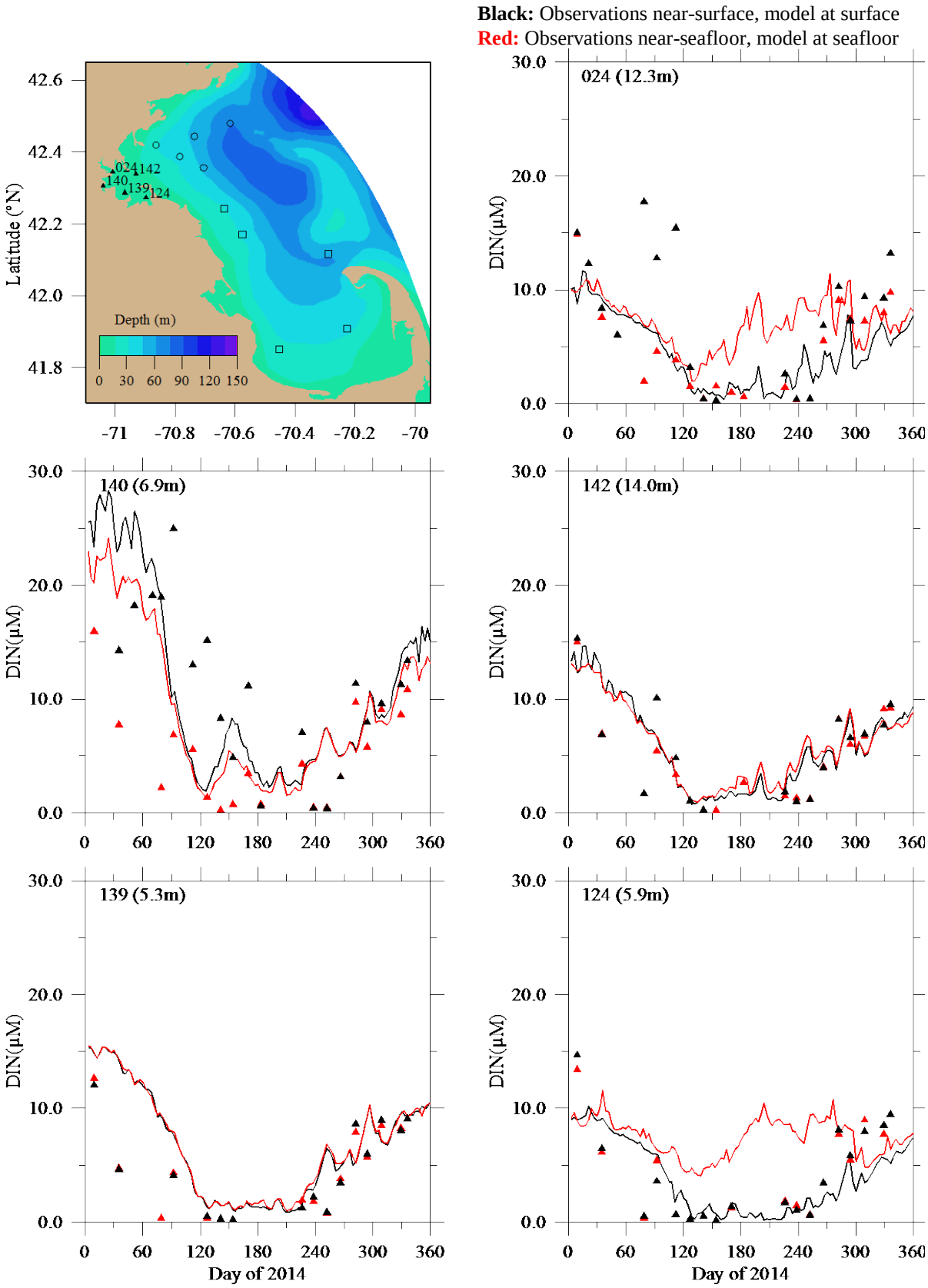

Figure 5-3c. Dissolved inorganic nitrogen. Harbor stations. Model-observation comparisons.

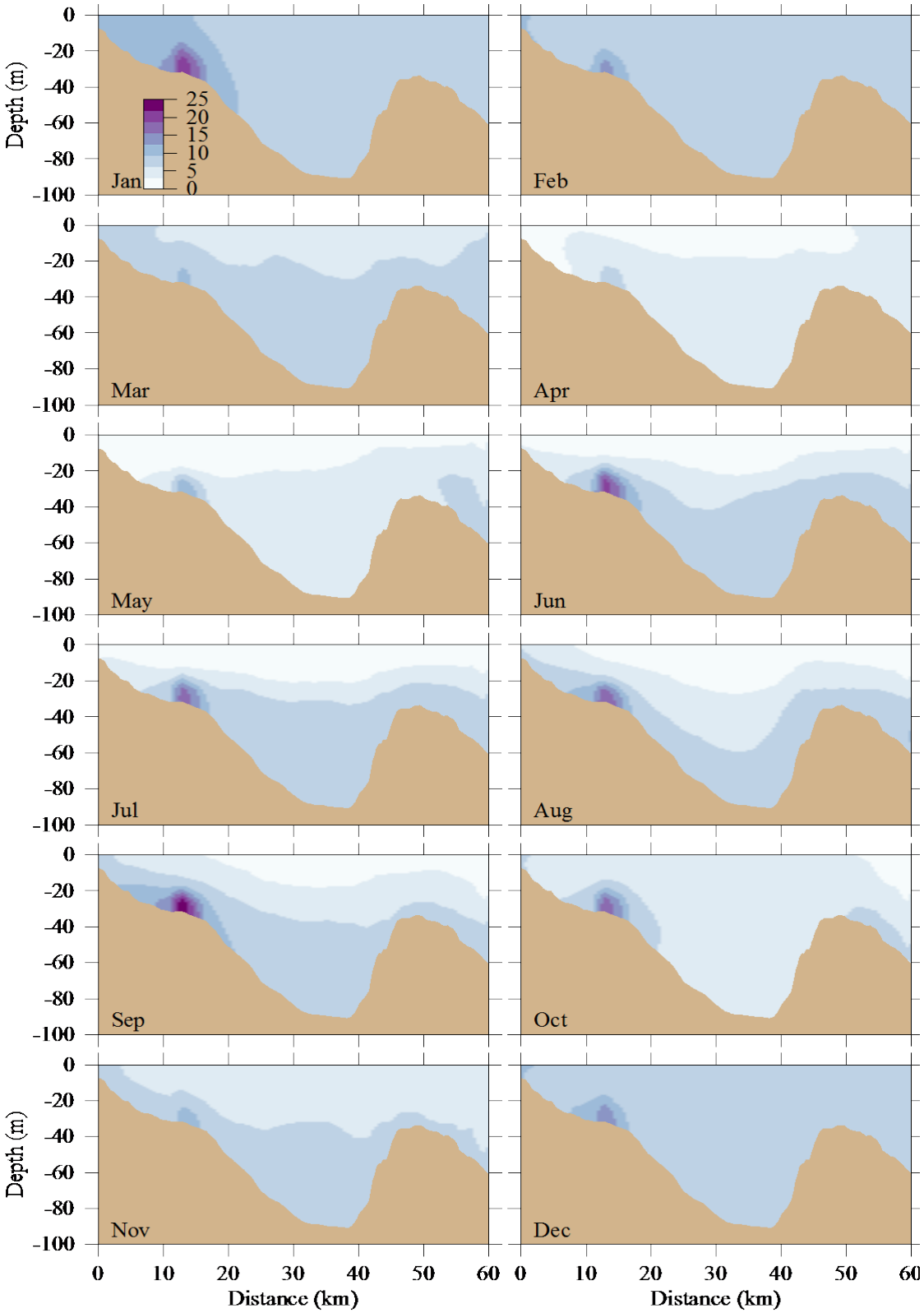

Figure 5-3d. Dissolved inorganic nitrogen (μM). Model results, east-west transect (Fig. 3-7). Horizontal axis is distance eastward from coast; outfall is on seafloor at approximately 13 km.

5.3 *Chlorophyll*

Model chlorophyll concentrations at Massachusetts Bay and Cape Cod Bay stations in 2014 (Figure 5-4a,b) generally included low values in the early months, peaks during spring at both the shallow and deep depths, then intermediate levels during summer and early fall when values near the surface were higher than near the seafloor, before a return to lower levels. Compared to the observations the model had less pronounced temporal variability. The model was generally within the observed ranges, with the exception of stations in and near Cape Cod Bay, for which there was a bias with model levels higher than the observations during most of the year. Deep concentrations in the model generally exceeded those near the surface for most of the duration of the springtime increase; in the observations, deep values were higher than shallow values only for one early May survey, during which the highest values of the year occurred due to a senescing *Phaeocystis* bloom (Libby et al., 2015).

At harbor stations (Figure 5-4c) the seasonal cycle of chlorophyll in the model featured increased levels during most of spring and summer, instead of blooms earlier in spring as seen outside the harbor, and at most stations (except stations 024 and 124) deep concentrations were generally higher than near-surface levels. The model values were biased low compared to observations and the observations included higher ranges of variability than the model as well as smaller differences between shallow and deep concentrations.

Model chlorophyll on the east-west transect (Figure 5-4d) had relatively low and vertically uniform concentrations early in the year. They increased in March and reached peak values in April, with highest levels at mid-depth, particularly offshore. In May they were high and mostly uniform in depth, and through the summer months there was a near-surface layer of high values with low concentrations deeper. Concentrations decreased again in the fall. In contrast to DIN, in model chlorophyll there was not a strong signature of the outfall plume.

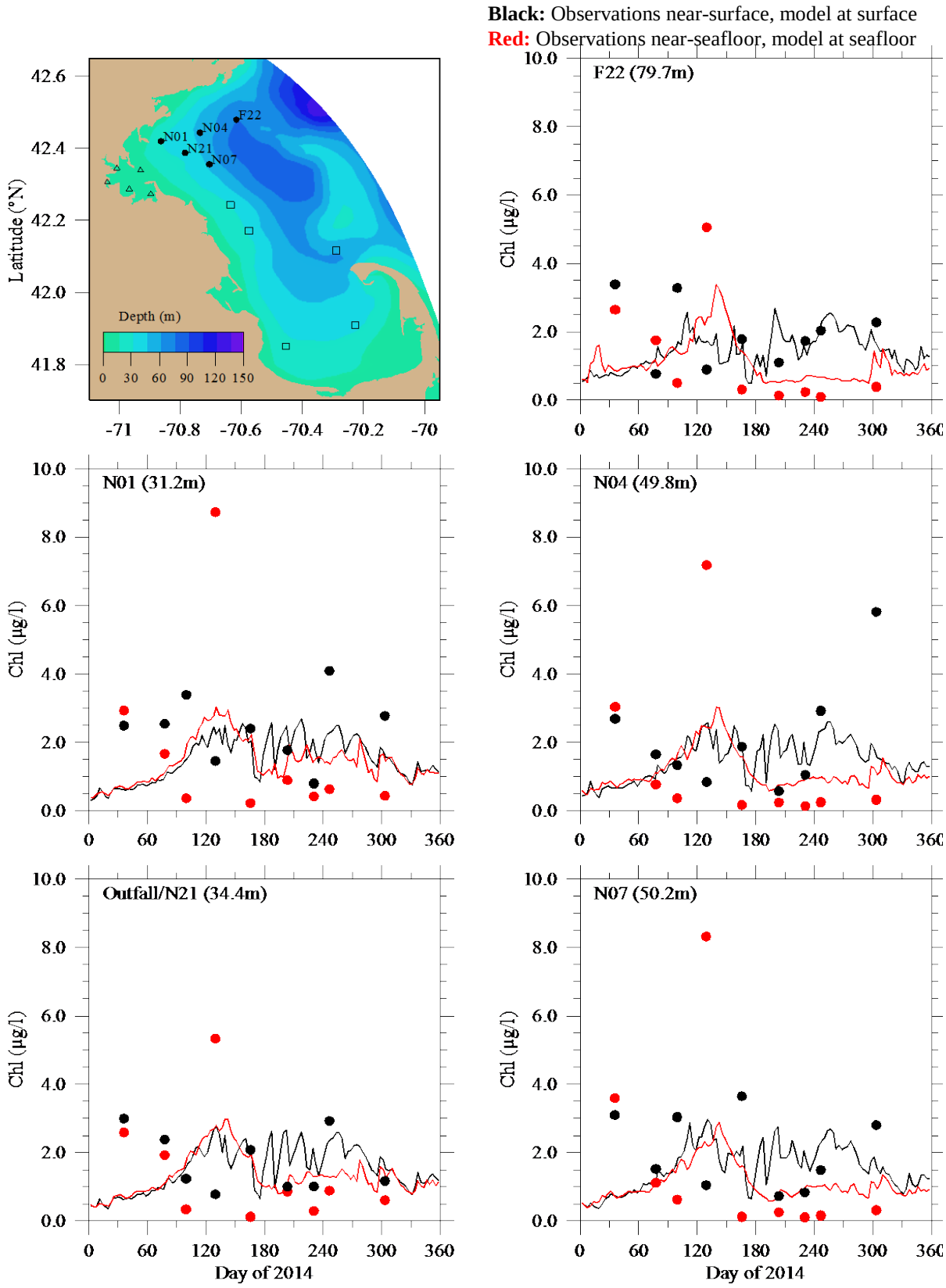

Figure 5-4a. Chlorophyll. Northern stations. Model-observation comparisons.

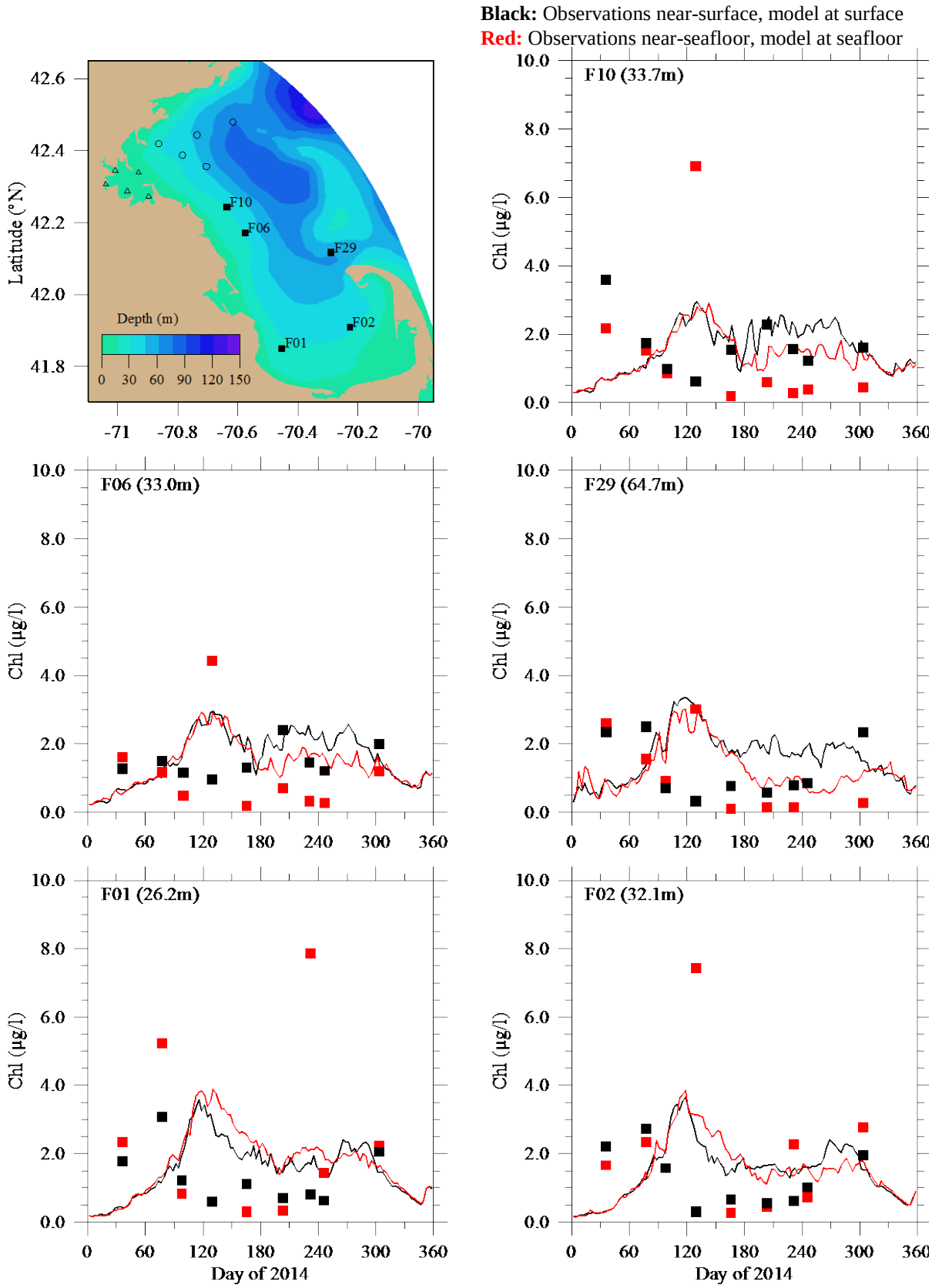

Figure 5-4b. Chlorophyll. Southern stations. Model-observation comparisons.

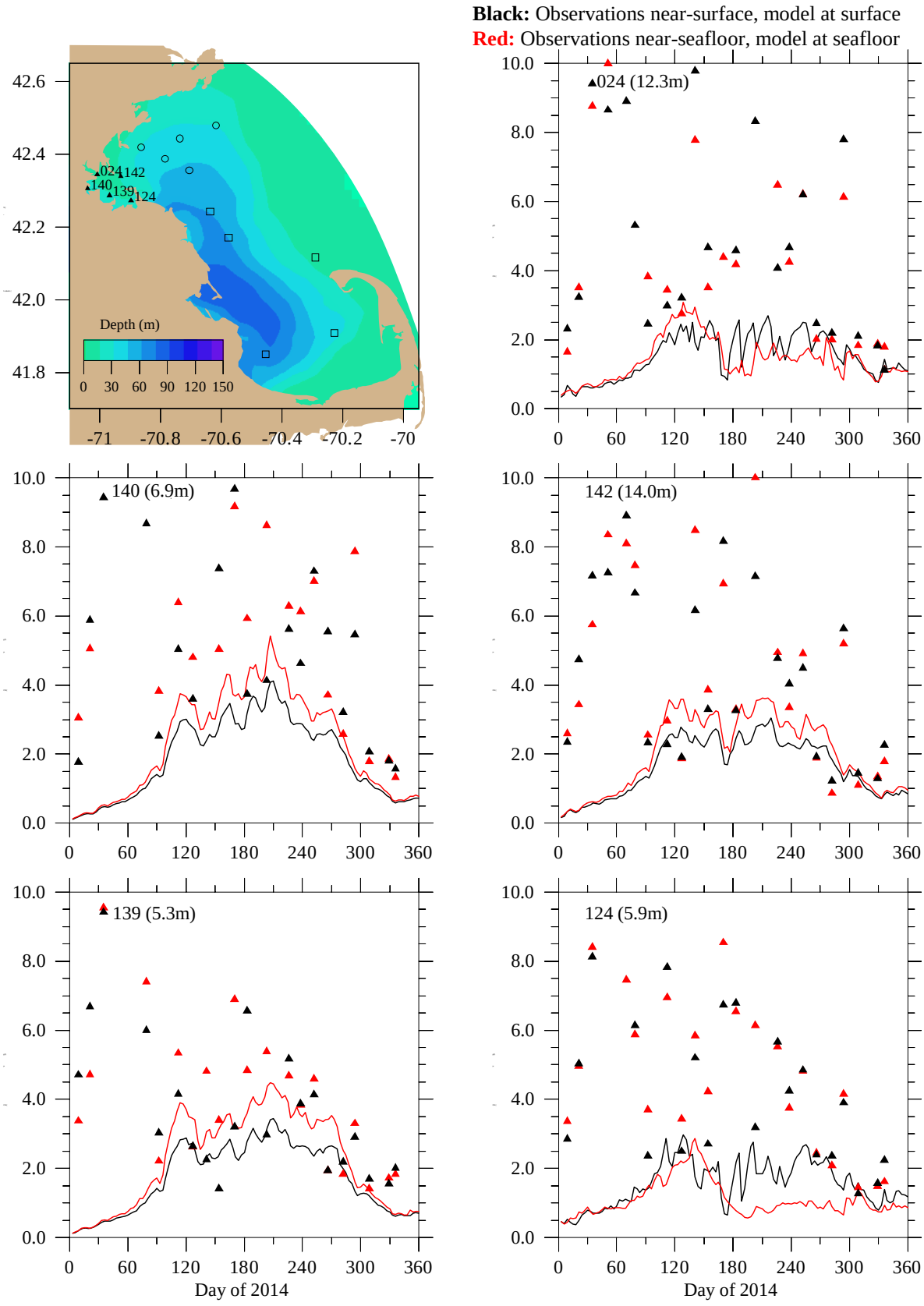

Figure 5-4c. Chlorophyll. Harbor stations. Model-observation comparisons.

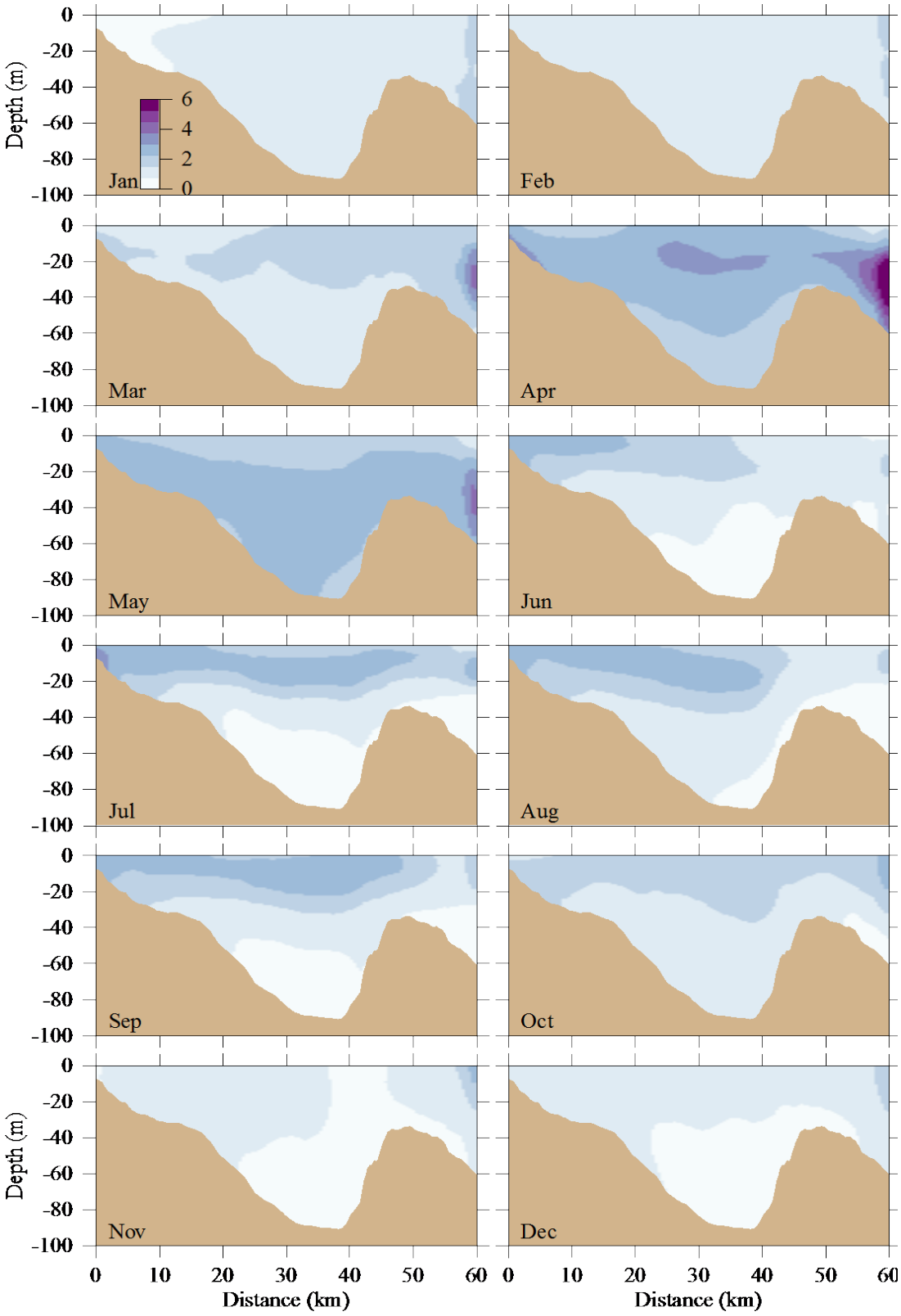

Figure 5-4d. Chlorophyll (µg L^{-1}). Model results, east-west transect (Fig. 3-7).

Horizontal axis is distance eastward from coast; outfall is on seafloor at approximately 13 km.

5.4 *Primary productivity*

Primary productivity in the 2014 model run is shown in Figure 5-5 at three monitoring stations (F23 at the mouth of BH; N04 to the northeast of the outfall; and N18 nearest to the outfall) where observations of primary productivity had been made in past years. Ongoing field sampling no longer includes primary productivity measurements, but for context the observations from 1995-2010 are superimposed as box-whisker plots on the model outputs (a review of the field results is included as part of Keay et al 2012; methods are described in Appendix C of Libby et al., 2005). The box-whisker plots consist of a box with the 25^{th} and 75^{th} percentiles at its lower and upper bounds and a horizontal line bisecting the box at the median (50^{th} percentile), with whiskers that extend to the 9^{th} and 91^{st} percentiles. For most of the year, 2014 modeled primary productivity was within ranges of historic observations. The springtime increase in 2014 was modest and occurred mainly in the second half of April, slightly later than was observed in many past years at N04 and N18. In fall 2014, primary productivity decreased to low levels earlier than was observed in many past years.

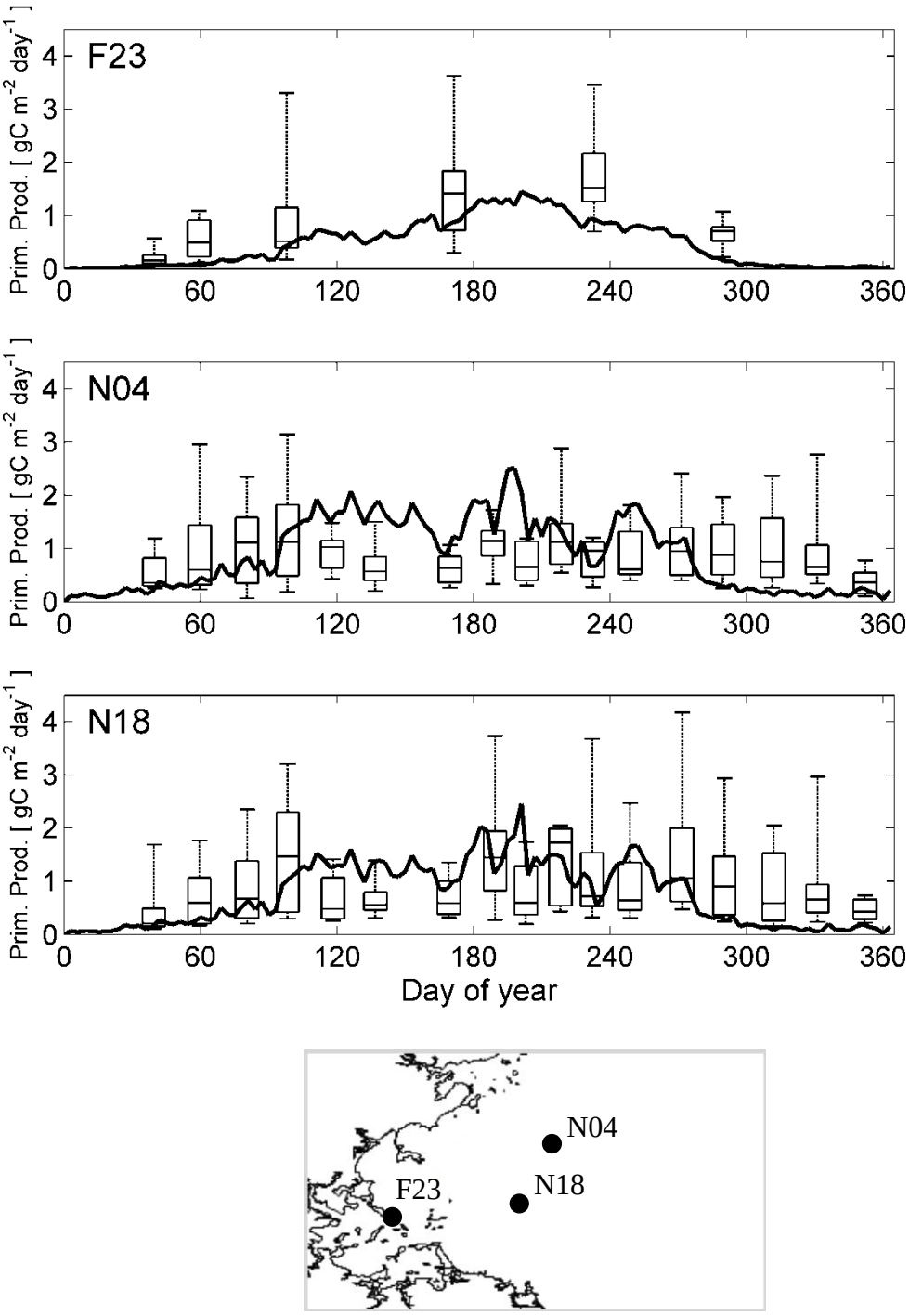

Figure 5-5. Primary production, vertically integrated, model-observation comparison.

Line is 2014 model result. Box-whiskers are 1995-2010 observations; box shows 25th, 50th, and 75th percentiles and whiskers are 9th and 91st percentiles.

5.5 *Dissolved and particulate organic nitrogen*

Model dissolved organic nitrogen (DON) levels during 2014 were generally within the range of variability of observations (Figure 5-6a,b), with evidence of low bias at some stations (F10, F06). Temporal variability in the model was weaker than in observations and did not include a strong seasonal cycle. Vertical differences in model DON were modest, with surface values slightly higher, particularly in the late summer, as evidenced in the east-west transect results (Figure 5-6).

Model particulate organic nitrogen (PON) during 2014 showed a stronger seasonal cycle, with low concentrations in winter, then elevated levels in spring and summer that slowly decreased through fall (Figure 5-7a,b); at most stations, deep concentrations were modestly less than shallow concentrations. The range of temporal variability in the model was less than in observations, and at most stations the deep observed values remained markedly lower than shallow values for all or most of the year, a feature the model did not capture. The east-west transect results for PON (Figure 5-7c) demonstrate that the seasonal changes and vertical structure just described generally occurred regionwide.

As noted for chlorophyll above, in both model and observations there was not a persistent anomalous signal near the outfall in either DON or PON. This is evidence supporting the conclusion that these model variables are not detectably influenced by outfall effluent.

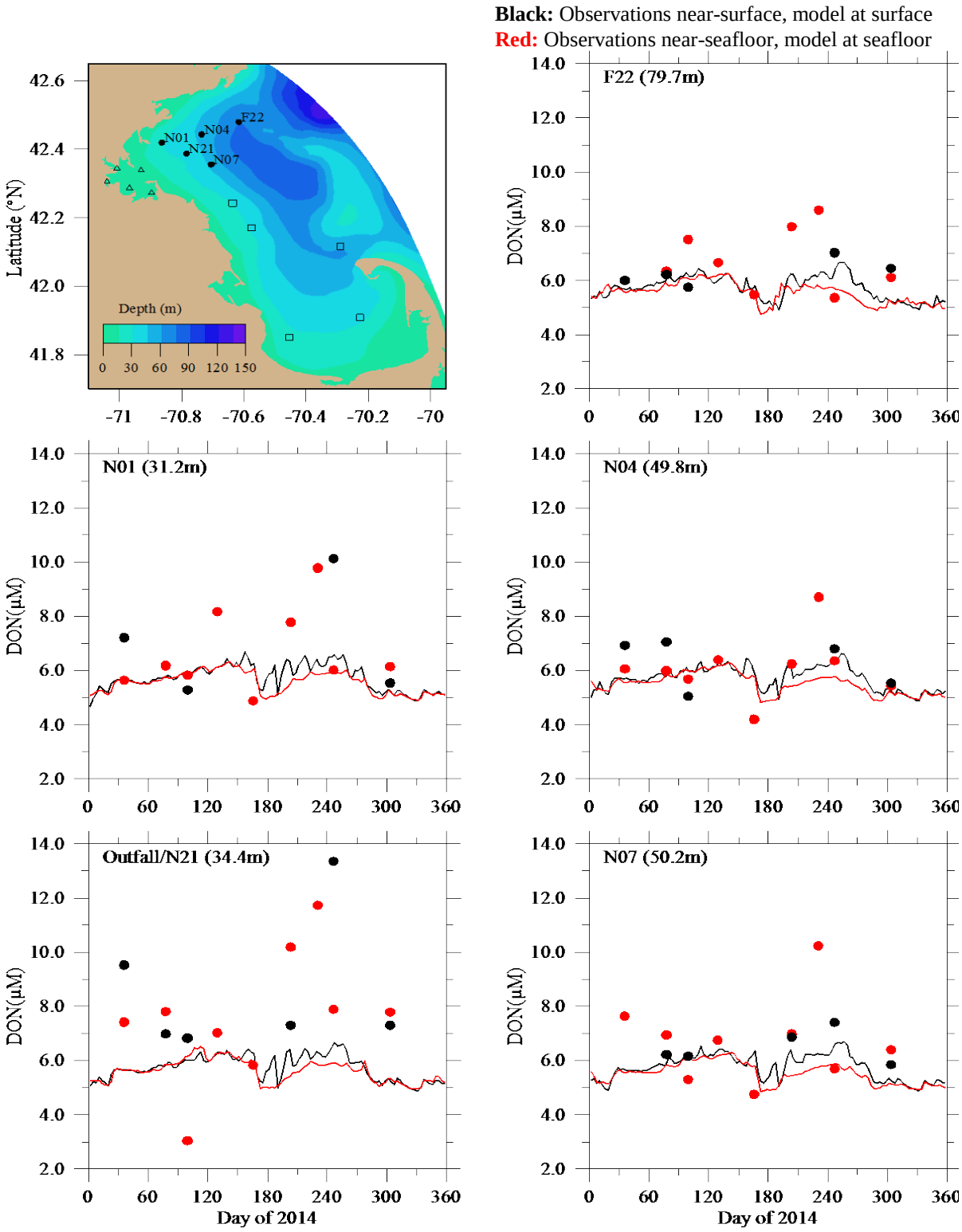

Figure 5-6a. Dissolved organic nitrogen. Northern stations. Model-observation comparisons.

Because observed DON is computed using measurements of TDN (total dissolved nitrogen), NO2, NO3, and NH4, if any of those four measurements was unavailable the observed DON does not appear on these plots. This was the case for many near-surface samples during the summer months.

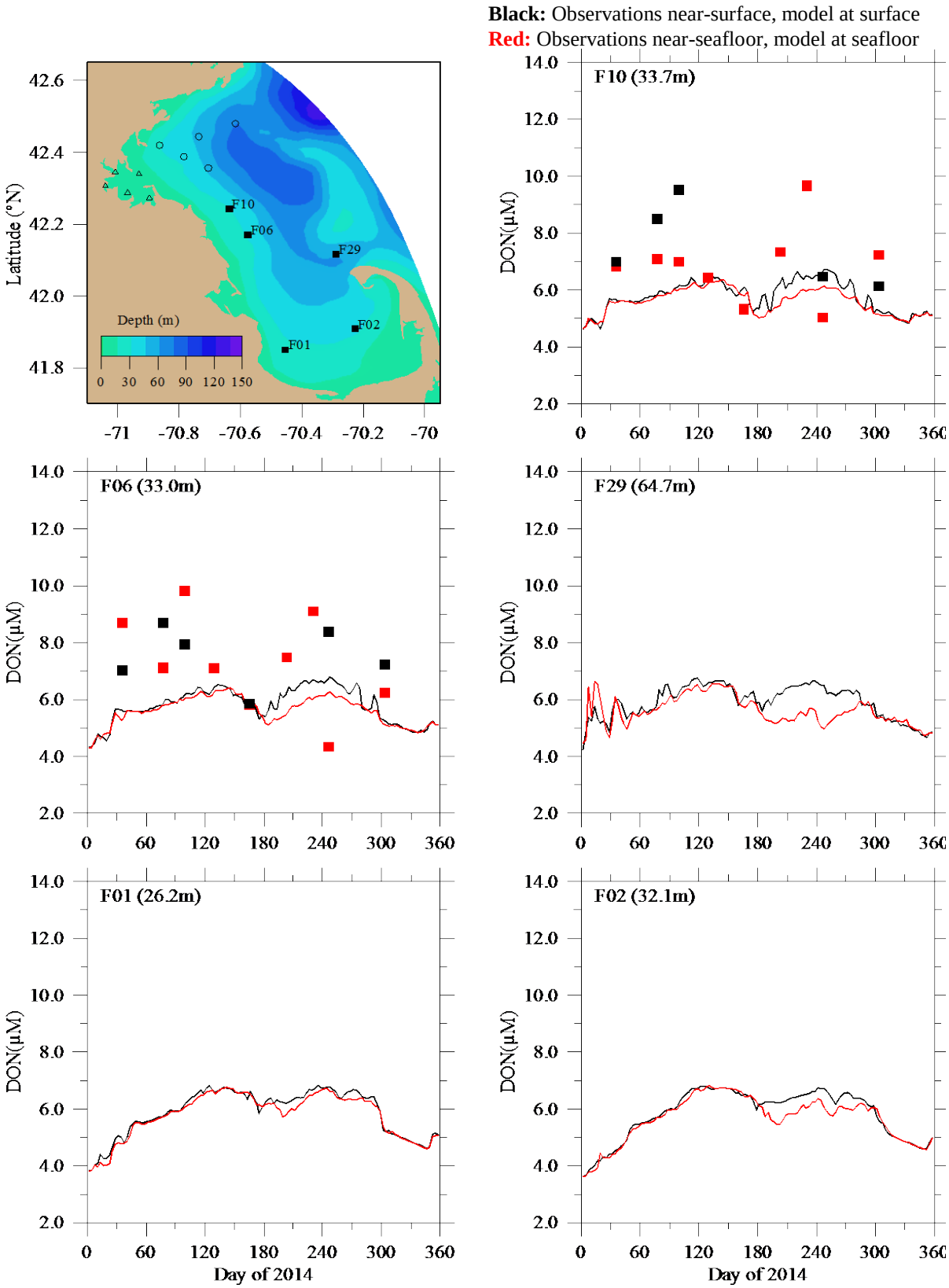

Figure 5-6b. Dissolved organic nitrogen. Southern stations. Model-observation comparisons. No observations were collected at stations F29, F01, or F02.

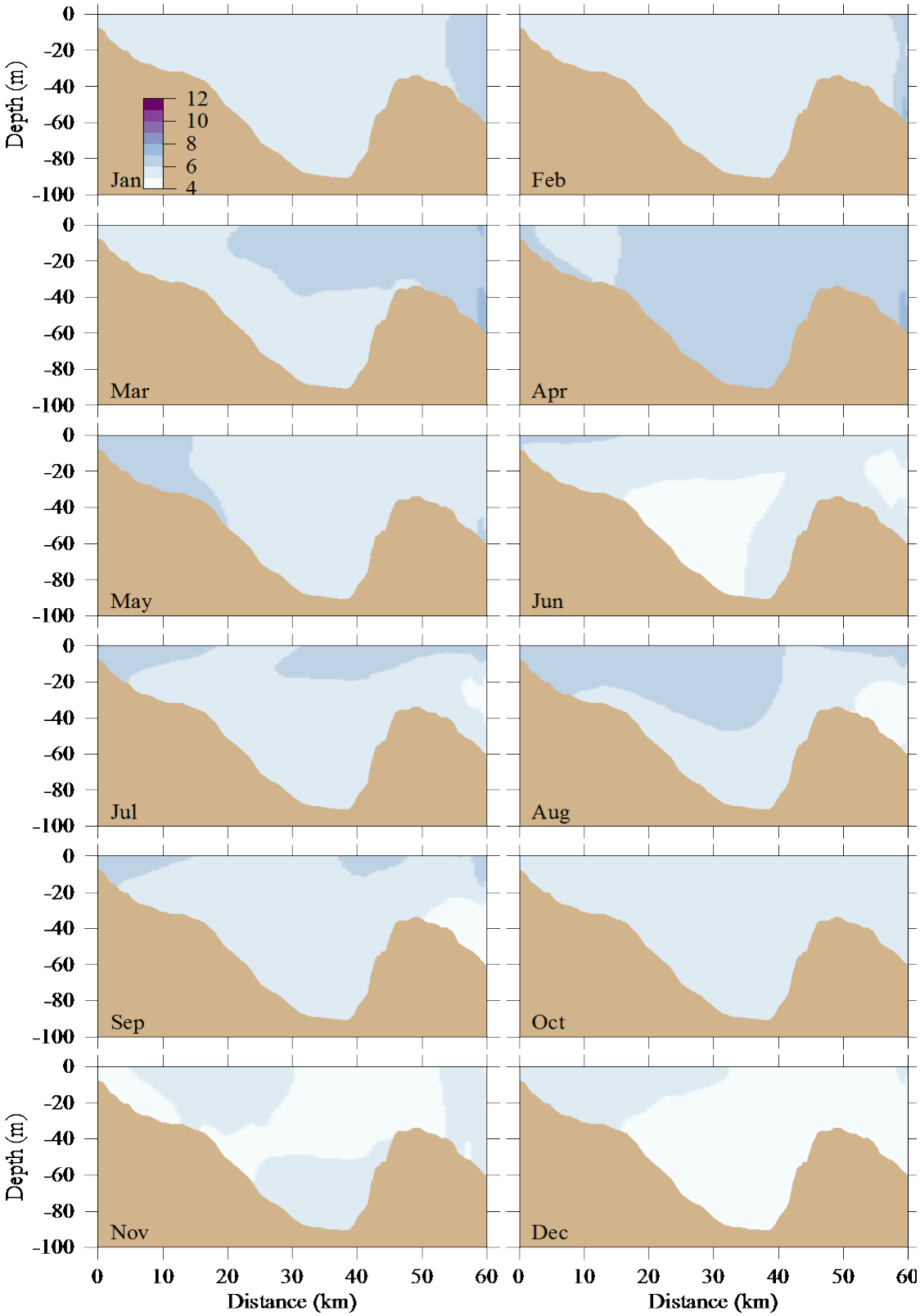

Figure 5-6c. Dissolved organic nitrogen (μM). Model results, east-west transect (Fig. 3-7). Horizontal axis is distance eastward from coast; outfall is on seafloor at approximately 13 km.

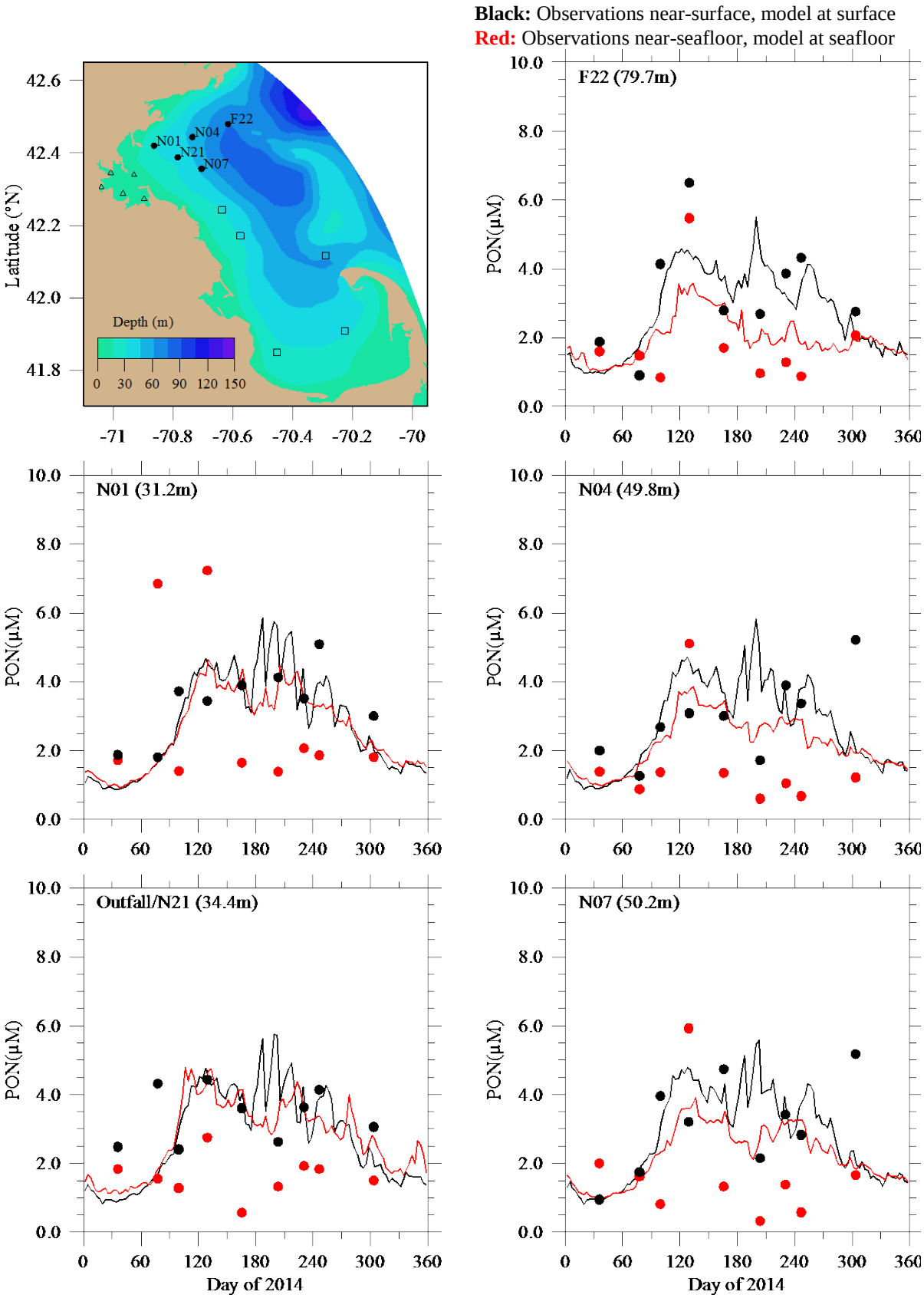

Figure 5-7a. Particulate organic nitrogen. Northern stations. Model-observation comparisons.

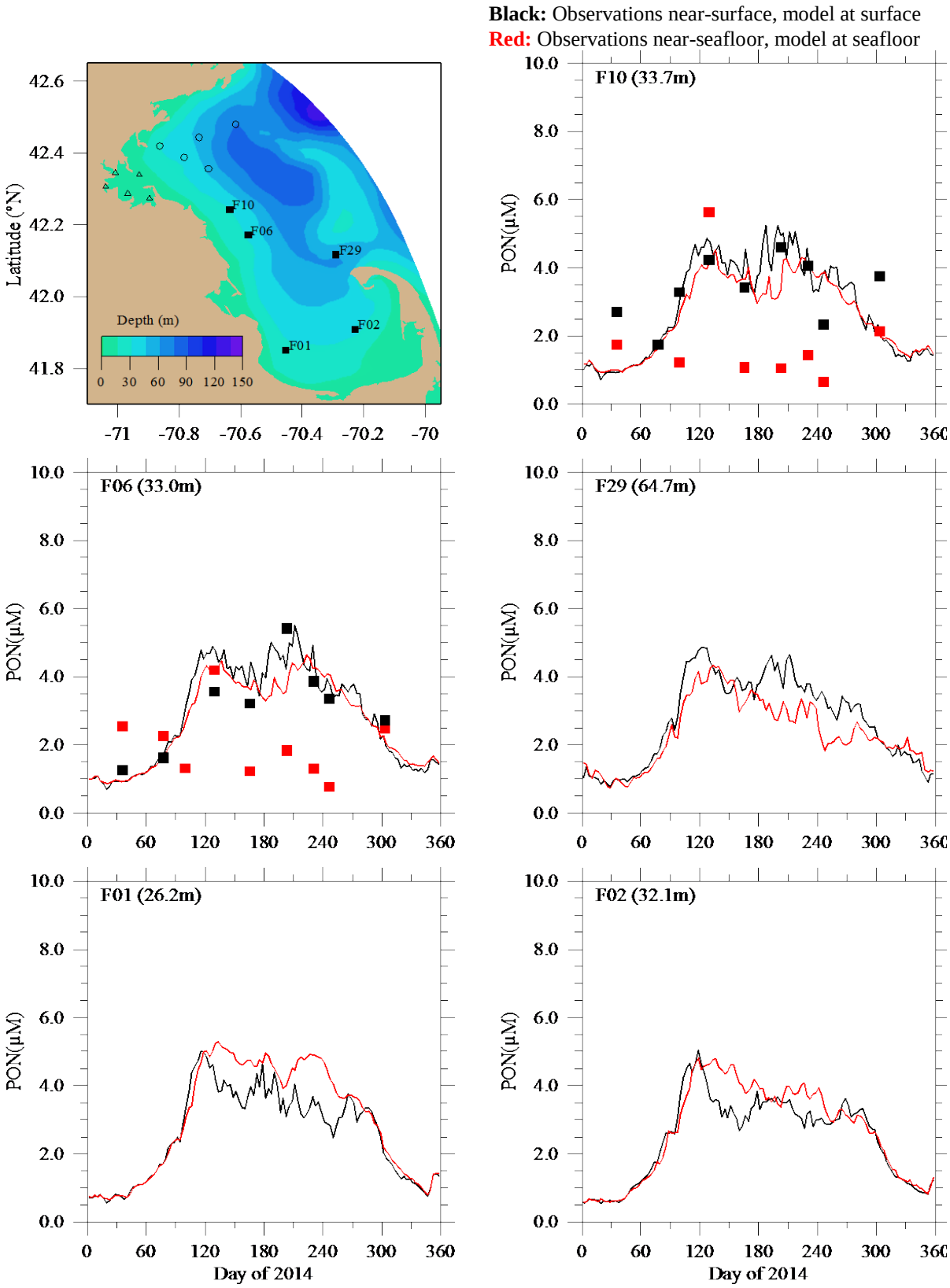

Figure 5-7b. Particulate organic nitrogen. Southern stations. Model-observation comparisons. No observations were collected at stations F29, F01, or F02.

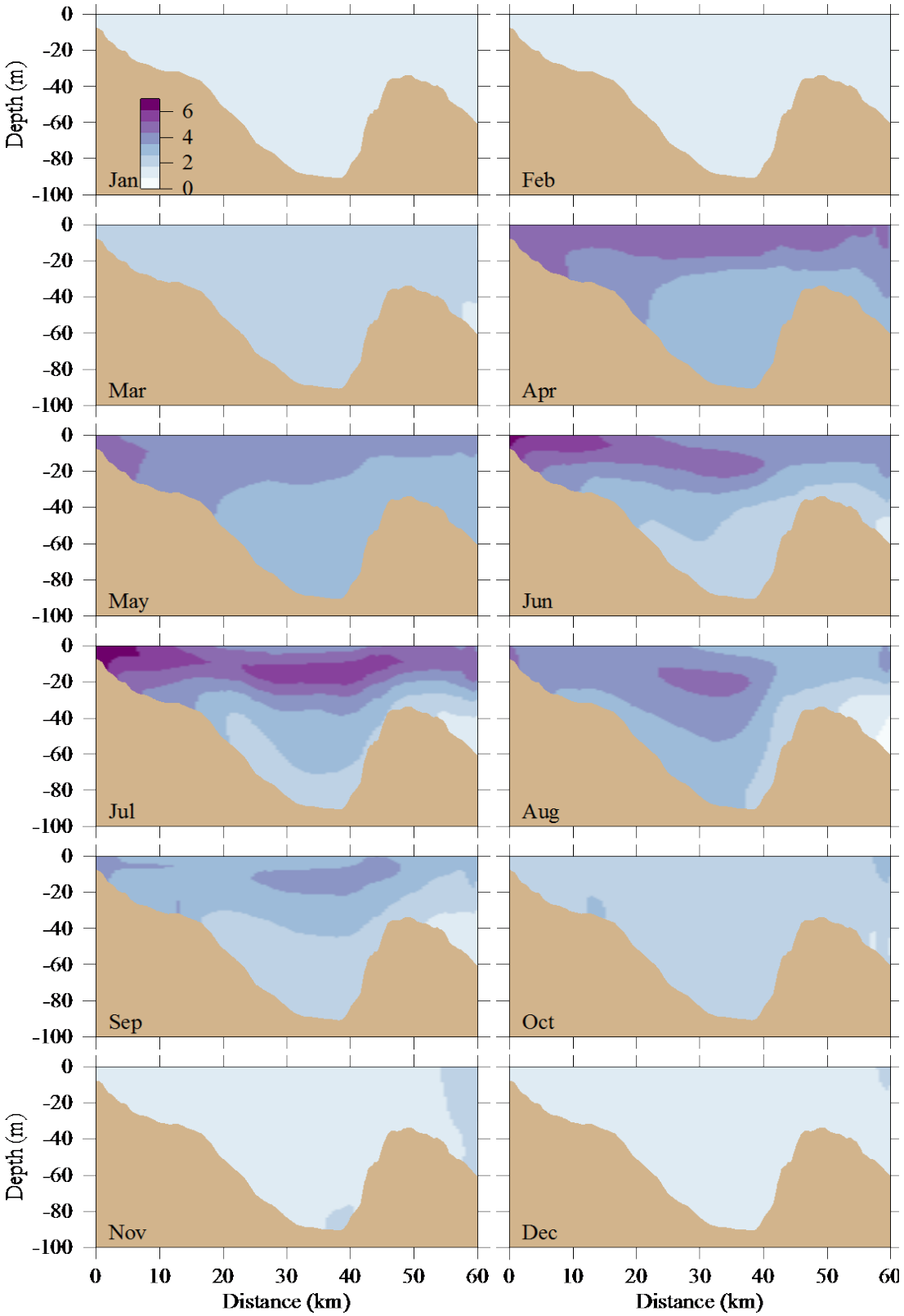

Figure 5-7c. Particulate organic nitrogen (μM). Model results, east-west transect (Fig. 3-7). Horizontal axis is distance eastward from coast; outfall is on seafloor at approximately 13 km.

5.6 *Particulate organic carbon*

The seasonal cycle in model particulate organic carbon (POC) during 2014 at Massachusetts Bay stations was clear (Figure 5-8a,b) and included minimum values in February and highest levels from late spring through early fall, with deep and shallow values typically similar to each other throughout the year. The ranges of model values were generally near the range of observed values, but at many stations the model results were biased higher than observations. In the observations, deep concentrations were almost all substantially lower than shallow values, while the opposite was true for much of the year at many stations in the model. This mismatch between the vertical structure of POC in the model and observations is apparently due to parameterization of biogeochemical processes in UG-RCA, given that the hydrodynamic model is capturing observed variations of vertical structure (stratification) well, as described above.

Model POC on the east-west transect in 2014 (Figure 5-8c) showed a region-wide pattern with the highest concentrations from April to June and the lowest concentrations during January and February. During January and February there was evidence of slightly elevated concentrations near the seafloor within 5-10 km of the outfall. Concentrations were otherwise generally homogenous in the vertical for most of the year, except during higher concentrations of May-August, when values between 20-30 m deep and the surface were higher than at deeper depths.

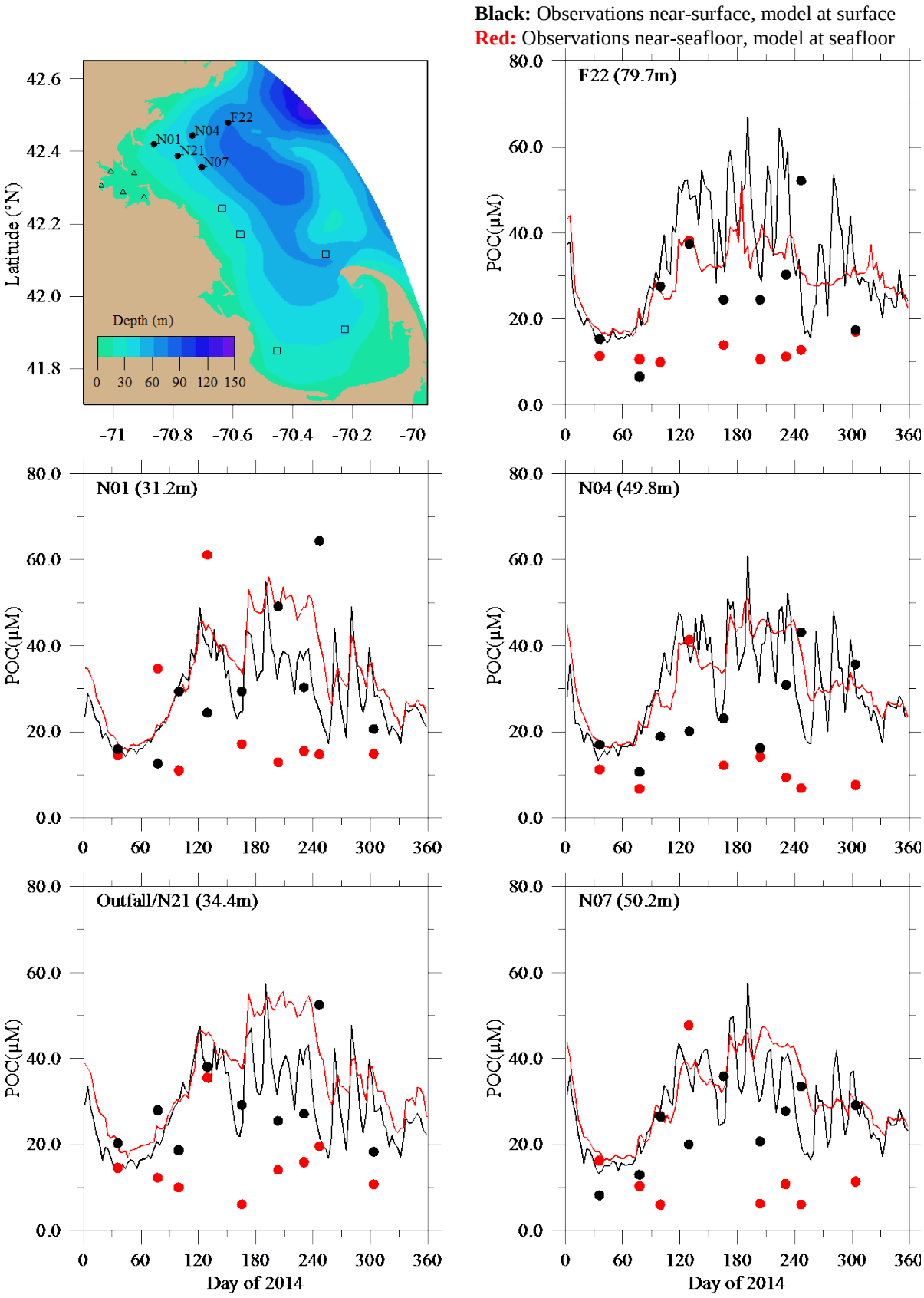

Figure 5-8a. Particulate organic carbon. Northern stations. Model-observation comparisons.

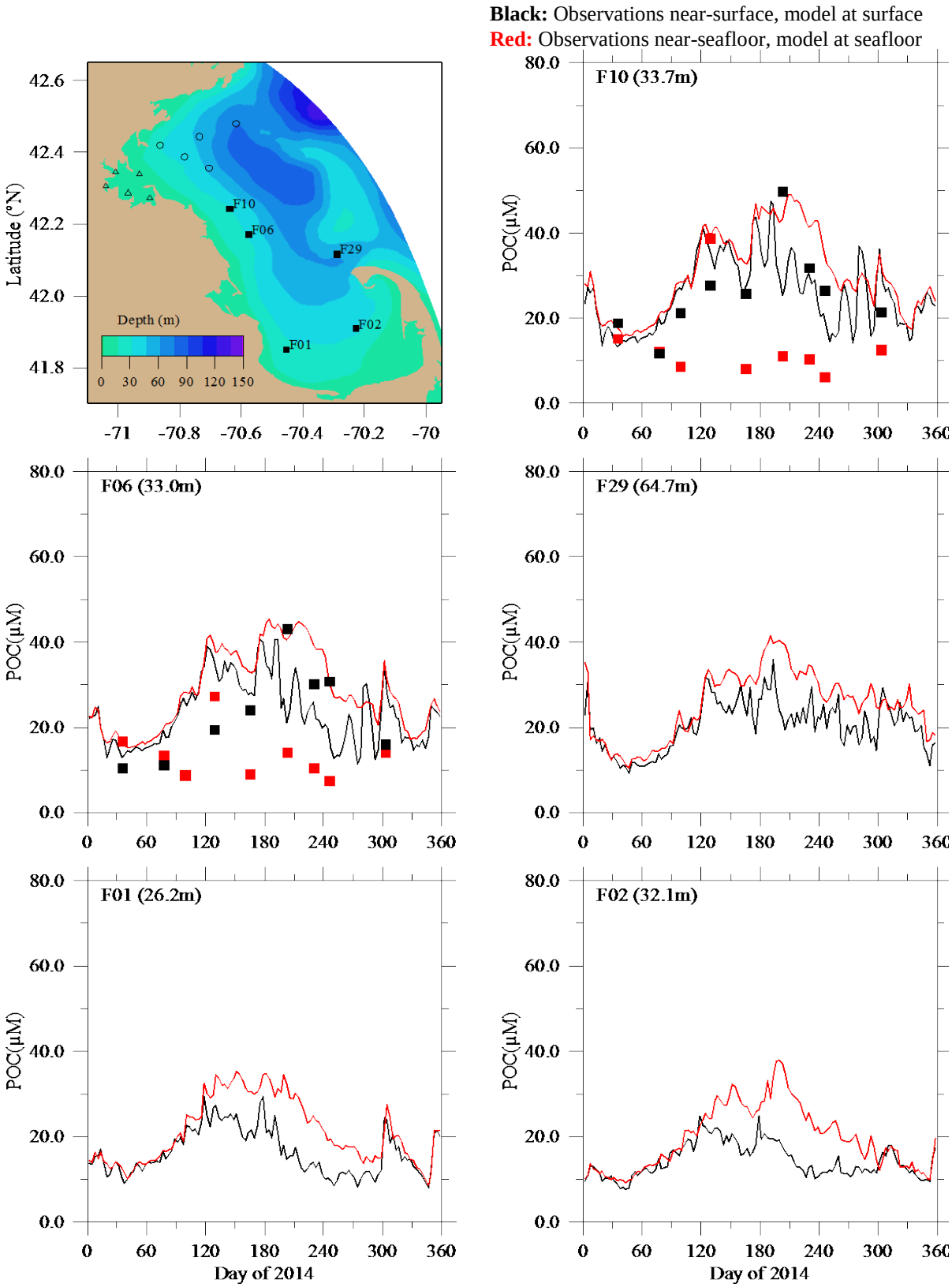

Figure 5-8b. Particulate organic carbon. Southern stations. Model-observation comparisons. No observations were collected at stations F29, F01, or F02.

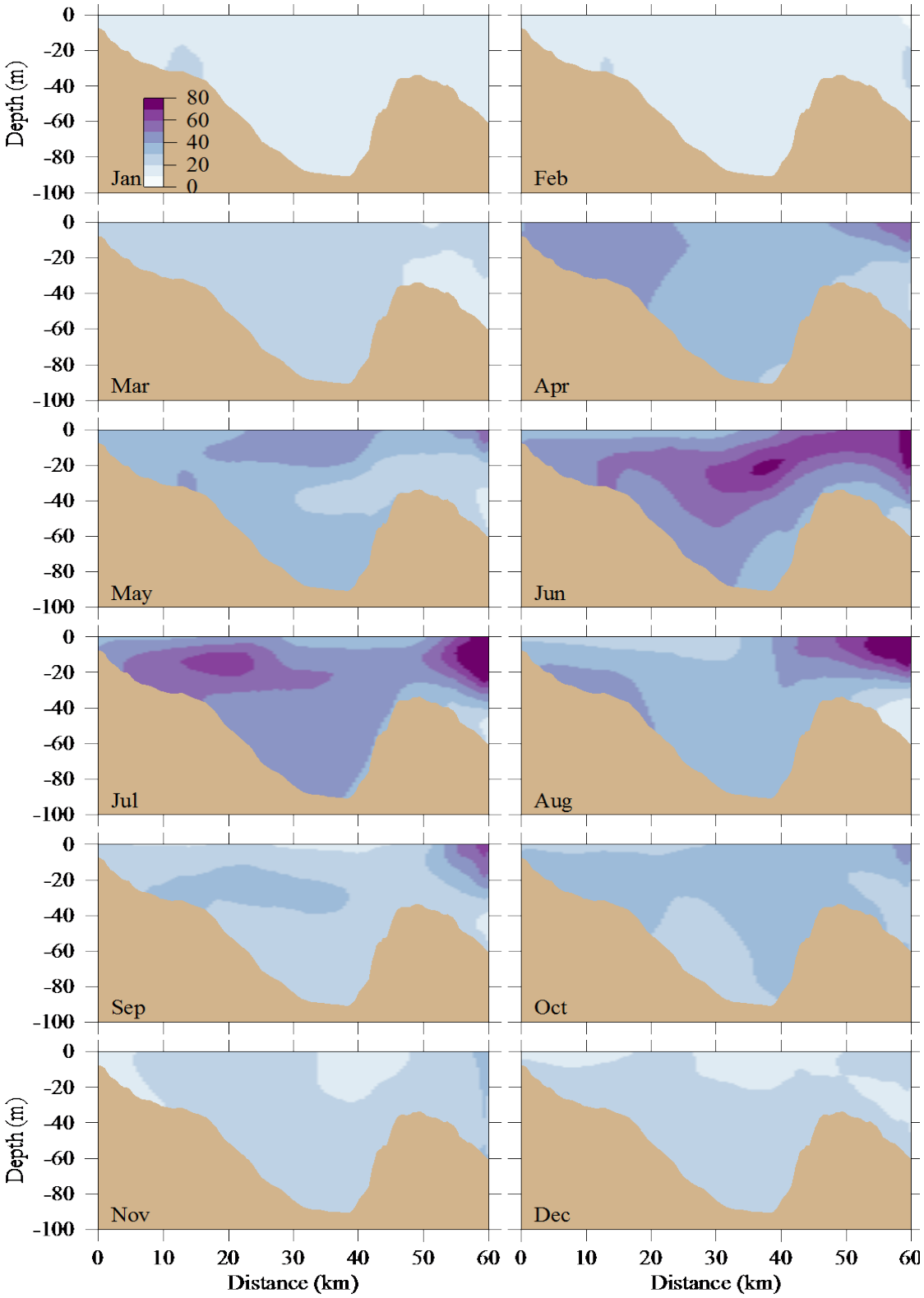

Figure 5-8c. Particulate organic carbon (μM). Model results, east-west transect (Fig. 3-7). Horizontal axis is distance eastward from coast; outfall is on seafloor at approximately 13 km.

5.7 *Dissolved oxygen*

The observed seasonal cycle in dissolved oxygen concentration (peak in spring, decrease through summer to minimum in late fall, then increase) in 2014 was reproduced by the model reasonably well at Massachusetts Bay and Cape Cod Bay stations (Figure 5-9a,b). The model included bias toward underestimation at both the surface and bottom, compared to observations. As noted above (Figure 5-1) the correlation between modeled and observed DO concentrations was 0.90 near the bottom, with root-mean square (RMS) error of 0.67 mg L^{-1}. Concentrations are highest in spring and lowest in late summer, with values near the surface generally higher than near the bottom. The model-observation differences in the 2014 simulation were similar in magnitude to those of previous years. Model DO concentration on the west-east transect (Figure 5-9c) showed the same general patterns as those found in previous years.

DO percent saturation depends on temperature and salinity as well as oxygen concentration, and is a useful quantity to help understand the relative influence of temperature and photosynthesis on DO. Percent saturation above 100% can result from photosynthetic production. We computed DO saturation from observations of DO concentration, temperature, and salinity using the approximate relation given in equation 2.3 of Zhao et al. (2012). Comparisons between this result and observed DO saturation (Figure 5-10a,b) reveal reasonable agreement. The pattern is similar at most stations, and on the east-west transect (Figure 5-10c), with reaeration due to exchange between atmosphere and ocean playing a dominant role as described by Xue et al (2014). In winter, DO saturation levels are modest due to weaker reaeration, and vertical mixing keeps them nearly vertically uniform; in spring, photosynthesis increases surface values, which remain higher through summer when reaeration is most active, while levels in deeper water steadily decrease because they are isolated by stratification. The deep minimum is reached in late summer, after which the fall overturn returns the system to winter conditions.

Finally, model DO concentration and percent saturation have also been compared (Figure 5-11) directly to the only available time series observations, from near the surface (2 m deep) and 51 m deep at the Mooring A01 site (see Figure 1-1) in northeastern Massachusetts Bay. In order to minimize the influence of intermittent sensor noise due to bubble sweepdown, daily medians of the raw hourly near-surface measurements are used; also, there were no near-surface observations from Jan - May. The general patterns of seasonal variations in the model, as described above, agree well with observations. The oxygen concentration at depth in the model is biased high compared to the

observations, particularly during late summer. Near the surface, model concentrations overestimated observations during summer then underestimated them through the fall. In percent saturation, model-observation differences at 51 m were less pronounced than for concentration.

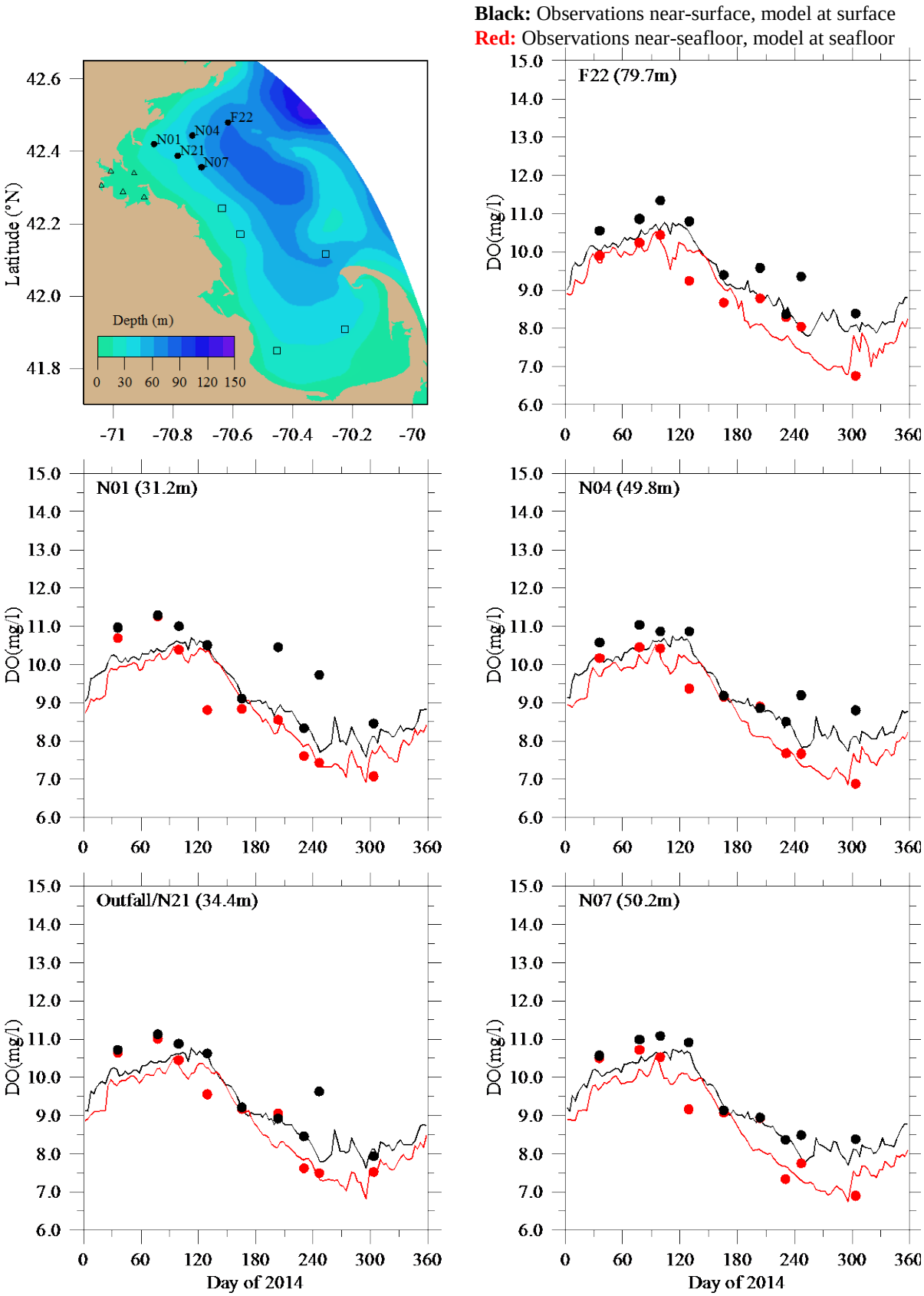

Figure 5-9a. Oxygen concentration. Northern stations. Model-observation comparisons.

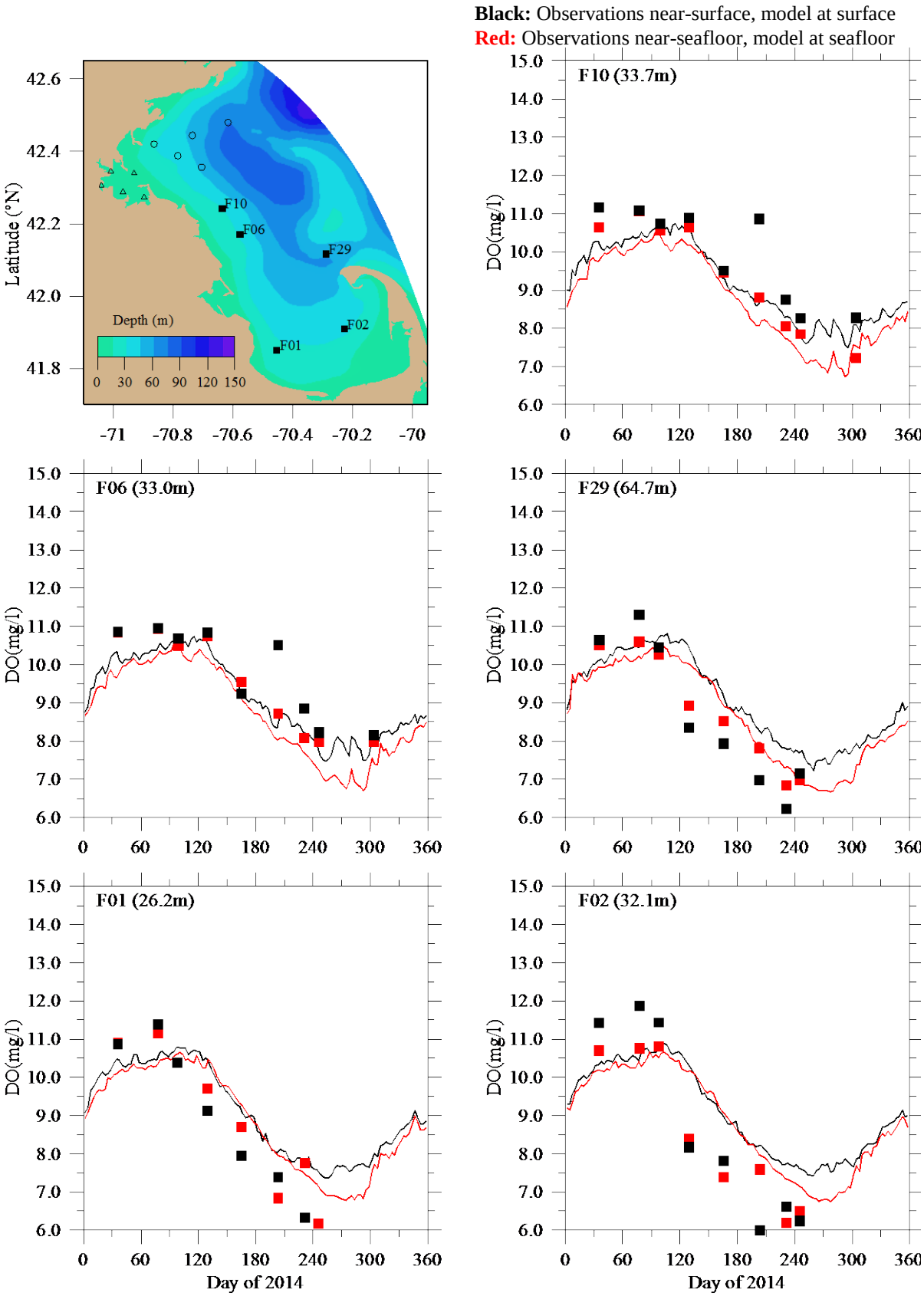

Figure 5-9b. Oxygen concentration. Southern stations. Model-observation comparisons.

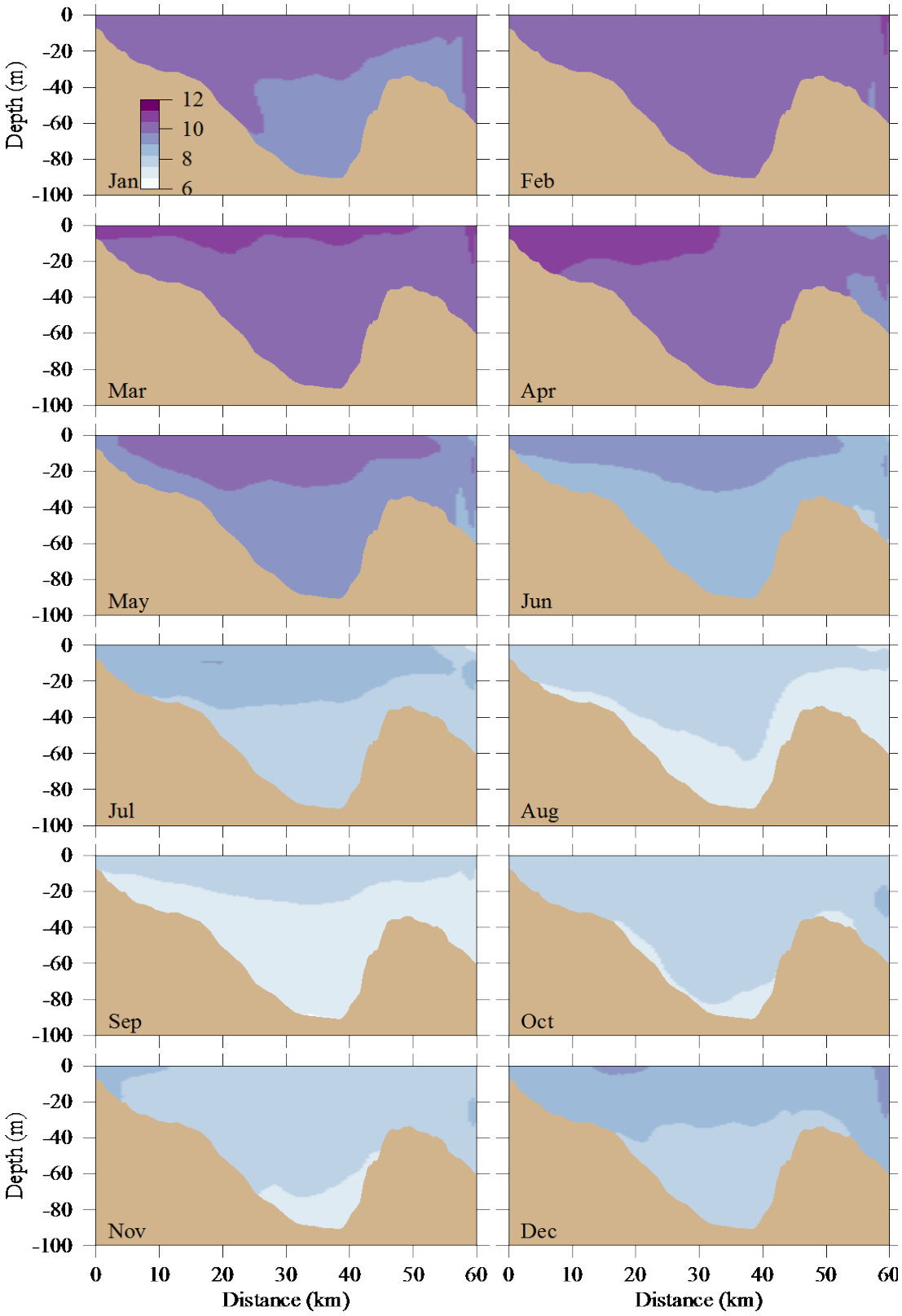

Figure 5-9c. Oxygen concentration (mg L^{-1}). Model results, east-west transect (Fig. 3-7). Horizontal axis is distance eastward from coast; outfall is on seafloor at approximately 13 km.

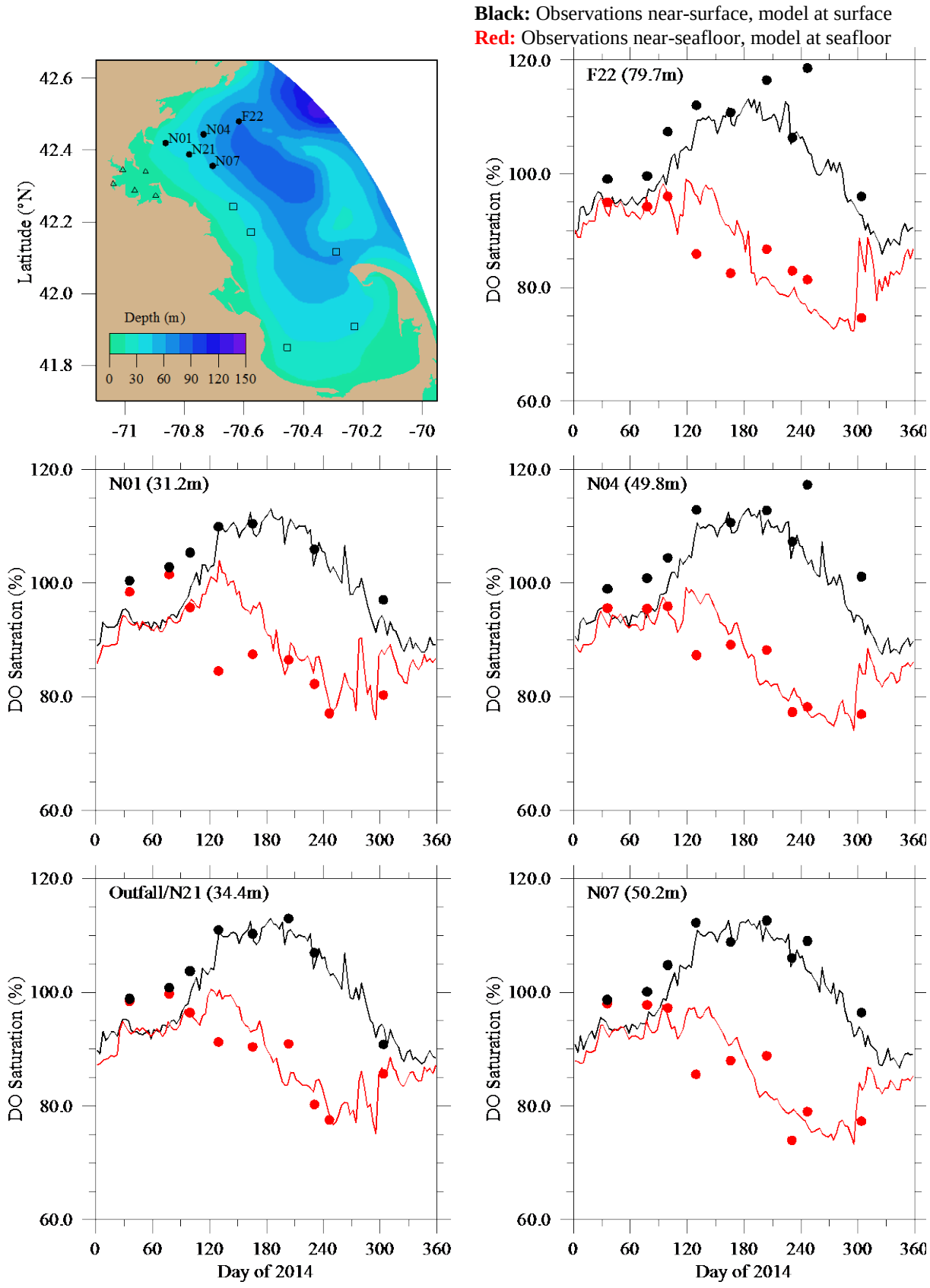

Figure 5-10a. Oxygen percent saturation. Northern stations. Model-observation comparisons.

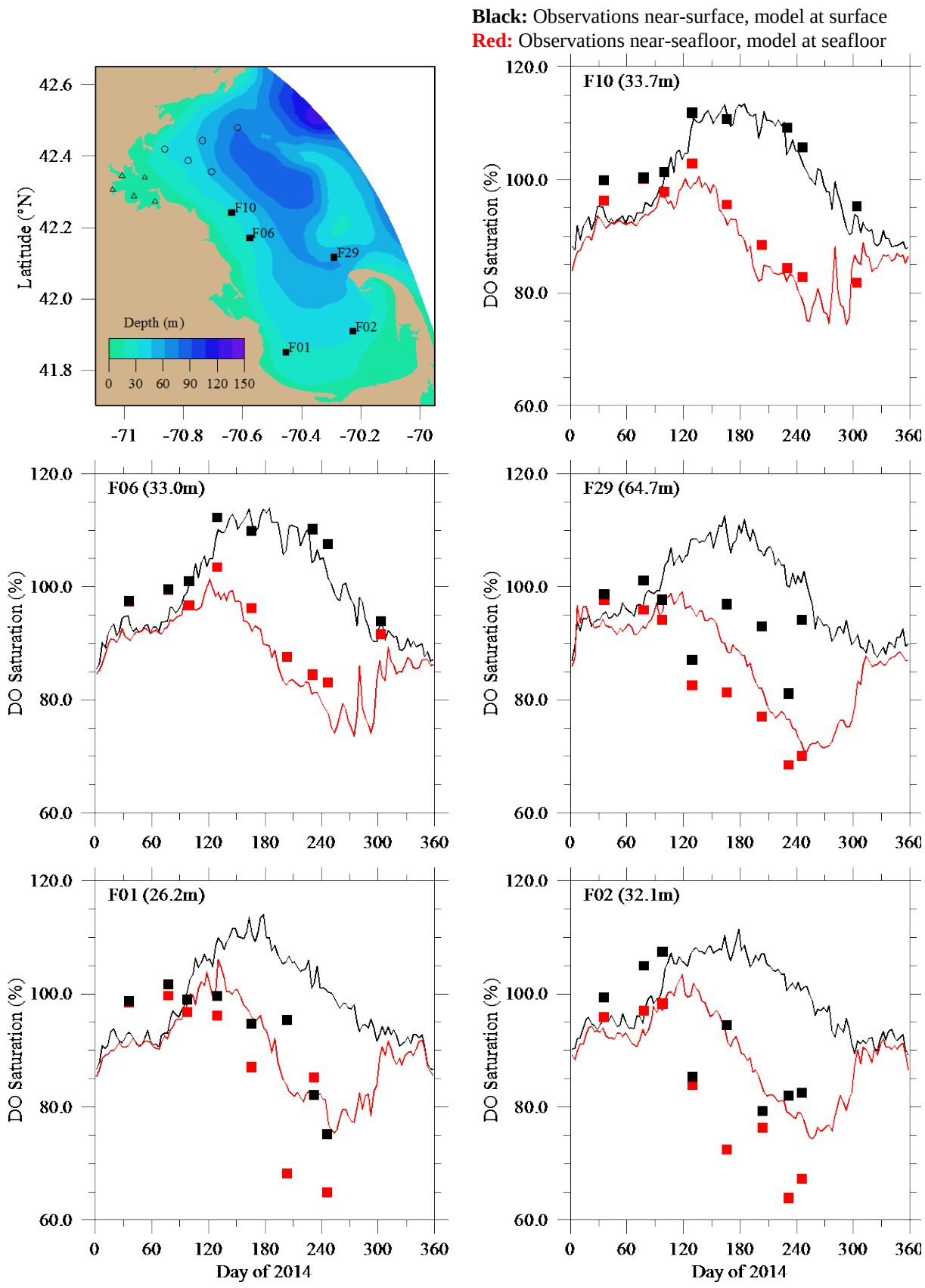

Figure 5-10b. Oxygen percent saturation. Southern stations. Model-observation comparisons.

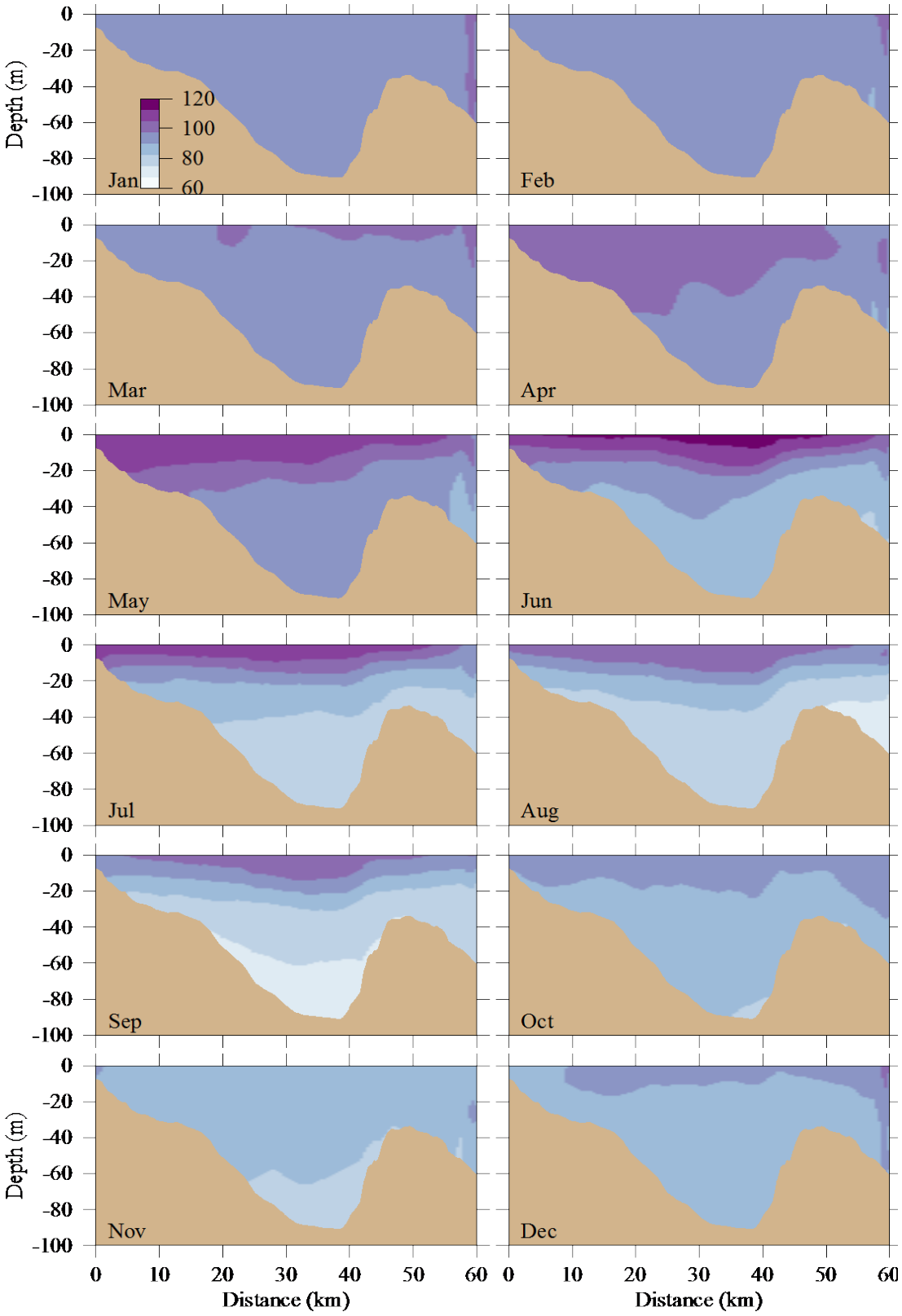

Figure 5-10c. Oxygen percent saturation. Model results, east-west transect (Fig. 3-7). Horizontal axis is distance eastward from coast; outfall is on seafloor at approximately 13 km.

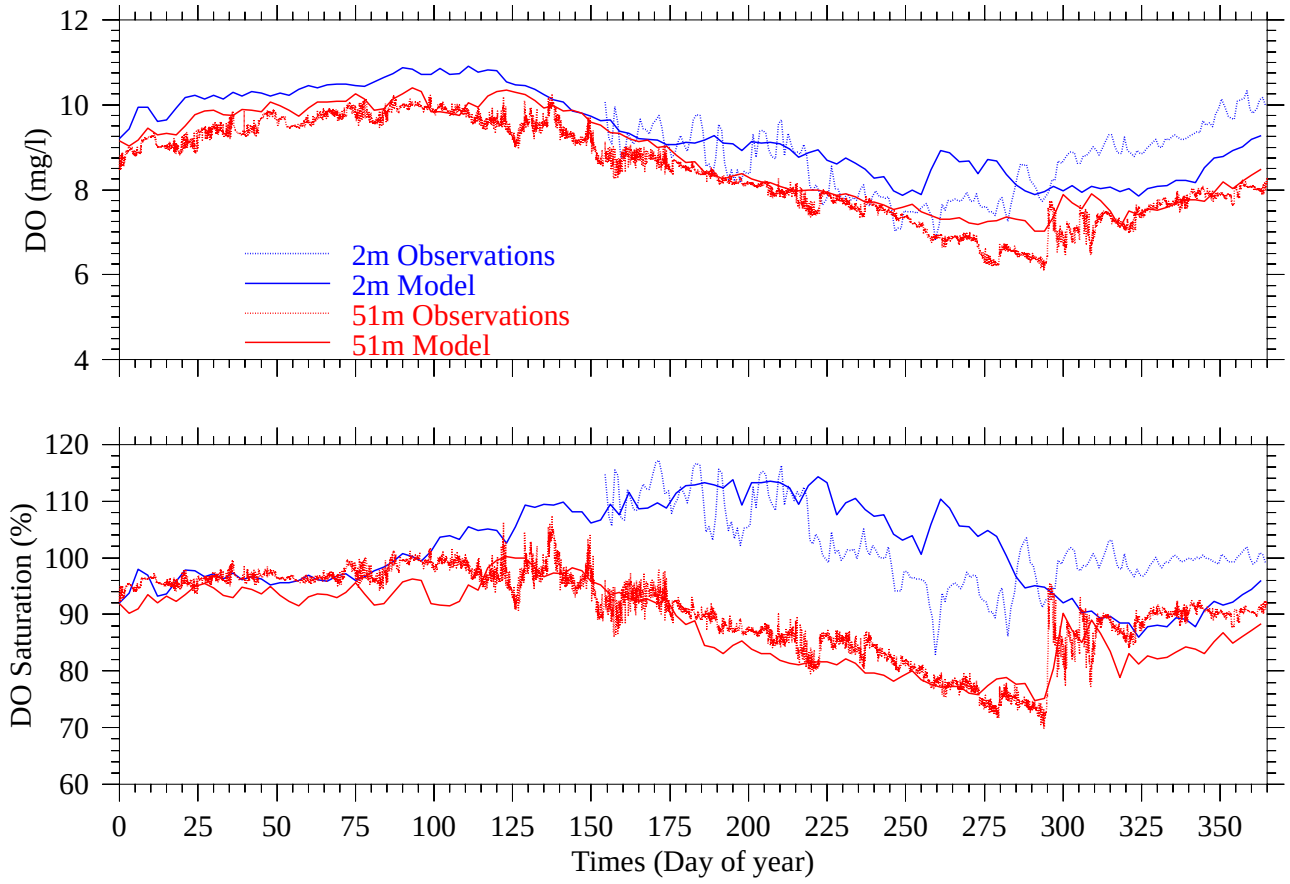

Figure 5-11. Oxygen time series, Mooring A01 site, model-observation comparison.

5.8 *Sediment fluxes*

Sediment NH_4^+ fluxes and sediment oxygen demand (SOD) from the 2014 simulation are shown in Figure 5-12 and Figure 5-13 from the Massachusetts Bay and Boston Harbor stations where flux measurements had been made most consistently in earlier years, to best facilitate model-observation comparisons. Ongoing field sampling no longer includes these benthic fluxes, but to provide context the observations from 2000-2010 are superimposed as box-whisker plots (as described in Section 5.4) on the model results (the field program and its results are described in MWRA technical reports, for example Tucker et al., 2010). Observations from prior to 2001 were not included, because diversion of the outfall to its current location occurred in 2000. At harbor stations the model NH_4^+ flux in 2014 was nearly zero except during about 5 months from summer to early fall, and systematically lower than the range of observed values. At bay stations it was nearly zero except between May and December, and had values within the range of prior observations although with notable bias higher than them at station MB05. Model SOD at harbor stations exhibited seasonality, and low bias relative to observations, similar to the NH_4^+ flux there. At bay stations, model SOD had similar seasonality to the NH_4^+ flux there; relative to the range of observations, model values were low in the spring and early summer, near the lower end of the range in summer, and within the range in fall. These characteristics and relationships to observations for the 2014 simulation are similar to those of simulations from earlier years.

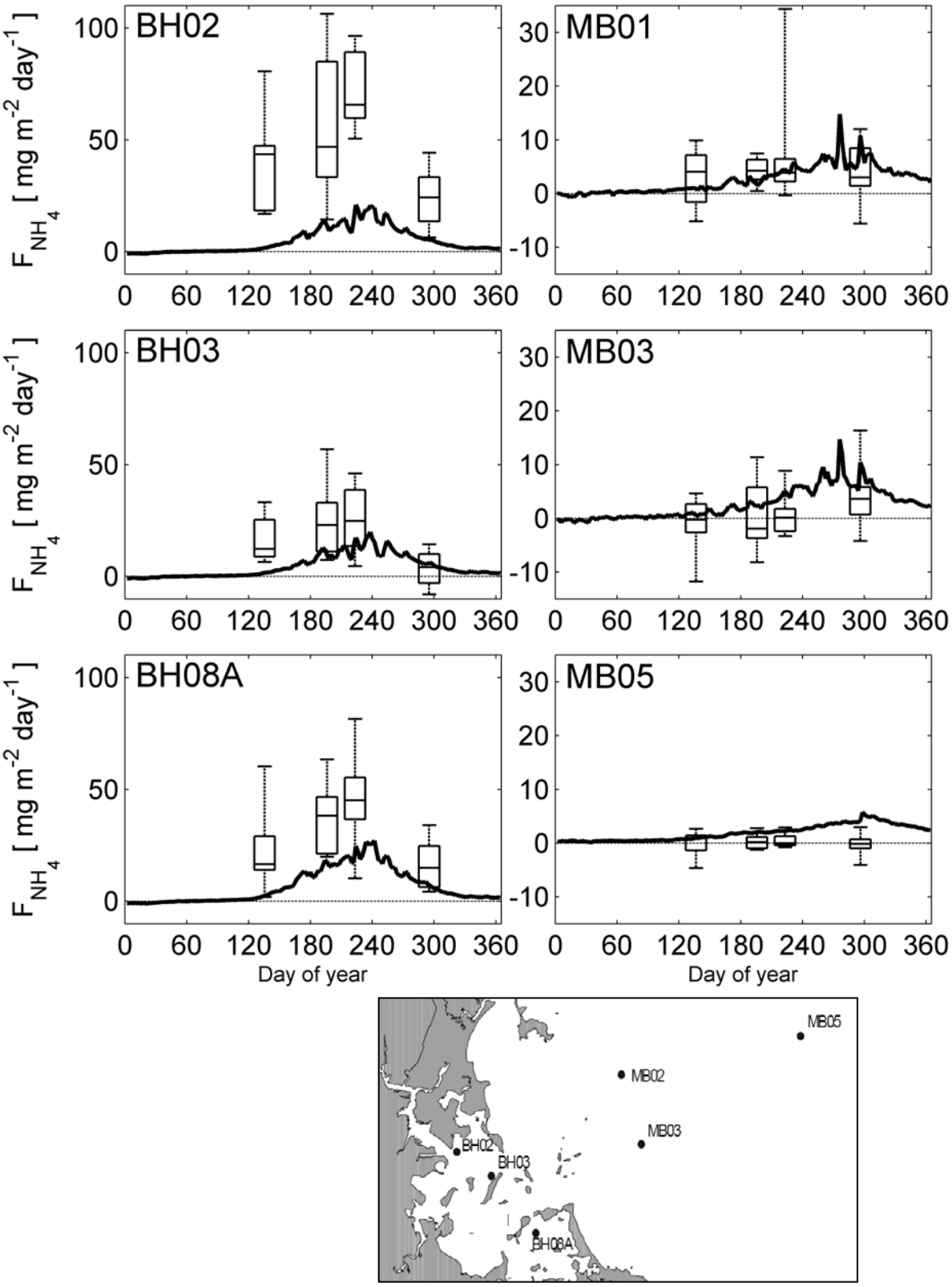

Figure 5-12. Sediment NH4+ flux. Model 2014 (line), observed 2001-2010 (box-whiskers). Select Boston Harbor stations (left column) and Massachusetts Bay stations (right column).

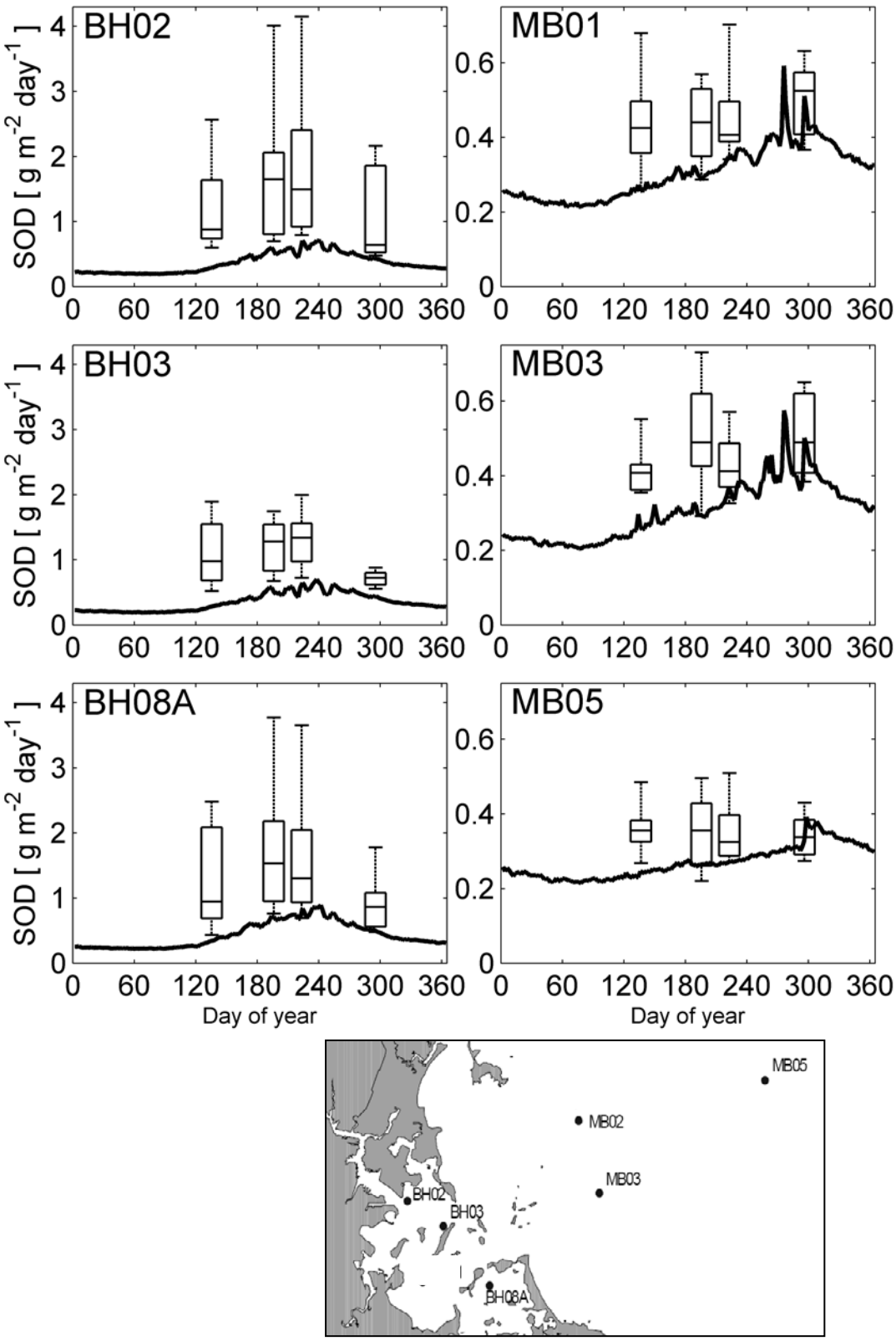

Figure 5-13. Sediment oxygen demand. Model 2014 (line), observed 2001-2010 (box-whiskers). Select Boston Harbor stations (left column) and Massachusetts Bay stations (right column).

5.9 *Summary*

In summary, the UG-RCA 2014 simulation captured many of the observed seasonal and vertical variations of an array of key water quality parameters examined here. Among them, agreement of the model with observations was generally strongest for DIN and DO, modest for light, DON, and PON, and weakest for POC and chlorophyll. Temporal and spatial variability in the model is typically less than observed, and at most stations surface-bottom differences in the model are smaller than observed.

6. Notable features during 2014

The modeling team worked with scientists from the MWRA field monitoring program to identify features of observed 2014 conditions to investigate with additional, more focused, model analyses. They identified two main features. The first feature was the unusually late duration of winter temperatures, which may have delayed the winter-spring phytoplankton bloom (Libby et al. 2015). The second feature was the spring onset and fall breakdown of density stratification, in particular the nature of its short-timescale (days to weeks) progression and vertical structure; during 2014, the spring onset included a brief but prominent destratification event, and the fall breakdown was unusually early at shallow depths (Libby et al. 2015).

6.1 *Delayed onset of winter-spring phytoplankton bloom*

As described by Libby et al. (2015) and summarized in Section 1c above, the MWRA monitoring program field observations revealed that the 2014 winter-spring bloom, which was modest in strength, was delayed by about a month compared to a typical year, until late April and May. The observations also demonstrated that temperatures during March and April of 2014 were much colder than in past years, while the timing of stratification was not particularly different from a typical year. Inter-annual variations such as these are relatively common. It is important to understand the extent to which they are captured by the water quality model.

We focus here on the timing of the spring increases and decreases in nutrients, particulate organic carbon, and chlorophyll in the model, in an effort to assess the degree to which they corresponded to the delayed bloom seen in the observations. During a typical bloom the nutrients phytoplankton consume, such as dissolved inorganic nitrogen, are drawn down to low concentrations near the surface. At about the same time, particulate organic carbon and chlorophyll concentrations rise due to increased phytoplankton abundance.

The seasonal cycles of dissolved inorganic nitrogen, particulate organic carbon, and chlorophyll in the model at outfall station N21 during 2014 were plotted in comparison to the long-term average seasonal cycles based on the 1995-2014 BEM simulations, and the standard deviations of individual years about the long-term mean (Figure 6-1a,b). The long-term average and standard deviations in dissolved inorganic nitrogen (lines in top frames of figures) portray the typical pattern, with shallow concentrations falling off in March and April and remaining low through summer while deep concentrations are sustained relatively high. Both near-surface and near-bottom 2014

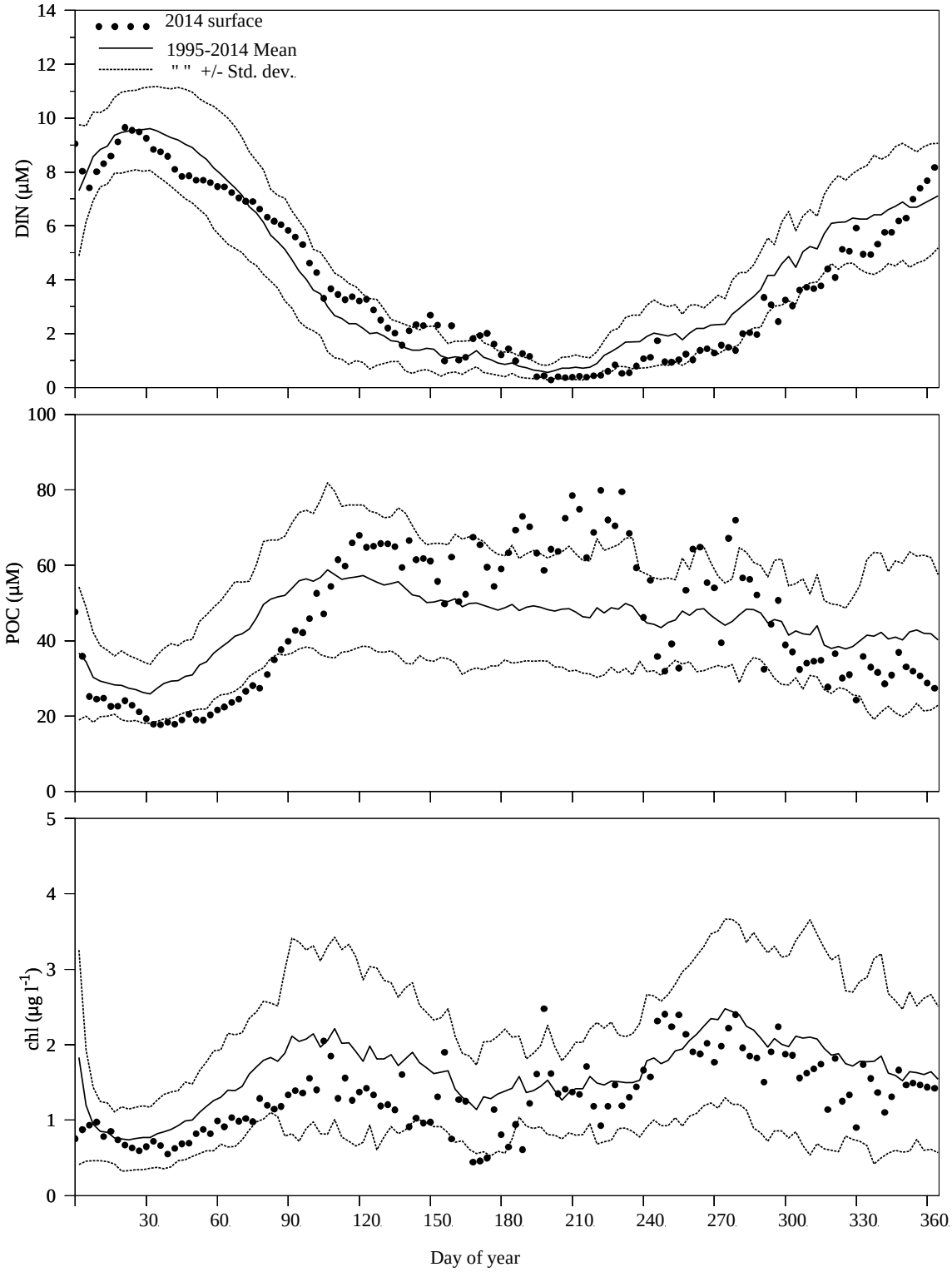

Figure 6-1a. Model DIN, POC, chlorophyll; 2014 compared to 1995-2014 conditions. Surface.

Top frame: Dissolved inorganic nitrogen. Middle frame: Particulate organic carbon. Bottom frame: chlorophyll.

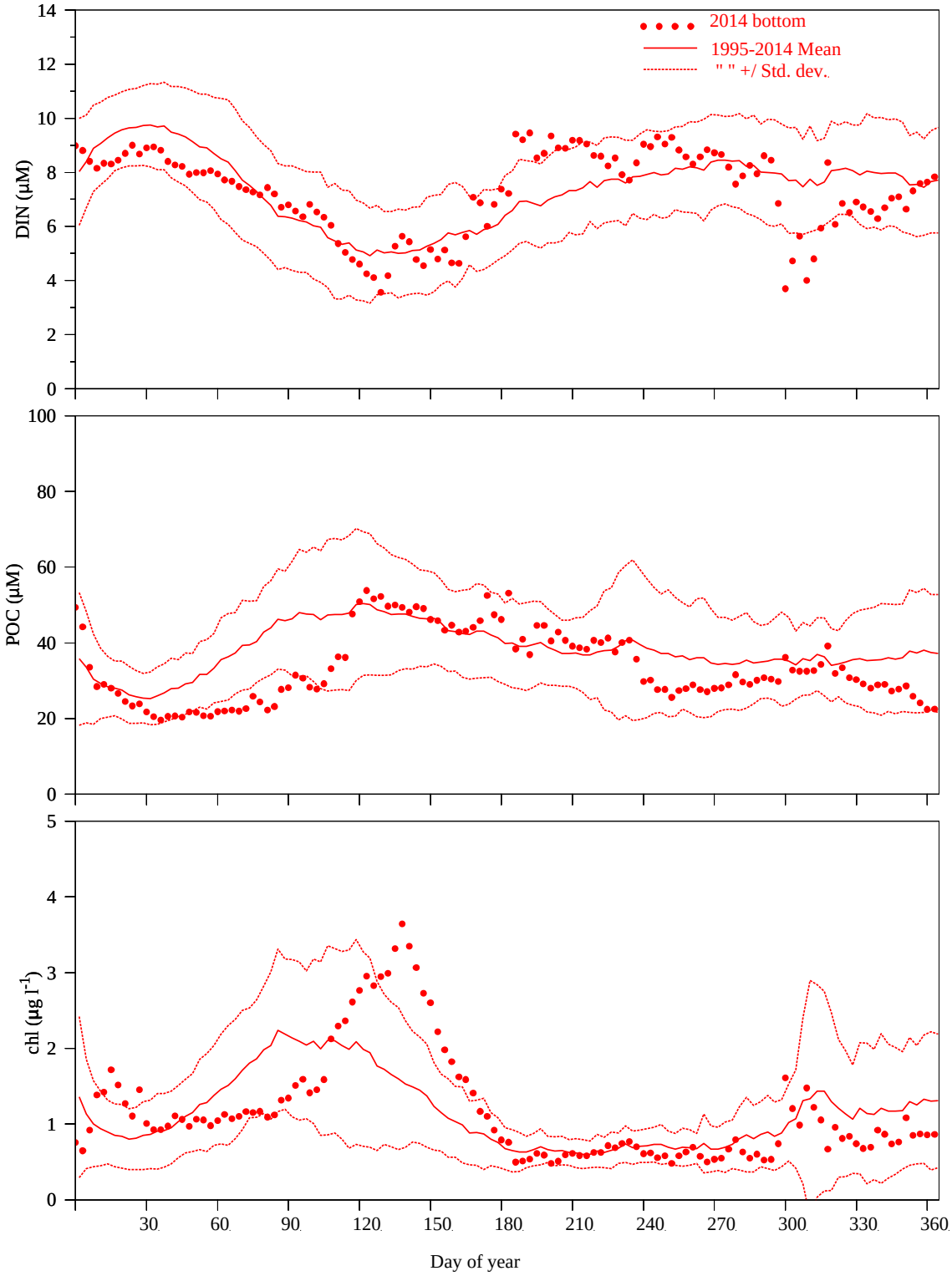

Figure 6-1b. Model DIN, POC, chlorophyll; 2014 compared to 1995-2014 conditions. Seafloor.

Top frame: Dissolved inorganic nitrogen. Middle frame: Particulate organic carbon. Bottom frame: chlorophyll.

dissolved inorganic nitrogen (dots in top frames) followed the pattern of the long-term means and generally remained within one standard deviation of the mean. The springtime decrease in shallow concentrations was later than average, to a modest degree, with the concentration remaining higher than the long-term mean during nearly all of April and May but by less than one standard deviation.

For particulate organic carbon, long-term mean near-surface and near-seafloor conditions (lines in middle frames of Figure 6-1a,b) are similar to each other. Both are minimal in winter, peak in spring, then decrease slightly but remain elevated through summer and most of fall. The near-bottom concentrations are generally less than surface concentrations year-round, but nearest to them during the fall and winter. The amplitude of the springtime increase in the long-term mean seasonal cycle is comparable to or less than the ranges of interannual variability. In 2014, the onset of the spring increase in both shallow and deep concentrations (dots in middle frames) was delayed by between one and two months relative to the long-term mean, with both being lower than the mean by more than one standard deviation until late March. Shallow concentrations then rose to above the long-term mean by late April, and deep concentrations reached the long-term mean by the start of May. These characteristics are consistent with the observed late timing of the 2014 spring increase in phytoplankton.

In chlorophyll, although the inter-annual variability is also pronounced, the long-term mean and standard deviations (lines in bottom frames of Figure 6-1a,b) reveal a springtime peak centered on April at both depths, with a secondary surface increase through late summer and fall. The 2014 chlorophyll results (dots in bottom frames) from the surface include a springtime peak that was weaker than average and not notably later than the typical growth period; bottom concentrations include a peak that is both one month later than typical and reaches substantially more than one standard deviation higher than the long-term mean. The observations of high concentrations in May, identified as a senescing bloom of *Phaeocystis* by Libby et al. (2015), were most pronounced at depth.

In summary, many important features of DIN, POC, and chlorophyll in the 2014 simulation were unusual compared to long-term model means and variability, in ways that are consistent with the late winter-spring bloom observed during 2014. Unlike the 2014 observations, in the 2014 simulation the shallow chlorophyll increase was not later than typical and the deep chlorophyll had a larger than typical spring peak. However, prominent aspects of the 2014 simulation were

consistent with the unusual 2014 observations, including surface DIN that decreased later than typical, and both POC and deep chlorophyll that increased substantially later than is typical.

6.2 *Development and breakdown of stratification*

The spring onset and fall breakdown of density stratification are complex processes involving responses to multiple factors including surface heating, wind-driven mixing, and advection. Vertical density differences (stratification) typically vary strongly on timescales of days to weeks, and are themselves characterized by detailed vertical structure within the water column. Prominent examples of these features were on display in the 2014 observations (Libby et al., 2015). Stratification had begun to develop during early April, when a storm led to full destratification for several days, after which new stratification was established that grew and persisted through the summer season. In the fall, storms broke down stratification in the upper water column earlier than usual, but stratification at depth persisted at least a month longer.

These variations in the timing and vertical structure of stratification are an important factor influencing water quality, through their effects on plankton growth and dissolved oxygen distributions. It is therefore useful to assess model fidelity in properly representing them. Detailed time series of vertical structure of density stratification in the model has been compared to observations from Mooring A01 in northeastern Massachusetts Bay during spring (Figure 6-2a) and fall 2014 (Figure 6-2b).

For the spring onset of stratification (Figure 6-2a) there is close agreement between BEM and the observations, with regard to both temporal evolution and vertical structure. Gradual seasonal-timescale changes are punctuated by several storm events, which include both temperature and salinity signatures. The general characteristics of each event in the observations are present in the model. This includes the event on about April 15 when the initially developed stratification was effectively entirely removed, after which stratification developed again and persisted. The most prominent differences in temperature are at the middle (20 m) and deeper (50 m) of the three depths shown. At the middle depth, temperature events in the model track the observations less well than at the surface, but the long-term bias is not prominent; in contrast, at the deeper depth, model temperatures are systematically higher than observations, by up to 2 degrees. In salinity, the most notable differences are at the shallowest and deepest depths; near the surface, model salinity decreases during short-term events are stronger than observed, while at the deepest depth the model is systematically fresher than observations. Both the higher temperature and lower salinity in the

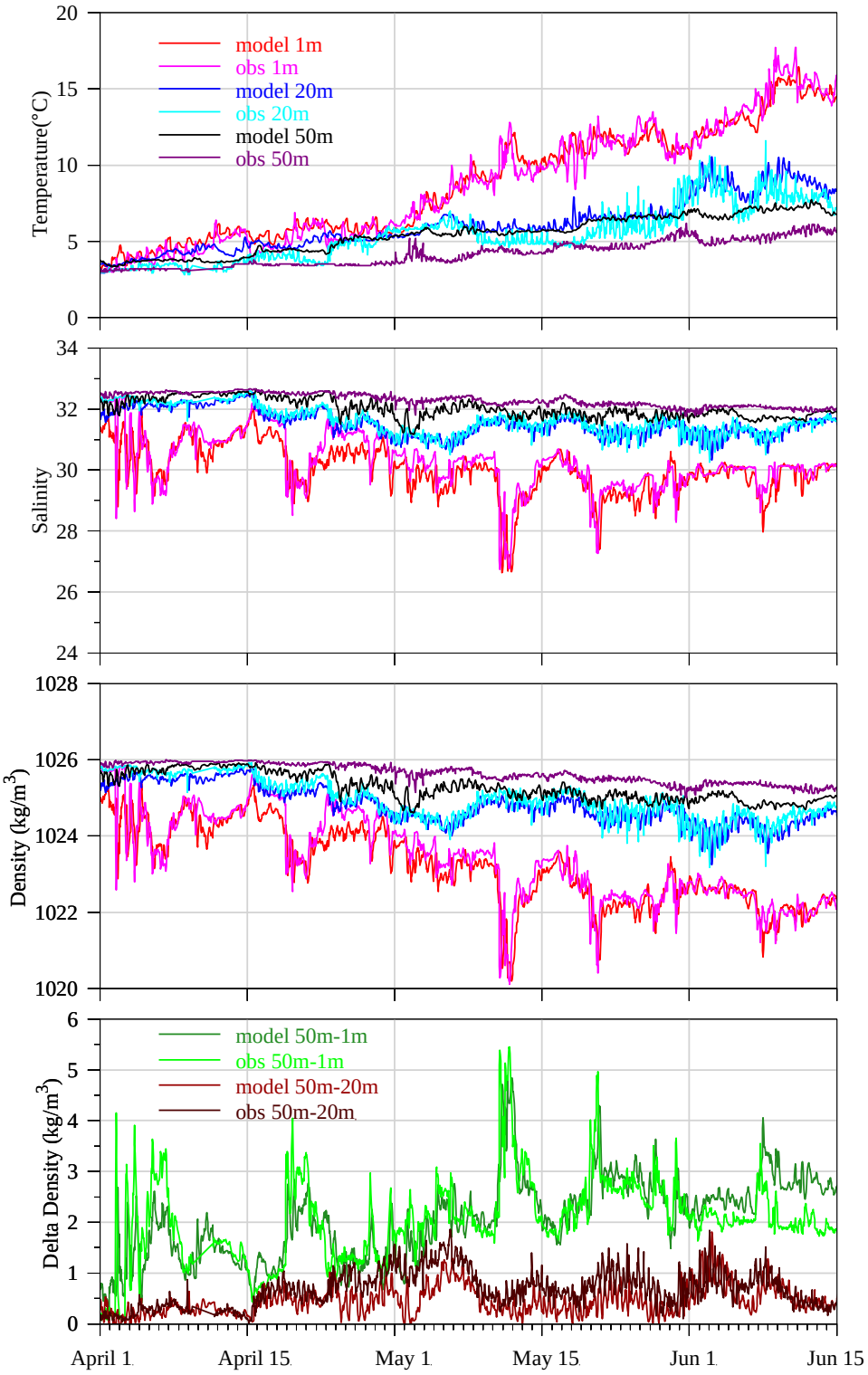

Figure 6-2a. Spring onset of density stratification, model-observation comparison.

Top frame: Temperature. Second frame: Salinity. Third frame: Density. Bottom frame: Stratification, vertical difference in density.

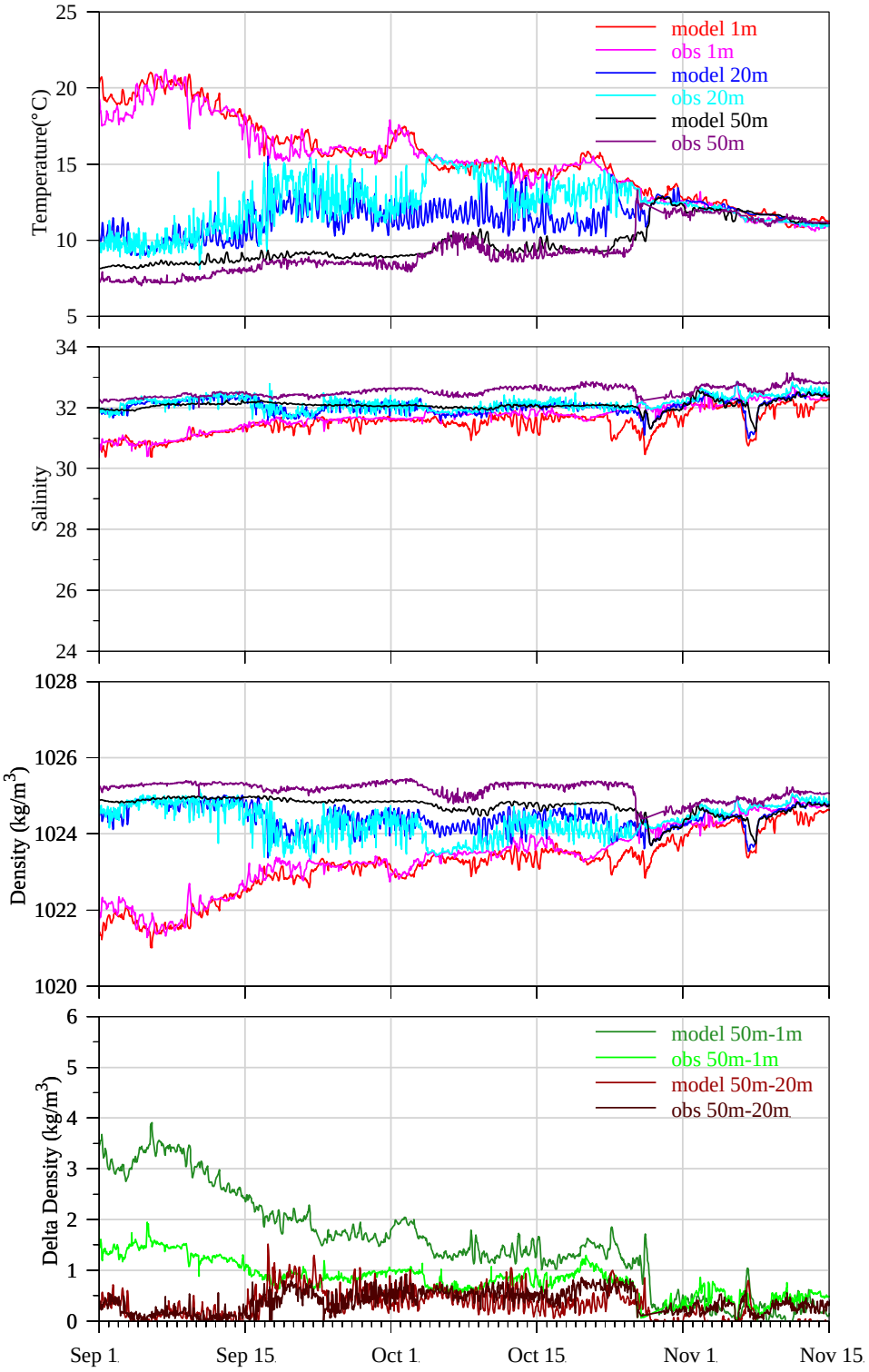

Figure 6-2b. Fall breakdown of density stratification, model-observation comparison.

Top frame: Temperature. Second frame: Salinity. Third frame: Density. Bottom frame: Stratification, vertical difference in density.

model at 50 m compared to observations cause the modeled deep density to be lower than observed. This leads to model stratification that is weaker than observed, as is particularly evident in the 50m-20m density difference (bottom, Figure 6-2).

During the fall breakdown (Figure 6-2b) model-observation agreement is comparable to that in spring, but reveals certain differences that are more pronounced. Surface temperatures agree best. Mid-depth temperature agrees well during most of the record, with the notable exception of a period in early October when the model did not warm to match surface temperatures as the observations did, in association with destratification at shallow depths. Deep model temperatures were biased high, as during spring, though by a smaller amount. Model salinities showed more pronounced differences from observations. Agreement was best at the middle depth. At the shallow depth, freshening events were more common and more pronounced in BEM than in observations. At the deepest depth, model salinities were markedly less variable than observations, with a systematic low bias that was stronger (up to 0.75) than that during the springtime. The net effect on density stratification was that the model strongly overestimated upper water column stratification for most of the time period, missed the shallow destratification event during early October, and had some spurious short-duration peaks due to shallow freshening. The model did however capture well the abrupt destratification later in October.

These comparisons to field measurements are a demanding test of hydrodynamic model performance and confirm that the simulation is capturing many detailed aspects of the observations.

7. Summary

The Marine Ecosystem Dynamics Modeling Laboratory at University of Massachusetts Dartmouth simulated hydrodynamic and water quality parameters for calendar year 2014 in Massachusetts Bay, Cape Cod Bay, and Boston Harbor using the unstructured-grid models MB-FVCOM and UG-RCA respectively. The methods were as in the prior year's simulation (described in Zhao et al., 2015b).

The main features of observed seasonal cycles in temperature and salinity were captured well by the hydrodynamic model. The seasonal cycle of stratification in the model also agreed reasonably well with observations. Comparisons of observed currents were favorable.

Overall patterns in seasonal variations and vertical structure of many water quality parameters in the model were in good agreement with observations. In comparison to field measurements, the model typically showed a smaller range of values, and smaller surface-bottom differences during the stratified season. The well-known observed spring/summer reduction in shallow DIN concentrations due to phytoplankton uptake, and later fall replenishment due to enhanced mixing when stratification breaks down, were apparent in the model and consistent with observations. The model also reproduced the main characteristics of the observed seasonal cycle of DO, with peaks in spring when shallow values increase due to phytoplankton growth, continuous decreases through summer and early fall, followed by replenishment during the winter mixed period. In addition to these bay-wide patterns, near the seafloor local to the outfall (within 10-20 km) dissolved inorganic nitrogen was elevated, but this was not the case for other water quality parameters including chlorophyll. Agreement of model DON and PON with observations was modest, and model POC showed relatively poor agreement with measurements, particularly with regard to vertical structure. In summary, model-observation agreement was generally strongest for DIN and DO, modest for DON and PON, and weakest for POC and chlorophyll. Overall, the simulations support the conclusions of the field monitoring program, that the outfall does not have an appreciable influence on bay-wide ecosystem function.

Agreement with observations was generally better for the hydrodynamic model than for the water quality model. This is not unusual, in the context of current research methods for simulations of coastal waterbodies such as Massachusetts Bay and Cape Cod Bay. In part this is a result of the less complete scientific understanding of the complex biological and chemical processes that are represented in water quality models. The model must include such processes but can only use

substantially simplified formulations for them, leading to larger differences when compared to observations. In addition, for the biological and chemical parameters of the water quality model, observations available to drive and verify the model are less spatially and temporally extensive compared to parameters important to the hydrodynamic model. An example of the latter is that water temperatures, and the strength and direction of winds, are monitored at least hourly at multiple Gulf of Maine locations. In contrast, the most substantial field sampling effort for water quality parameters has been the MWRA Ambient Monitoring program, which consists of vessel-based surveys 3-4 weeks apart and focuses on measuring and understanding outfall effects, so can only partially characterize the regional nutrient and plankton dynamics.

Focused investigations of two notable features identified in 2014 observations were carried out, in order to help gauge the fidelity of the model in representing them. The first feature was the timing of the winter-spring bloom, which was observed to occur 1-2 months later than in a typical year, in association with the correspondingly late duration of cold winter temperatures even though stratification did not develop later than in a typical year. In the water quality model, although some aspects of springtime conditions did not agree well with observations, other key characteristics differed from results of prior years' modeling in ways that were consistent with the observations. In the 2014 simulation the shallow increase in chlorophyll was not later than typical and the deep chlorophyll increase was notably larger than in a typical year, neither of which were noted aspects of the 2014 observations. However, in the 2014 simulation the timing of DIN depletion from shallow waters was later than typical, and both the particulate organic carbon and deep chlorophyll were substantially later than in a typical year. These are prominent features of the winter-spring bloom that were consistent with the 2014 observations. This is an indication of the effectiveness of forcing the water quality model with offshore boundary conditions that are determined using monitoring survey observations.

The second notable feature of 2014 observations that was examined carefully in the 2014 simulations was the detailed timing (on timescales of days to weeks) and vertical structure of stratification during its spring development and fall breakdown. To gauge model fidelity, the temperature, salinity, and density structure of the 2014 hydrodynamic model results was compared directly to hourly timeseries measurements from Mooring A01 south of Cape Ann. During the springtime stratification development the model-observation agreement for temporal variations and vertical structure of stratification was very good, including during a prominent short-term

destratification event. During the fall breakdown of stratification, the model was stratified more strongly than observed, due mainly to bias in the deep salinity and temperature, and did not capture the short timescale variations as thoroughly as during spring. The high overall level of model-observation agreement is an indication of the effectiveness of assimilation of temperature and salinity observations by the hydrodynamic model. It confirms that representation of stratification in the hydrodynamic model should not be a major limitation to the fidelity of the water quality model.

References

Beardsley RC, EE Adams, D Harleman, A Giblin, JR Kelly, JE O'Reilly, and JF Paul, 1995. Report of the MWRA hydrodynamic and water quality model evaluation group. MWRA Enviro. Quality Dept. Misc. Rpt. No. ms-37. Boston: Massachusetts Water Resource Authority. 58pp. http://www.mwra.state.ma.us/harbor/enquad/pdf/1995-ms-37.pdf

Becker S, 1992. The seasonal distribution of nutrients in Massachusetts and Cape Cod Bays. Masters Thesis, University of New Hampshire, Durham. 127pp.

Blumberg A, Z Ji, and CK Ziegler, 1996. Modeling outfall plume behavior using a far field model, *J. Hydraulic Engineering*, 112: 610-616.

Chen C, B Beardsley, GW Cowles, J Qi, Z Lai, G Gao, D Stuebe, Q Xu, P Xue, J Ge, R Hu, R Ji, R Tian, H Huang, H Wu, H Lin, Y Sun, and L Zhao, 2013. An Unstructured grid, Finite-Volume Community Ocean Model-FVCOM User Community-FVCOM user manual, School for Marine Science and Technology, University of Massachusetts Dartmouth, New Bedford, Fourth Edition. SMAST/UMASSD Technical Report-13-0701, 404pp.

Chen C, R Tian, RC Beardsley, J Qi, and Q Xu, 2010. Modeling 2008 in Massachusetts Bay using an upgraded unstructured-grid Bays Eutrophication Model. Boston: Massachusetts Water Resources Authority. Report 2010-15. 127pp. http://www.mwra.state.ma.us/harbor/enquad/pdf/2010-15.pdf

Chen, C, H Haung, RC Beardsley, Q Xu, R Limeburner, GW Gowles, Y Sun, J Qi and H Lin, 2011. Tidal dynamics in the Gulf of Maine and New England Shelf: An application of FVCOM. *J. Geophys. Res., 116*. C12010, doi: 10.1029/2011JC007054.

Fitzpatrick JJ and RA Isleib, 2003. Post-audit analysis of the impacts of wastewater treatment plant outfall relocation on Boston Harbor, Massachusetts Bay and Cape Cod Bay water quality Proceedings of the Water Environment Federation, WEFTEC 2003, pp. 530-555.

Hunt CD, RK Kropp, JJ Fitzpatrick, P Yodzis, and RE Ulanowicz, 1999**.** A Review of Issues Related to the Development of a Food Web Model for Important Prey of Endangered Species in Massachusetts and Cape Cod Bays. Boston: Massachusetts Water Resources Authority. Report ENQUAD 99-14. 62 pp. http://www.mwra.state.ma.us/harbor/enquad/pdf/1999-14.pdf

HydroQual, 1993. A water quality model for Massachusetts and Cape Cod Bays. Boston: Massachusetts Water Resources Authority. Report 1993-05. 222pp. http://www.mwra.state.ma.us/harbor/enquad/pdf/1993-05.pdf

HydroQual, 1995. A water quality model for Massachusetts and Cape Cod Bays: Calibration of the Bay Eutrophication Model (BEM). Boston: Massachusetts Water Resources Authority. Report 1995-08. 402pp. http://www.mwra.state.ma.us/harbor/enquad/pdf/1995-08.pdf

HydroQual, 2000. Bays Eutrophication Model (BEM): modeling analysis for the period 1992-1994. Boston: Massachusetts Water Resources Authority. Report 2000-02. 158pp. http://www.mwra.state.ma.us/harbor/enquad/pdf/2000-02.pdf

HydroQual, 2002a. Sensitivity of the Bays Eutrophication Model (BEM) to changes in algal model coefficients. Boston: Massachusetts Water Resources Authority Report 2002-16. 236pp. http://www.mwra.state.ma.us/harbor/enquad/pdf/2002-16.pdf

HydroQual, 2002b. Addendum to the 1998-1999 hydrodynamic modeling report. Boston: Massachusetts Water Resources Authority. Report 2002-17. 82pp. http://www.mwra.state.ma.us/harbor/enquad/pdf/2002-17.pdf

HydroQual, 2004. "User's Guide for RCA, Release 3.0", Hydroqual, Inc, New Jersey.

Jiang M, GT Wallace, M Zhou, PS Libby and CD Hunt, 2007. Summer formation of a high-nutrient low-oxygen pool in Cape Cod Bay, USA, *J. Geophys. Res*., **112**, C05006, doi:10.1029/2006JC003889.

Jiang M, and M Zhou, 2004. Calibration of the Massachusetts and Cape Cod Bays hydrodynamic model: 2000-2001. Boston: Massachusetts Water Resources Authority. Report 2004-08. 71pp. http://www.mwra.state.ma.us/harbor/enquad/pdf/2004-08.pdf

Keay KE, WS Leo, and PS Libby, 2012. Comparisons of Model-Predicted and Measured Productivity in Massachusetts Bay. Boston: Massachusetts Water Resources Authority. Report 2012-03. 11 p. plus Appendix. http://www.mwra.state.ma.us/harbor/enquad/pdf/2012-03.pdf

Li Y, PS Fratantoni, C Chen, JA Hare, Y Sun, RC Beardsley, R Ji, 2015. Spatio-temporal patterns of stratification on the Northwest Atlantic shelf. Prog. Oceanog. 134, p123-137. http://dx.doi.org/10.1016/j.pocean.2015.01.003

Libby PS, DG Borkman, WR Geyer, JT Turner, and AS Costa, 2015. 2014 Water column monitoring results. Boston: Massachusetts Water Resources Authority. Report 2015-09. 42 pp. http://www.mwra.state.ma.us/harbor/enquad/pdf/2015-09.pdf

Libby PS, C Gagnon, C Albro, M Mickelson, A Keller, D Borkman, J Turner, and CA Oviatt, 2005. Combined work/quality assurance plan for baseline water quality monitoring: 2004-2005. Boston: Massachusetts Water Resources Authority. Report 2005-09. Version 1. 76 pp., plus appendices. http://www.mwra.state.ma.us/harbor/enquad/pdf/2005-09.pdf

Limeburner, R (Editor), 1985. CODE-2: Moored Array and Large-Scale Data Report. Woods Hole Oceanographic Institution Technical Report 85-35, 234pp.

Menzie CA, JJ Cura, Jr, JS Freshman, and B Potocki, 1991. Boston Harbor: estimates of loadings. Boston: Massachusetts Water Resources Authority. Report 1991-04. 108pp. http://www.mwra.state.ma.us/harbor/enquad/pdf/1991-04.pdf

Menzie-Cura and Associates, 1991. Sources and loadings of pollutants to the Massachusetts Bay. Report to the Massachusetts Bays Program. Report No. MBP-1991-01.

Montoya JP, KM Rathbun, and CS Mayo, 2003. Information Briefing to Outfall Monitoring Science Advisory Panel. Recent nitrogen isotope data from Massachusetts and Cape Cod Bays. January 6, 2003. 8 pp.

Sun, C & co-authors, 2010. "The Data Management System for the Global Temperature and Salinity Profile Programme" in Proceedings of OceanObs.09: Sustained Ocean Observations and Information for Society (Vol. 2), Venice, Italy, 21-25 September 2009. Hall, J, DE Harrison, and D Stammer, Eds., ESA Publication WPP-306, doi:10.5270/OceanObs09.cwp.86.

Taylor DI, 2015. Boston Harbor Water Quality 1994-2014. Boston: Massachusetts Water Resources Authority. Report 2015-05. 11 p. http://www.mwra.state.ma.us/harbor/enquad/pdf/2015-05.pdf

Tian, RC, C Chen, Q Xu, PF Xue, GW Cowles, RC Beardsley, and B Rothschild, 2009. Massachusetts Bay Eutrophication Model: 2006-2007 Simulation. Boston: Massachusetts Water Resources Authority. Report 2009-11. 147pp. http://www.mwra.state.ma.us/harbor/enquad/pdf/2009-11.pdf

Tian, RC, C Chen, LZ Zhao, P Xue, WS Leo, MJ Mickelson, 2010. Modeling 2009 in Massachusetts Bay using the unstructured-grid Bays Eutrophication Model. Boston: Massachusetts Water Resources Authority. Report 2010-22. 100pp. http://www.mwra.state.ma.us/harbor/enquad/pdf/2010-22.pdf

Tucker J, and AE Giblin, 2002. Stable isotope analyses of sediment and invertebrate samples from Boston Harbor and Massachusetts Bay. Boston: Massachusetts Water Resources Authority. Report 2002-21. 24 p. http://www.mwra.state.ma.us/harbor/enquad/pdf/2002-21.pdf

Tucker J, AE Giblin, CS Hopkinson, Jr, and D Vasiliou, 2000. Benthic nutrient cycling in Boston Harbor and Massachusetts Bay: 1999 annual report. Boston: Massachusetts Water Resources Authority. Report 2000-11. 63 p. http://www.mwra.state.ma.us/harbor/enquad/pdf/2000-11.pdf

Tucker J, S Kelsey, and AE Giblin, 2010. 2009 benthic nutrient flux annual report. Boston: Massachusetts Water Resources Authority. Report 2010-10. 27 p. http://www.mwra.state.ma.us/harbor/enquad/pdf/2010-10.pdf

Werme C, KE Keay, PS Libby, D Wu, DI Taylor, DL Codiga, K Coughlin, 2015. 2014 Outfall monitoring overview. Boston: Massachusetts Water Resources Authority. Report 2015-11. 70 p. http://www.mwra.state.ma.us/harbor/enquad/pdf/2015-11.pdf

Xue, P, C Chen, J Qi, RC Beardsley, R Tian, L Zhao, and H Lin, 2014. Mechanism studies of seasonal variability of dissolved oxygen in Mass Bay: A multi-scale FVCOM/UG-RCA application. *Journal of Marine Systems*. 131, 102-119.

Zhao L, C Chen, RC Beardsley, DL Codiga, WS Leo, and MJ Mickelson, 2015a. Modeling 2012 in Massachusetts Bay Using the Unstructured-Grid Bays Eutrophication Model. Boston: Massachusetts Water Resources Authority. Report 2015-02. 102p. http://www.mwra.state.ma.us/harbor/enquad/pdf/2015-02.pdf

Zhao L, C Chen, RC Beardsley, DL Codiga, WS Leo, and MJ Mickelson, 2015b. Modeling 2013 in Massachusetts Bay Using the Unstructured-Grid Bays Eutrophication Model. Boston: Massachusetts Water Resources Authority. Report 2015-03. 102p. http://www.mwra.state.ma.us/harbor/enquad/pdf/2015-03.pdf

Zhao, L, C Chen, WS Leo, and MJ Mickelson, 2012. Modeling 2011 in Massachusetts Bay using the unstructured-grid Bays Eutrophication Model. Boston: Massachusetts Water Resources Authority. Report 2011-13. 135pp. http://www.mwra.state.ma.us/harbor/enquad/pdf/2012-13.pdf

Zhao L, R Tian, P Xue, C Chen, WS Leo, and MJ Mickelson, 2011. Modeling 2010 in Massachusetts Bay using the unstructured grid Bay Eutrophication Model. Boston: Massachusetts Water Resources Authority. Report 2011-09. 118 p. http://www.mwra.state.ma.us/harbor/enquad/pdf/2011-09.pdf

Massachusetts Water Resources Authority
Charlestown Navy Yard
100 First Avenue
Boston, MA 02129
(617) 242-6000
www.mwra.com